2005

Vibration fatigue assessment finite element analysis and test correlation

Ziad A. Hanna
University of Windsor

Vibration Fatigue Assessment
Finite Element Analysis and Test Correlation

By

Ziad A. Hanna

A Thesis

Submitted to the Faculty of Graduate Studies and Research

through the Department of Civil and Environmental Engineering

In Partial Fulfillment of the Requirements for the

Degree of Master of Applied Science at the

University of Windsor

Windsor, Ontario, Canada

2005

Your file Votre référence
ISBN: 0-494-09817-1
Our file Notre référence
ISBN: 0-494-09817-1

ABSTRACT

During the design process of a new component, it is necessary to investigate its resistance to fatigue. Fatigue life assessment techniques can use experimental and/or modeling approaches. Conducting fatigue experimental test is time consuming and in most cases expensive. On the other hand, modeling approaches are fast and economical. However, there is still a need to calibrate a model to experimental finding before conducting parametric studies on fatigue performance results.

There exist three approaches for modeling fatigue, these are: stress based, strain based and fracture mechanics approach. In many engineering applications, particularly in the automotive industry, the loading is in general random by nature, therefore fatigue analysis of automotive component is based on random vibration.

In most cases fatigue life assessment is conducted in conjunction with finite element methods. The model of a component is developed to calculate the stress/strain distribution. Because fatigue life assessment is very sensitive to the stress/strain used, it is very important that the finite element model results are as close to the physical test results. The objective of this project is to develop a methodology of combining finite element modeling with experimental result for the fatigue life assessment of an automotive component.

In developing the finite element model, it is necessary to make simplifying assumptions with regards to the material behavior, boundary conditions and loading application. Generally, these assumptions lead to discrepancies between the FE results and experimental test. This research focuses on developing a methodology to construct a reliable finite element model that reproduces the observed behavior during the experiment despite the simplifying assumptions.

The proposed methodology is applied to the study of the fatigue life of an ABS-bracket supporting the electronic control unit (ECU). An experimental program is conducted to

assess the fatigue life of this component. A finite element model using MSC.PATRAN, MSC.NASTRAN software's is developed. The strain history obtained from experimental test is used to calibrate the FE model. The model update technique is used based on an optimization procedure for the stiffness of the bushings connecting the ECU to the bracket. Special attention is paid for modeling the boundary conditions at the connection of the bracket on the car body.

After obtaining a finite element model consistent with the observed experimental results, the fatigue life of the bracket is predicted using existing model. The MSC.FATIGUE software is used for this task.

Through this research, it is shown that the calibration of this finite element model is mandatory before using it for fatigue life assessment. The developed methodology can be generalized for other types of components.

ACKNOWLEDGMENTS

The author would like to thank his advisors Dr. Faouzi Grib and Dr. Peter Frise for their support, guidance, effort and patience throughout the course of this research. Their supervision is deeply appreciated.

My appreciation goes out to my industrial advisors, Mr. Mohammed Malik and Mr. Adrian Triffan of Daimler Chrysler Canada Inc., whose support, humility and technical expertise is inspirational. They have patiently sat through discussions with me on the project while answering my questions carefully and helping me to overcome any obstacles that have appeared through this course of research.

Furthermore, I would like to acknowledge all the people at ARDC especially the RTS lab and the durability steering lab for their support during this project, their time, resources and the access to the testing equipment which was essential to complete this project successfully. The author would also like to thank University of Windsor personnel for their help, time and support in conducting experimental tests.

Last but not least, I would like to thank all of my family members, my wife Ruoah, my sons Marwan and Tareq without whom I would have never succeeded this far.

TABLE OF CONTENTS

LIST OF FIGURES

LIST OF TABLES

LIST OF ABBREVIATIONS

ARDC: Automotive Research and Development Center

LEFM: Linear Elastic Fracture Mechanics Approach

ASTM: American Society for Testing and Materials

SAE: Society of Automotive Engineers

ECU: Electronic Control Unit

PSD: Power Spectral Density

MPCs: Multi-Point Constraints

RBE2: Rigid Beam Element

Hz: hertz

kg: kilogram

N: newton

RPC: Remote Parameter Control

LIST OF SYMBOLS

A: Amplitude ratio

A': Effective area

A_o: Original area

A_f: Area at fracture

a: Crack length.

b1: First fatigue strength exponent.

b: Fatigue strength exponent

c: Fatigue ductility exponent

d: Effective diameter

d_o: Original diameter

$\frac{da}{dN}$: The crack growth rate

D: Damage variable

E: Young modulus of elasticity

E_o: Expected numbers of zero crossings

E_p: Expected numbers of peaks

{f(t)}: Forcing function

F: Harmonic excitation force amplitude

$f(g)$: Correction factor that depends on specimen and crack geometry

G: Shear modulus

I_x: Inertia in x-direction

I_y: Inertia in y-direction

I_z: Inertia in z-direction

I_{xz}: Inertia in xz-direction

I_{xy}: Inertia in xy-direction

I_{yz}: Inertia in yz-direction

K_x: Stiffness in x- direction

K_y: Stiffness in y- direction

K_z: Stiffness in z- direction

K_{xy}: Stiffness in xy- direction

K_{xz}: Stiffness in xz- direction

K_{yz}: Stiffness in yz- direction

K_{Ic}: Fracture toughness

k_t^{eq}: Equivalent stress concentration factor

K: Strength coefficient

K': Cyclic strength coefficient

ΔK : The stress intensity range

ΔK_{th}: Threshold stress intensity factor

l: Effective length

l_o: Original length

$m_n(S)$: Spectral moment

n: Strain hardening exponent

n': Cyclic hardening exponent

N: Number of cycles

N_f: Number of cycles to failure

P: Applied force

P_f : Load at fracture

PSD: The mean square amplitude of a random signal

P(S): Probability density function

RA: Reduction in area

R : Stress range

r: Distance from crack tip

S: Nominal stress

S_e : Fatigue or endurance limit

S_u : Ultimate strength

SRI1: The stress range intercepts.

[M]: N*N mass matrix

[K]: N*N stiffness matrix

[C]: N*N damping matrix

[D]: ω.[C]

$[M_{ss}]$: Mass matrix for secondary DOF

$[M_{sp}]$: Mass matrix for primary DOF

$[K_{ss}]$: Stiffness matrix for secondary DOF

$[K_{sp}]$: Stiffness matrix for primary DOF

$[M^R]$: Reduced system mass matrix

$[K^R]$: Reduced system stiffness matrix

$[T]$: Transformation matrix

$[Z_u]$: Updated stiffness matrix

$[Z_A]$: Original stiffness matrix

u_s : Displacement vector for the secondary DOF

u_p : Displacement vector for the primary DOF

n_s : Number of secondary DOF

n_p : Number of primary DOF

r^{th} : Mode number in a model

${}_A\phi$: The analytical mode

${}_X\phi^E$: Expanded experimental modes

η : Damping loss factor

λ^2: Complex eignvalues

$[\phi]$: Normalized eigenvectors

$\{\phi\}$: Mode shape vector

[I]: Diagonal Identity matrix

[ω]: Eigenvalue matrices

$\alpha(\omega)$: The response of the system

$\Delta Z(\omega)$: The error in the dynamic stiffness matrix

$\{I\}_j$: The j^{th} column of the identity matrix

j: The location of the input force

$\dot{P}$: The parameter values for the original FE model

[S]: Sensitivity matrix

υ: Poisson's ratio

σ: Local stress

$\sigma_1, \sigma_2, \sigma_3$: Principal stresses

σ_m: Mean stress

σ_a : Stress amplitude

$\Delta\sigma$: Stress range

σ_{eq}: Equivalent stress

σ'_f: Fatigue strength coefficient

${}^e\sigma^{eq}$: Elastic equivalent stress

σ_{max}: Maximum stress

σ_{min}: Minimum stress

ε: Local strain

$\varepsilon_1, \varepsilon_2, \varepsilon_3$: Principal strain

ε_q: Equivalent strain

ε_f: True strain at final fracture

ε_e: Elastic strain component

ε_p: Plastic strain component

$\Delta\varepsilon$: Strain range

ε_f' : Fatigue ductility coefficient

τ_f' : Shear fatigue strength

γ_f' : Shear fatigue ductility coefficient

γ_{max} : Maximum shear strain

$\frac{\Delta\gamma_{max}}{2}$: Maximum shear strain amplitude.

$\Delta\varepsilon_n$: Normal strain range

γ : Irregularity factor

$\{\ddot{x}\}$: N*1 vector of the varying acceleration response

$\{\dot{x}\}$: N*1 vector of the varying velocity response

$\{x\}$: N*1 vector of the varying displacement response

ω : Natural frequency

$\overline{X}$: Complex amplitude of response

H(ω): System frequency response function FRF

CHAPTER ONE

PROBLEM DISCRIPTION

1.1 Introduction

The component under consideration is the ABS-Bracket supporting the electronic control unit (ECU). The bracket and the ECU are located in the bottom left and frontage of the car. Figures 1.1 and 1.2 show the shape and the location of the bracket, respectively.

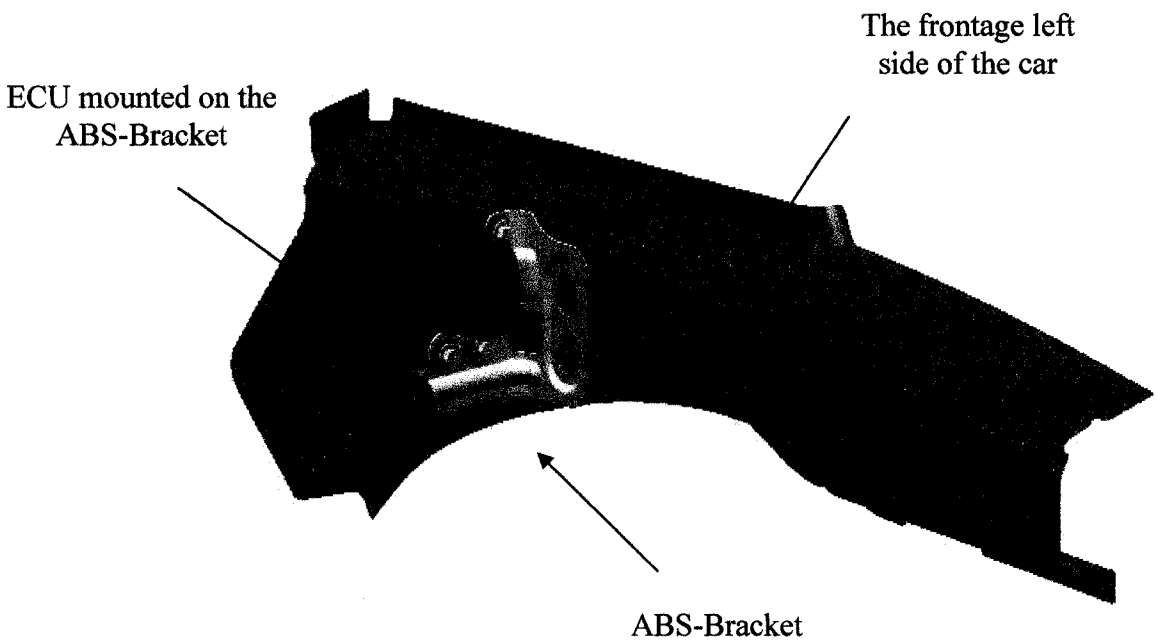

Figure 1.1 Location of the Bracket and the ECU in front left side of the car

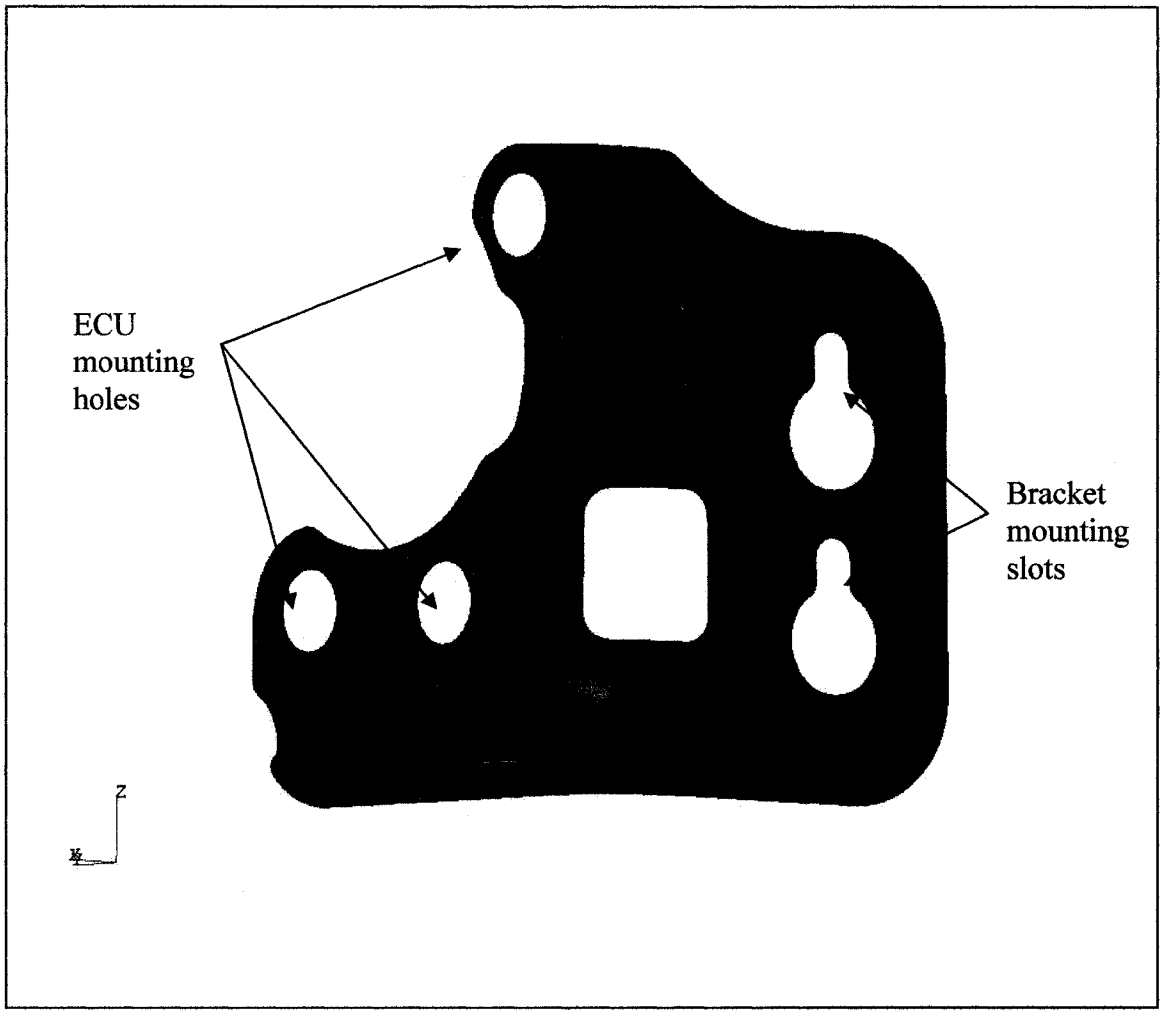

Figure 1.2 Geometry of the ABS-bracket

The bracket mass is 0.7 kg, the electronic control unit (ECU) mass is 3.15 kg and it is mounted on the bracket using three rubber bushings and three bolts tightened to the required torque. The ECU consists of three pieces (steel, aluminum and plastic) assembled together as one module using screws. The bracket is connected to the body of the car using 2 bolts tightened to the required torque as shown in Figure 1.3 below:

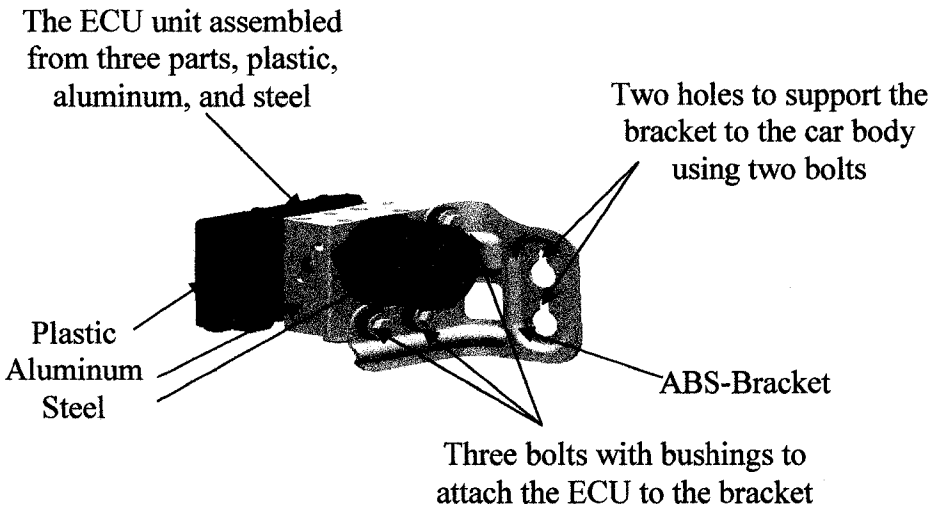

Figure 1.3 ECU component mounted on the bracket

1.2 Objective

The objective of this study is to develop a methodology for the durability analysis of the ABS-bracket using post-processing of finite element results. Durability tests are performed to assess the fatigue life experimentally. The actual bracket with the ECU is subjected to a vibration test on shaker table and is found to pass the durability test of target life on each excitation axis; no failure nor cracks was observed during the tests.

1.3 Loading history PSD

The vibration analysis of an automotive component is usually done in the frequency domain. The loading input is given in the form of acceleration Power Spectral Density

(PSD). The loading PSD is obtained through the transformation of the loading time history from the time domain to the frequency domain.

1. ***The Power Spectral Density Function (PSDF or PSD)*** of a signal $u_i(t)$ is denoted $S_j(\omega)$ and it is defined by equation 1.1 below and is the most common way of representing a signal that can be a loading force, acceleration, etc in the frequency domain. The PSD simply shows the frequency content of the time signal and is an alternative way to specify the time signal. It is obtained by utilizing the ***Fast Fourier Transform (FFT).***

$$S_i(\omega) = \lim_{T\to\infty} \frac{2}{T} \left| \int_0^T e^{-i\omega t} u_i(t) dt \right|^2 \qquad (1.1)$$

2. **PSD of signal** is representing the mean square amplitude of a random signal and it gives a statistical representation of stationary random process in the frequency domain. It is identified such that the area beneath the PSD represents the mean square amplitude of the random process.

$$\text{Mean square (f)} = \frac{1}{2}(amplitude)^2 \qquad (1.2)$$

The PSD of the loading history in each direction X, Y and Z direction are shown in Table 1.1. These PSDs depend on component designation and location in the car. They are calculated to excite parts subjected to random vibration loads. Directions X, Y and Z are the longitudinal, lateral and vertical direction of the car, respectively (Figure 1.1).

Table 1.1 Normalized PSD's Loading history with respect to the frequency in (X, Y and Z) direction

Frequency Hz	PSD in X G^2/Hz	Frequency Hz	PSD in Y G^2/Hz	Frequency Hz	PSD in Z G^2/Hz
5	0.105	5	0.121	5	0.094
10	1	8	1	10	1
190	0.072	12	1	60	0.595
370	0.004416	1000	0.004	200	0.0119
1000	0.004416			1000	0.00068

1.4 Finite element modeling

Finite element technique is one of the most powerful tools that allows modeling parts and conducting analysis for different types of structures and components. In most cases, the fatigue life assessment is conducted in conjunction with the finite element methods. The stress or strain histories obtained from the finite element analysis are used as a basis for fatigue life assessment.

1.4.1 Importing and meshing the part

The bracket is imported from CATIA to MSC.Patran software for preparing the FE model. The bracket is meshed using shell elements (QUAD 4), shell elements are used because the ratio $\frac{t}{l}$ of the bracket is $\frac{3}{80} < 0.1$. The (QUAD 4) elements are used because it has better characteristics than (TRI 3) elements and four gauss integration points. The material used for the bracket is not fully known; therefore the SAE material standard is used as a reference to determine the most likely material that can be used for this type of bracket. In this case, it is found that one of the stamped steel (SAE 1048, MAT-1, MAT-2, MAT-3) could be a good approximation.

1.4.2 Modeling the ECU in FE

The (ECU) is modeled using a concentrated mass element located at its center of gravity. This center of gravity of the mass (ECU) and its moment of inertia tensor components are computed using CATIA and MSC.Patran software, and the results are shown in Table 1.2. The bracket is made of stamped steel with modulus of elasticity, Poisson's ratio and density of 207,000 MPa, 0.29 and 7860 kg/m^3 respectively, these are generic properties for steel parts.

Table 1.2 Center of gravity and inertia tensor of the ECU unit

Center of gravity(mm)	$I_x\,(mm^4)$	$I_y\,(mm^4)$	$I_z\,(mm^4)$	$I_{xy}\,(mm^4)$	$I_{xz}\,(mm^4)$	$I_{yz}\,(mm^4)$
2054.85	8.35	-1.1004	12.78	1.0668	0.123	13.8285

Note: The values in the above table are scaled up for confidential purposes

Initially the rubber bushings were modeled using bushing elements available in MSC.Nastran software. These elements are an assembly of a generalized spring and a damper. The generalized spring element has six stiffness, 3 translational and 3 rotational stiffness at each end (see Table 1.3 and Figure 1.7).The used stiffness values where based on assumptions. The bushings were connected to the bracket and the mass using multi-point constraints (MPCs) elements called (RBE2) elements. The FEA model for the bracket and ECU is shown in Figure1.5

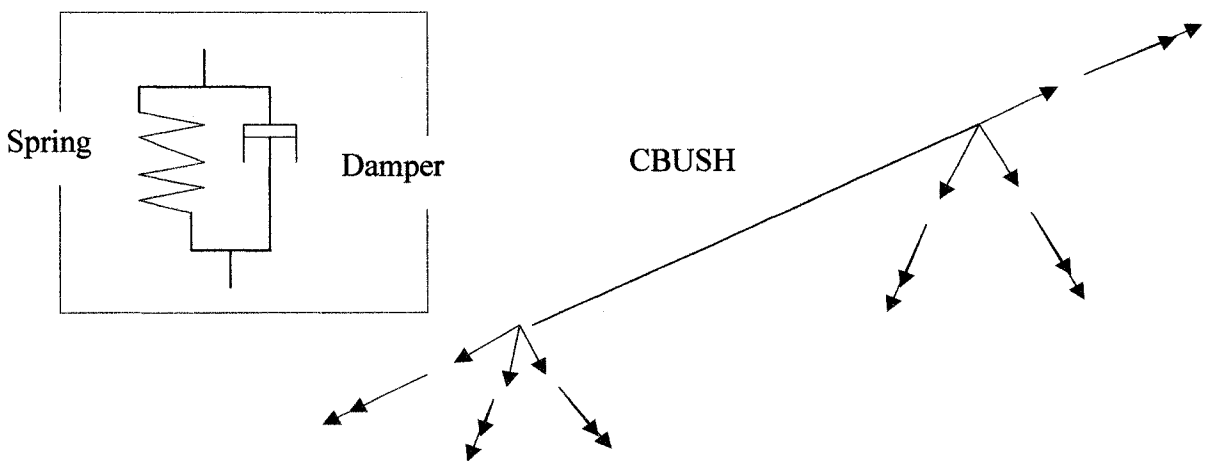

Figure 1.4 Bushing element in MSC.NASTRAN showing six degrees of freedom at each end

Table 1.3 Bushings stiffness

$K_x(N/mm)$	$K_y(N/mm)$	$K_z(N/mm)$	$K_{xy}(N.mm/rad)$	$K_{xz}(N.mm/rad)$	$K_{yz}(N.mm/rad)$
1050	1050	1050	105000	105000	105000

Note: The values in the above table are scaled up for confidential purposes

.

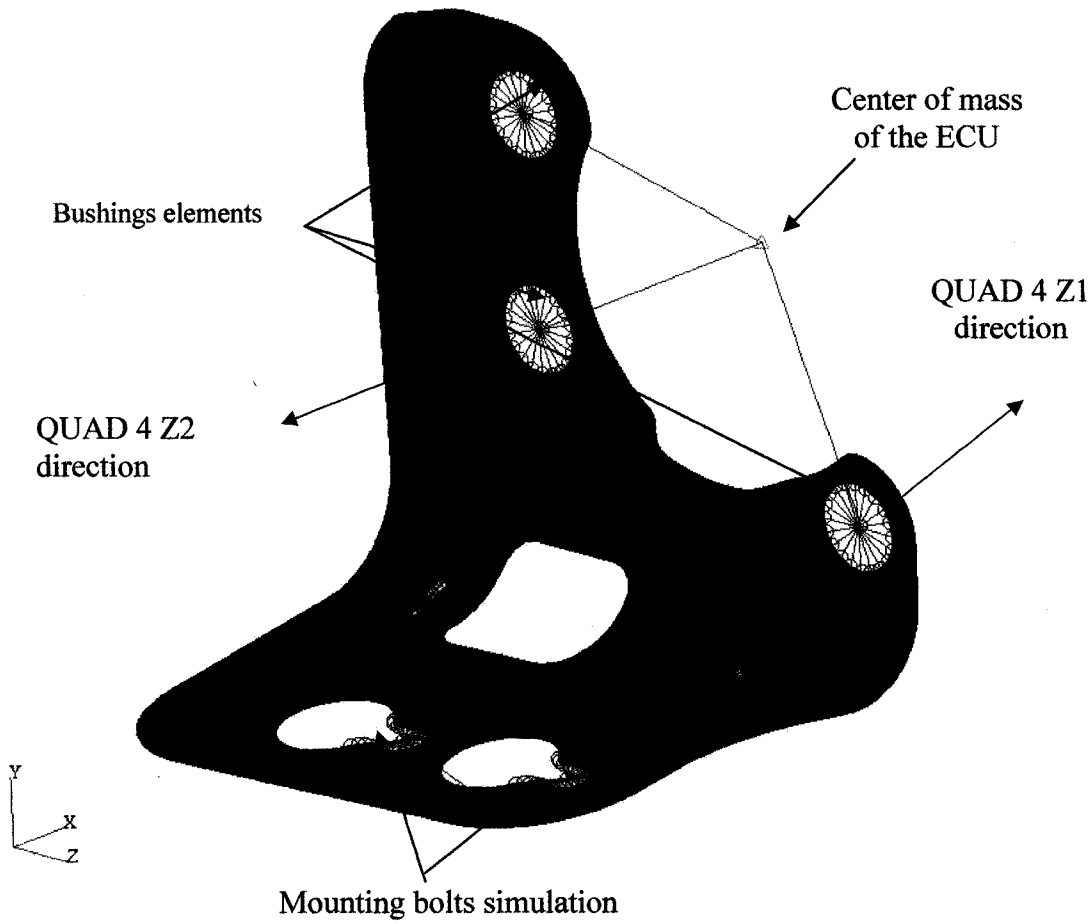

Figure 1.5 FEA model for the bracket and the ECU

1.4.3 Boundary conditions

The ABS-bracket is connected to the car body using two bolts. To model this in finite element, the nodes around the base holes of the FE model is assumed to be fully constrained in all six degrees of freedom at the base of the bracket. To model this accurately in NASTRAN a big mass of $1*10^8$ is created at the base input for this purpose. After completing the finite element model, finite element analysis is performed.

1.5 Finite element analysis

Finite element analysis of the bracket is conducted and consists of:

- Normal modes analysis to determine the basic dynamic behavior of the structure.
- Frequency response and random vibration analysis to calculate the RMS stresses and their critical locations.
- Fatigue assessment to predict the component life and damage locations.

1.5.1 Normal modes analysis

The durability analysis will be performed using spectral approach which is fundamentally a frequency based model. Therefore, the first step of the analysis is to determine the normal modes of the bracket. It is found that nine frequencies are in the range of the PSD excitation (0-1000 Hz), (Table 1.4). These frequencies will be used later to verify the degree of accuracy between the real component and the finite element model.

1.5.2 Frequency response and random vibration analysis

A point mass element at the base was created and used as an excitation input element in the Random Vibration analysis. The point mass is connected to the base holes nodes

using MPC's (RBE2 elements) (Figure 1.5). A frequency response analysis is conducted using unit acceleration and an initial critical damping of 4%. The stresses at the critical locations are reported in Table 1.5, and Figures 1.9 to 1.15.

Table 1.4 Normal modes analysis for different cases (values are scaled up for reason of confidentiality)

	FEA NORMAL MODES RANGE(0-1000)Hz (Scaled up for confidential purposes)			
MODE #	BRACKET ALONE WITH CONSTRAINT	BRACKET ALONE WITH NO CONSTRAINTS	ASSEMBLY WITH CONSTRAINT	ASSEMBLY WITH NO CONSTRAINT
1	385.041	230.212	60.012	235.530
2	883.198	505.047	151.787	512.515
3	1277.827	631.800	166.300	657.905
4		726.308	225.155	746.130
5			241.961	1028.895
6			434.533	1076.837
7			1156.621	1391.777
8			1648.746	1987.633
9			2038.515	

Table 1.5 Random vibration critical stress results and their locations

	NODE #	Z1	NODE #	Z2
MAX. STRESS IN X-DIR. (MPa)	6805.000	146.765	1324.000	178.536
MAX. STRESS IN Y-DIR. (MPa)	6805.000	74.212	1324.000	91.521
MAX. STRESS IN Z-DIR. (MPa)	4641.000	128.034	5196.000	136.333

Note: The values in the above table are scaled up for confidential purposes

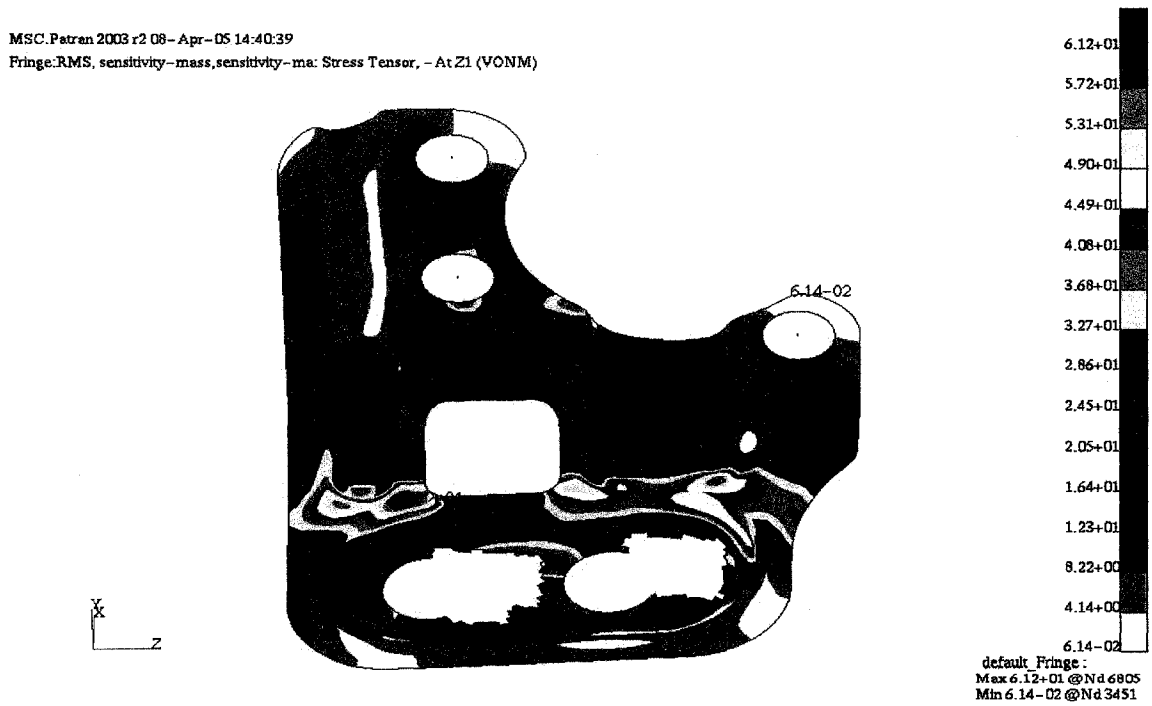

Figure 1.6 Von Mises stress contour (MPa) due to the X-PSD (Z1 direction)

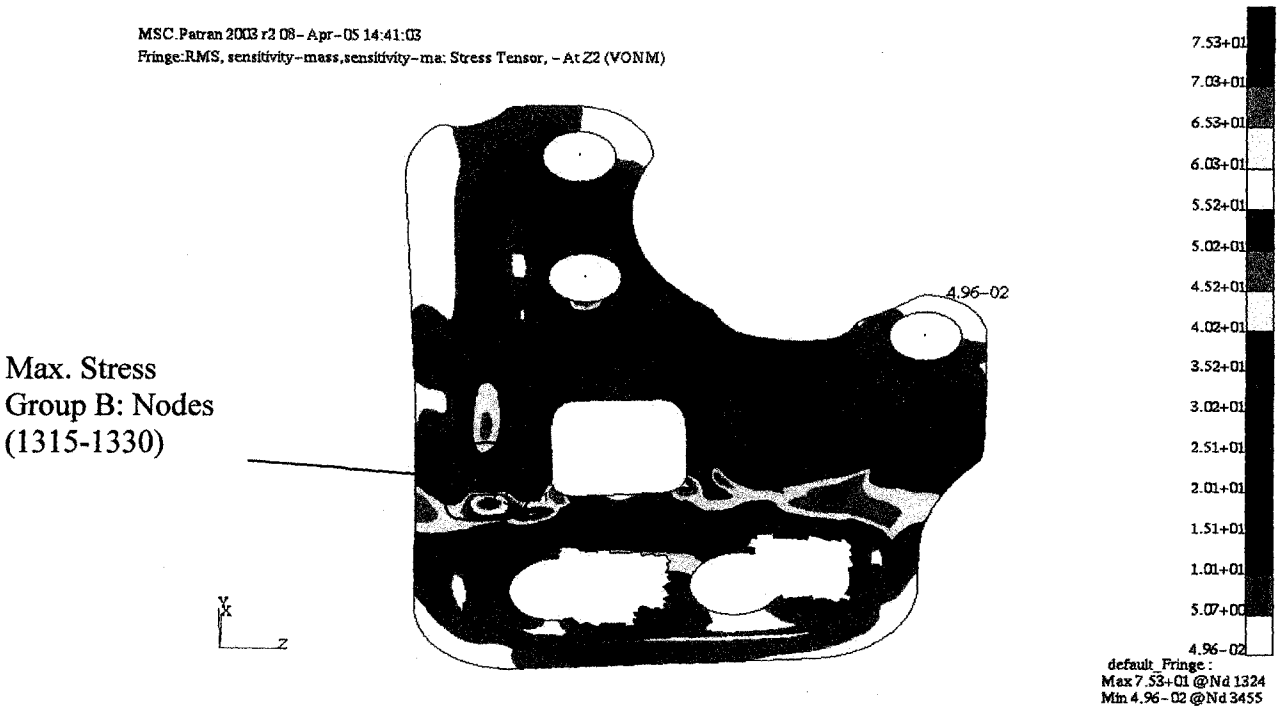

Figure 1.7 Von Mises stress contour (MPa) due to the X-PSD (Z2 direction)

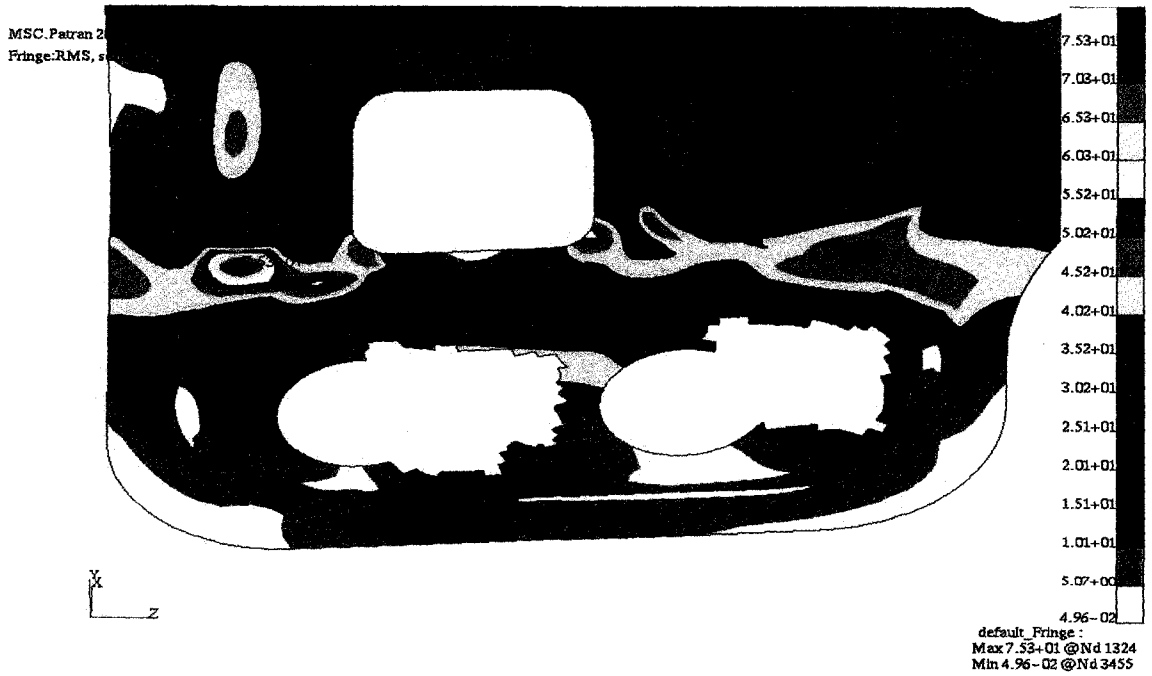

Figure 1.8 Von Mises stress contour (MPa) due to the X-PSD (Z2 direction)

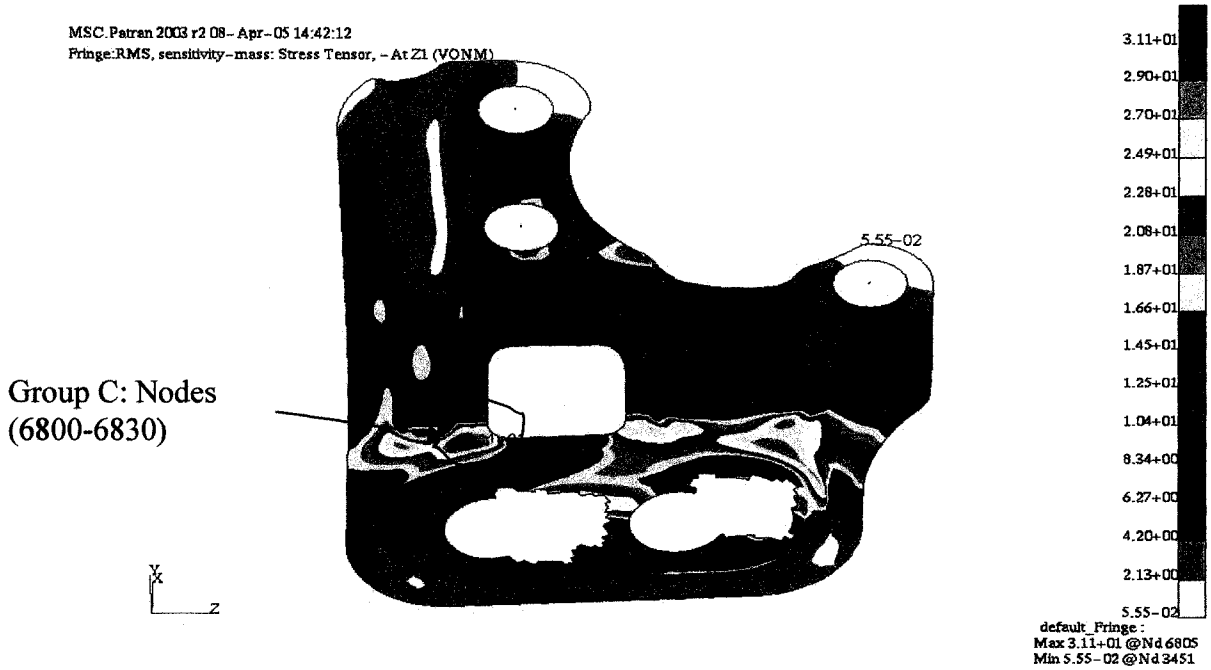

Figure 1.9 Von Mises stress contour (MPa) due to the Y-PSD (Z1 direction)

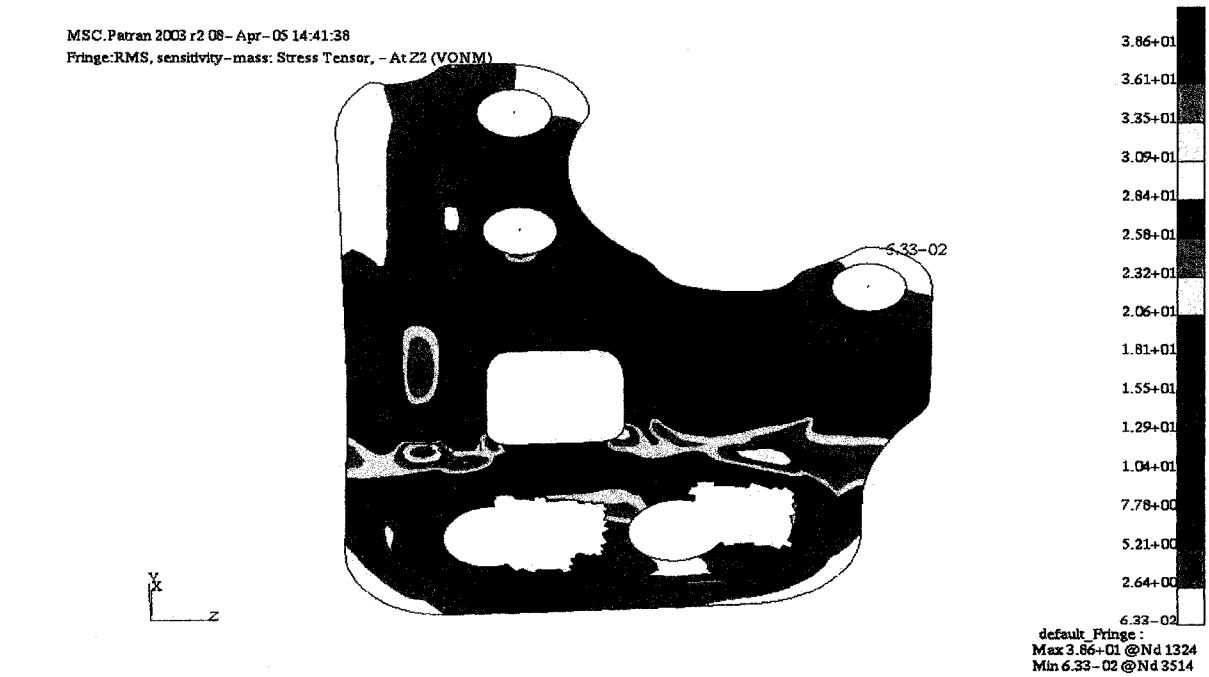

Figure 1.10 Von Mises stress contour (MPa) due to the Y-PSD (Z2 direction)

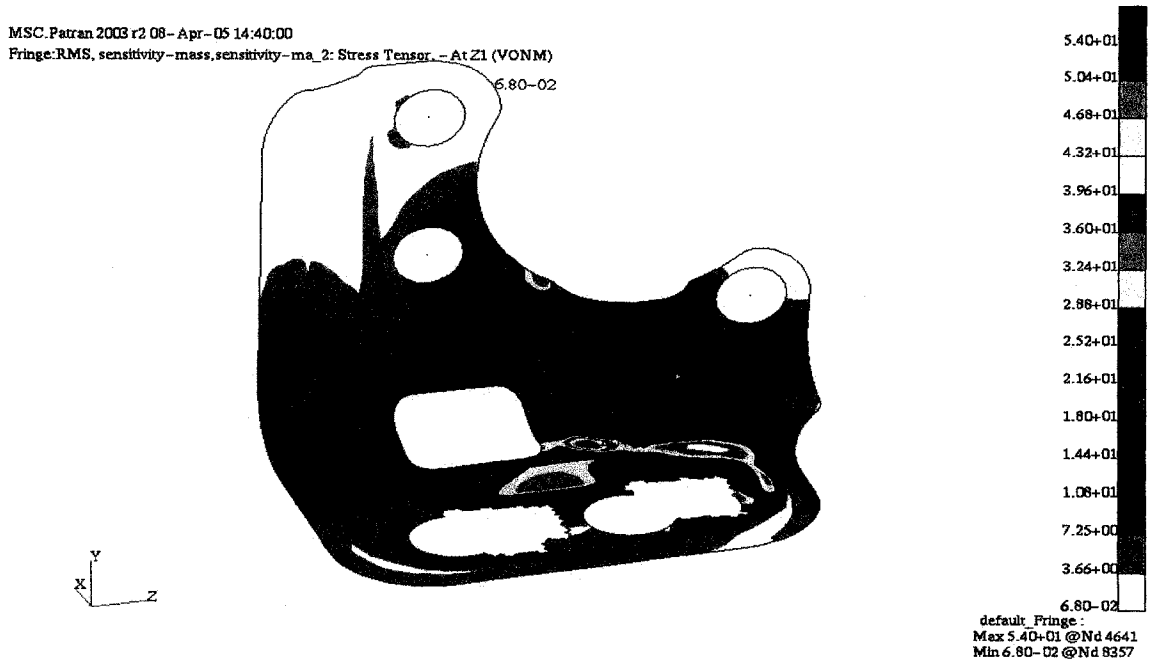

Figure 1.11 Von Mises stress contour (MPa) due to the Z-PSD (Z1 direction)

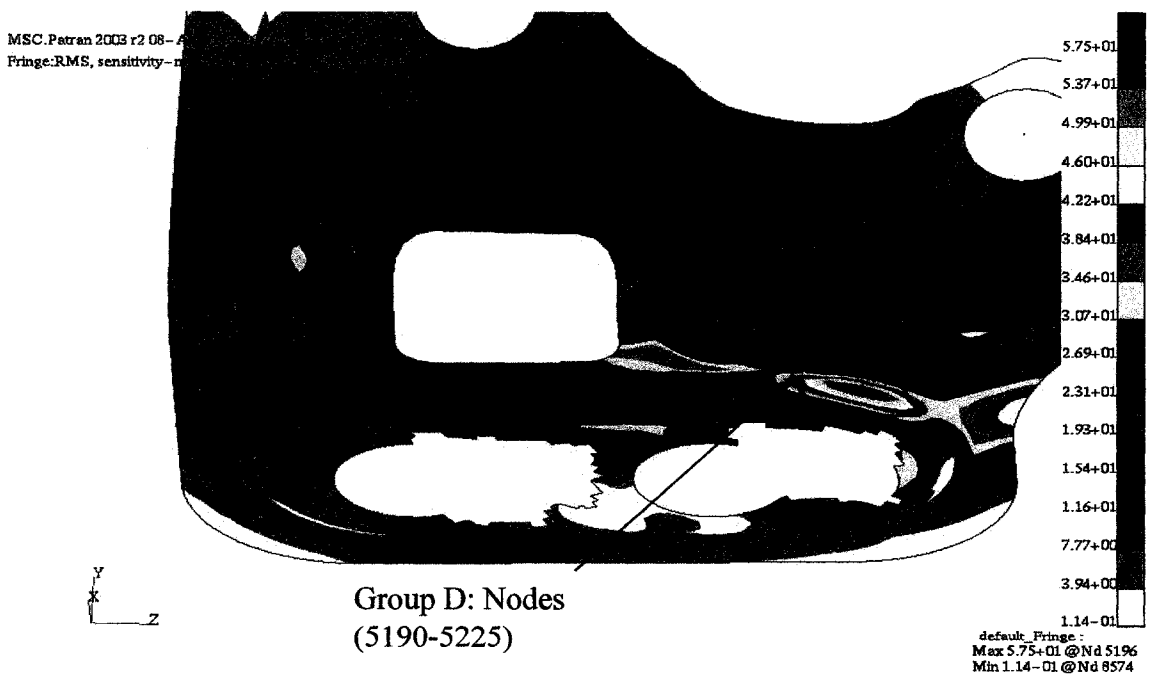

Figure 1.12 Von Mises stress contour (MPa) due to the Z-PSD (Z2 direction)

1.5.3 Fatigue assessment

After obtaining RMS of the stresses and the strains from the random vibration analysis, a fatigue life assessment is conducted using MSC.Fatigue software and the vibration fatigue model. Dirlik method is used which is considered the most appropriate method for automotive applications. The Maximum absolute principal stresses from the frequency response analysis were used to estimate the life at the nodes. The material used is SAE 1048 as mentioned earlier; the results are summarized in Table 1.6.

TABLE 1.6 Fatigue lives for critical nodes in the three directions

X-DIRECTION		Y-DIRECTION		Z-DIRECTION	
NODE #	LIFE (SECONDS)	NODE #	LIFE (SECONDS)	NODE #	LIFE (SECONDS)
1324.000	1219.935	1318.000	46766.610	5197.000	20972.655
1325.000	1414.735	1324.000	54551.305	5196.000	21001.875
1318.000	1434.215	1319.000	55515.565	5211.000	29974.850
1319.000	1699.630	1325.000	69959.985	5195.000	30883.105
1323.000	1784.855			5198.000	31036.510
1329.000	2722.330				

Note: The values in the above table are scaled up for confidential purposes

1.6 Conclusion

It can be seen that the fatigue lives obtained from the FE model are not realistic, since the experimental finding shows that the bracket pass the fatigue tests of 100 hours in each excitation axis without any damage. The low life obtained from FE analysis is an indicator of the fact that the model is far to be close to the actual component. The methodology of assessing the fatigue life of a real component is to be revised, and an investigation on what may be the cause of this discrepancy is to be performed.

CHAPTER TWO
LITERATURE REVIEW

2.1 Introduction

Fatigue is the process that may be the origin of damage or failure of mechanical components when they are subjected to repeated loading. Fatigue analysis is one of many key tools for the assessment of the behavior of automotive components. In automotive industry or any other industry, it is well known that fatigue is one of the most damaging phenomena. During the last 150 years, knowledge about fatigue process has been accumulating. A large amount of data and information is already available to design engineers and analysts. The purpose of this chapter is to summarize the existing literature on fatigue with focus on the analytical tools available for the assessment of fatigue life of metallic components.

There exist a wide range of methods for fatigue analysis. The existing literature for fatigue usually separates uniaxial fatigue from the more complex multiaxial fatigue theories. It is well established that fatigue process can be divided into three stages, initiation, nucleation and propagation of a crack. The existing methodologies for the analysis of each of these stages will be discussed in this chapter.

2.2 Existing fatigue theories

This section concentrates on existing uniaxial fatigue models with particular attention to stress based, strain based and fracture mechanics approaches.

The stress-based approach is the oldest technique that was initiated during 1850's when Whöler, a German engineer, developed the fundamentals of what is called today the S-N approach. It was the standard fatigue design method for almost 100 years. This approach is used mainly for high cycle fatigue where stresses and strains are elastic. The stress-based approach does not distinguish between initiation and propagation of a crack, it deals with total fatigue life of a component.

The second method is the strain-based approach which deals with localized yielding that may occur at stress raisers during cyclic loading. Initially, this approach was used only

when the plastic strains are not negligible. In this condition, the component has a short fatigue life. The strain-based approach is generalized to extend to high-cycle fatigue.
The third method of fatigue analysis uses the fracture mechanics approach to predict the propagation of a crack. This method is based on linear elastic fracture mechanics (LEFM) principles that was adapted for cyclic loadings. Fracture mechanics coupled with strain-life approach is sometimes used to predict a total fatigue life of a component for damage initiation, to crack propagation.

2.2.1 Stress-life approach:

The stress-life, called S-N approach, was the first method used to predict fatigue life. The number of cycles is calculated from the nominal stress acting in the system. This approach is still widely used in design applications where the stress is primarily within the elastic range of the material and the number of cycles to failure is large. This method doesn't work well for the low-cycle fatigue cases where the strain has a significant plastic component.

A typical cyclic load is shown in Figure 2.1. The following parameters are useful to define a generic cyclic load.

(i) the mean stress $\sigma_m = \left(\frac{\sigma_{\max} + \sigma_{\min}}{2} \right)$

(ii) the alternating range of stress $\sigma_a = \left(\frac{\sigma_{\max} - \sigma_{\min}}{2} \right)$

(iii)the stress range $\Delta\sigma = (\sigma_{\max} - \sigma_{\min})$

(iv) the stress ratio $R = \frac{\sigma_{\min}}{\sigma_{\max}}$

(v) the amplitude ratio $A = \frac{\sigma_a}{\sigma_{\min}} = \frac{1-R}{1+R}$

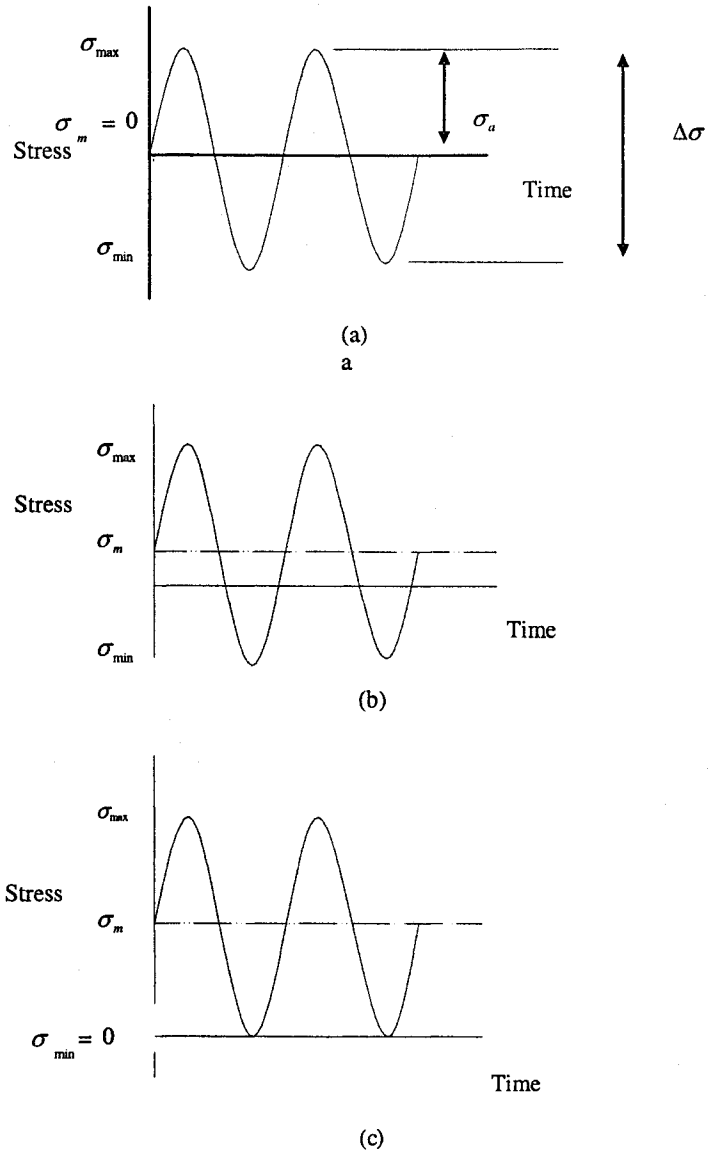

Figure 2.1 Several constant amplitude loading cycles. (a) Completely reversed, R=-1. (b) Non zero mean stress. (c) Zero compression, R=0 (Collins, 1981)

The S-N curve:

The S-N diagram is the base of stress-life method which is a plot of alternating nominal stress, S, versus the number of cycles at failure, N. The most common procedure for predicting the S-N data is the rotating bending test (Bannantine, 1990). An example is R.R.Moore test, which uses four points loading to apply a constant moment to a rotating (1750 rpm) cylindrical hourglass-shaped specimen. This loading procedure induces a fully reversed uniaxial state of stress, and the specimen is mirror polished with typical diameter in the test section of 0.25 to 0.3 in. The stress level at the surface of the specimen is calculated using the elastic beam equation even if the resulting value exceeds the yield strength of the material (Bannentine, 1990).

$$S=MC/I \qquad (2.1)$$

One of the major drawbacks of the stress-life approach is that it ignores the localized plasticity that may occur in the specimen. This plasticity may be significant, since the initiation of fatigue cracks may be caused by plastic deformation. The S-N approach is valid only if the plastic strains remain negligible.

For high cycle fatigue most metallic materials develop no significant plastic deformation, therefore the S-N approach is valid. In general, S-N data are presented on a plot with the actual S-N line representing the mean of the data. Certain materials, primarily steel have endurance or fatigue limit, noted, S_e, which is the stress level below which, the theoretical life is "infinite". In practice, the large numbers of cycles representing infinite life is taken of the order of 10^6 to 10^7.

Care must be taken when using endurance limit since it can disappear due:

(i) periodic overloads(which unpin dislocations)

(ii) corrosive environments (due to fatigue corrosion interaction)

(iii) high temperatures (which mobilize dislocations)

It should be pointed out that the effect of periodic overloads mentioned above relates to smooth specimens. Notched components may have completely different behavior due to residual stresses. The S-N curve plotted on scale is approximately a straight line, it can be represented by the following:

$$\sigma_a = AN_f^b \qquad (2.2\text{-a})$$

A and b are material properties and calculated for the test results.

This equation is often used in slightly different form:

$$\sigma_a = \sigma_f^{'}(2N_f)^B \qquad (2.2\text{-b})$$

Where A and B are fitting test data for unnotched axial specimen tested under completely reversed (σ_m=0) loading, the following equations describe the relation between the couple (A, b) and ($\sigma_f^{'}$, B):

$$A = 2^b \sigma_f', B = b \qquad (2.3)$$

When the ratio of the nominal and the yield stresses of the material is plotted as function of the number of cycles at failure, the curves of different materials tend to be the same. This suggest that the endurance limit (defined as the fatigue life of 10^6), S_6, is approximately equal to 50% S_u and the stress corresponding to 1000 cycles is about 90% S_u (refer to Figure 2.2).

$$S_6 = S_e = 0.5\ S_u \qquad \text{for } S_u < 1400 \text{ MPa} \qquad (2.4)$$

$$S_6 = S_e = 700 \text{ MPa} \qquad \text{for } S_u > 1400 \text{ MPa} \qquad (2.5)$$

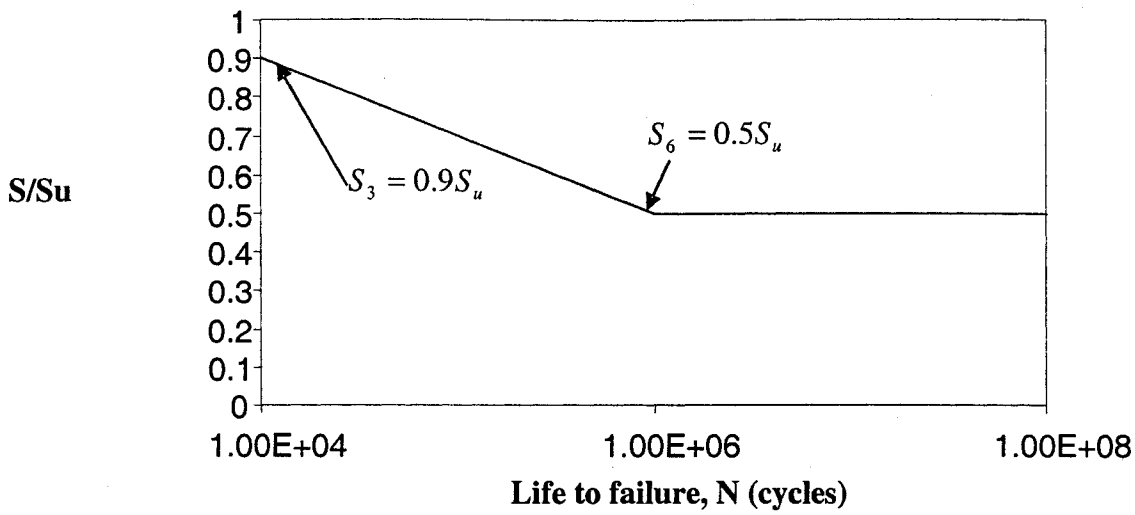

Figure 2.2 Generalized S-N curve for wrought steels

2.2.2 Strain-life approach:

Strain–life method emerged from the fact that in some critical locations such as notches, the material develops plastic strain and therefore, the stress approach is no longer applicable.

The strain–life method assumes similitude between the materials in a smooth specimen tested under strain–control and the material at the root of a notch, Figure 2.3. For a given loading history, the fatigue damage of the specimen and the notch root are considered to be equivalent (Bannantine, 1990).

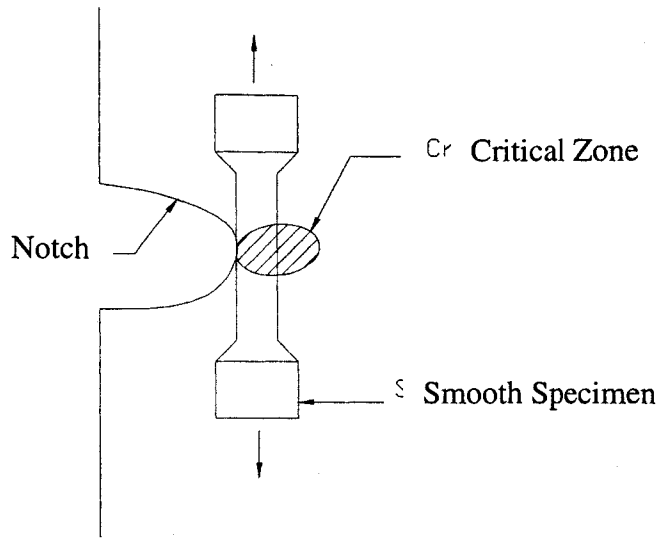

Figure 2.3 Equally stressed volume of material (Bannantine, 1990)

Crack growth is not explicitly accounted for in the strain-life method. Strain-life methods are often considered as initiation life estimates. The local strain-life approach has gained acceptance as useful method of evaluating fatigue life of a notched component. Both American Society for Testing and Materials (ASTM) and the Society of Automotive Engineers (SAE) have recommended procedures and practices for conducting strain-controlled tests and using these data to predict fatigue lives (Bannantine, 1990).

The strain versus life curve is a plot of strain amplitude versus the number of cycles to failure. This curve is referred to as ε-N curve. In notched components subjected to cyclic external loads, the strain based models are preferred for the fatigue life assessment. This concept has motivated the strain-life design method based on relating the fatigue life of notched parts to the life of small, unnotched specimens that are cycled to the same strains as the material at notch root (Stephens, Fatemi, 2001). Since fatigue damage is assessed directly in terms of local strain, this approach is called the "local strain approach" (Stephens, Fatemi, 2001). It is essential to know the stress-strain history at the critical location to study fatigue life for a component using strain-life approach.

i. The engineering stress is defined as:

$$\text{S=engineering stress} = \frac{P}{A_o} \tag{2.6}$$

Where:

P : is the force applied on the specimen

A_o : is the area of the specimen before applying the load.

The engineering strain is defined as:

ii. $$\text{e=engineering strain} = \frac{l - l_o}{l_o} = \frac{\Delta l}{l_o} \tag{2.7}$$

Where:

P : is the force applied on the specimen,

A_o : is the area of the specimen before applying the load

l_o : is the original length,

d_o : is the original diameter,

l : is the instantaneous length,

d : is the instantaneous diameter,

A' : is the instantaneous area.

In tension, the true stress is larger than the engineering stress, due to reduction in the cross area during deformation (Figure 2.4).

$$\sigma = \frac{P}{A'} \tag{2.8}$$

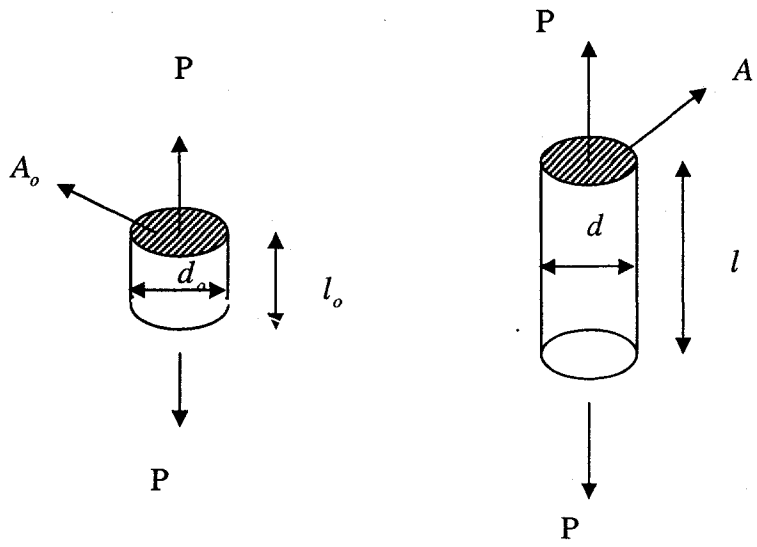

Figure 2.4 Original and deformed (instantaneous) configuration of test specimen (Stephens, Fatemi, 2001)

The true or natural strain, based on an instantaneous gage length, l, is defined as

$$\varepsilon = \int_{l_o}^{l} \frac{dl}{l} = \ln \frac{l}{l_o} \tag{2.9}$$

The true strain in terms of engineering strain is expressed as:

$$\varepsilon = \ln(1+e) \tag{2.10}$$

Equation 2.10 is valid up to necking which takes place when the ultimate tensile strength is reached, since after necking, plastic deformation becomes localized and the strain is no longer uniform through the gage section (Stephens, *et al.*, 2001).

Assuming that the volume of material remains constant during straining, one can write:

$$A_o l_o = Al = \text{ constant} \tag{2.11}$$

And therefore, we deduce

$$\frac{A_o}{A} = \frac{l}{l_o} \tag{2.12}$$

The true strain can be written in terms of cross-sectional area

$$\varepsilon = \ln\frac{l}{l_o} = \ln\frac{A_o}{A} \tag{2.13}$$

The true stress can expressed in terms of engineering stress as:

$$\sigma = S\frac{A_o}{A} \tag{2.14}$$

Combining equation (2.10) and equation (2.13) both valid up to necking, gives us:

$$\varepsilon = \ln(1+e) = \ln\frac{A_o}{A} \tag{2.15}$$

Therefore, true stresses can expressed as function of engineering stress and strain using equation (2.14) and (2.15). Figure 2.5 shows the plot of the engineering and true stress-strain relationship.

$$\sigma = S(1+e) \tag{2.16}$$

The total true strain, ε_t in tension test can be separated into elastic and plastic components, stated in equation form:

$$\varepsilon_t = \varepsilon_e + \varepsilon_p \tag{2.17}$$

The elastic strain is defined as

$$\varepsilon_e = \frac{\sigma}{E} \tag{2.18}$$

For most metals, a plot of true stress versus true plastic strain is a straight line. Consequently, this curve can be expressed using a power function:

$$\sigma = K(\varepsilon_p)^n \tag{2.19}$$

Where K is the strength coefficient and n is the strain-hardening exponent.

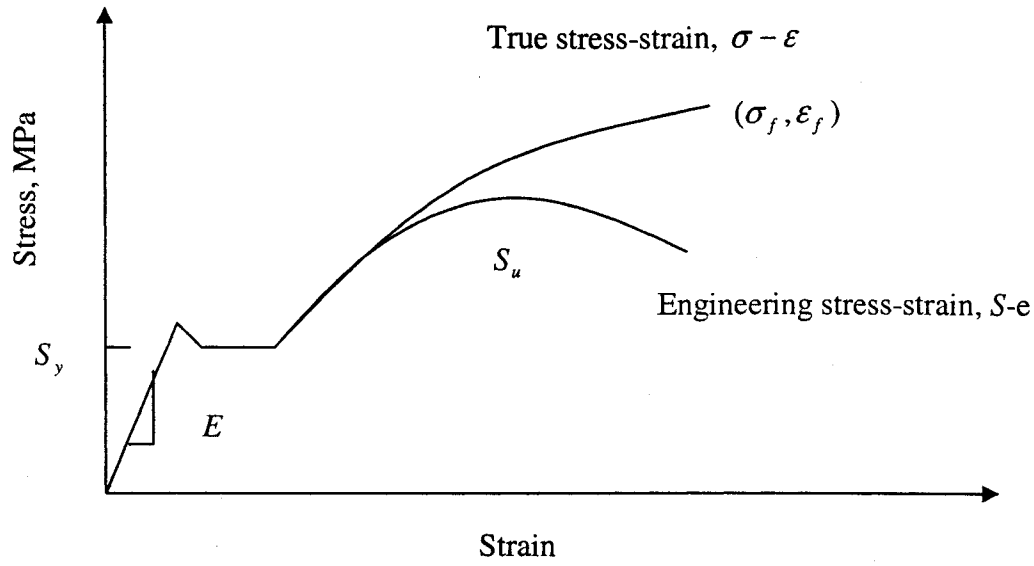

Figure 2.5 Comparison of engineering and true stress-strain, (Stephens, *et al.*, 2001)

At fracture, two important quantities can be defined: These are the true fracture strength and the true fracture ductility. True fracture strength, σ_f is the true stress at final fracture.

$$\sigma_f = \frac{P_f}{A_f} \qquad (2.20)$$

where:

A_f : is the area at fracture and

P_f : is the load at fracture.

True fracture ductility, ε_f : is the true strain at final fracture. This value can be defined in terms of the initial cross-sectional area and the area at fracture.

$$\varepsilon_f = \ln\frac{A_o}{A_f} = \ln\frac{1}{1-RA} \qquad (2.21)$$

where RA is defined as:

$$RA = \frac{A_o - A_f}{A_o} \qquad (2.22)$$

The strength coefficient, K, can be defined in terms of the true stress at fracture, σ_f and the true strain at fracture, ε_f, as:

$$K = \frac{\sigma_f}{\varepsilon_f^n} \qquad (2.23)$$

Therefore, the total strain can be written as:

$$\varepsilon_t = \frac{\sigma}{E} + \left(\frac{\sigma}{K}\right)^{\frac{1}{n}} \qquad (2.24)$$

Cyclic stress-strain behavior

Cyclic stress-strain curves are necessary for accessing the durability of structures and components subjected to repeated loading. The response of material subjected to cyclic inelastic loading is generally represented in the form of hysteresis loop, as shown in Figure 2.6. The total width of the loop is $\Delta\varepsilon$ or the total strain range. The total height of the loop is, $\Delta\sigma$ or the total stress range.

The total strain is the sum of the elastic and plastic strain ranges,

$$\Delta\varepsilon = \Delta\varepsilon_e + \Delta\varepsilon_p \qquad (2.25)$$

Or in terms of amplitudes,

$$\frac{\Delta\varepsilon}{2} = \frac{\Delta\varepsilon_e}{2} + \frac{\Delta\varepsilon_p}{2} \qquad (2.26)$$

Using the Hooke's law, the elastic term may be replaced by $\frac{\Delta\sigma}{E}$.

$$\frac{\Delta\varepsilon}{2} = \frac{\Delta\sigma}{2E} + \frac{\Delta\varepsilon_p}{2} \qquad (2.27)$$

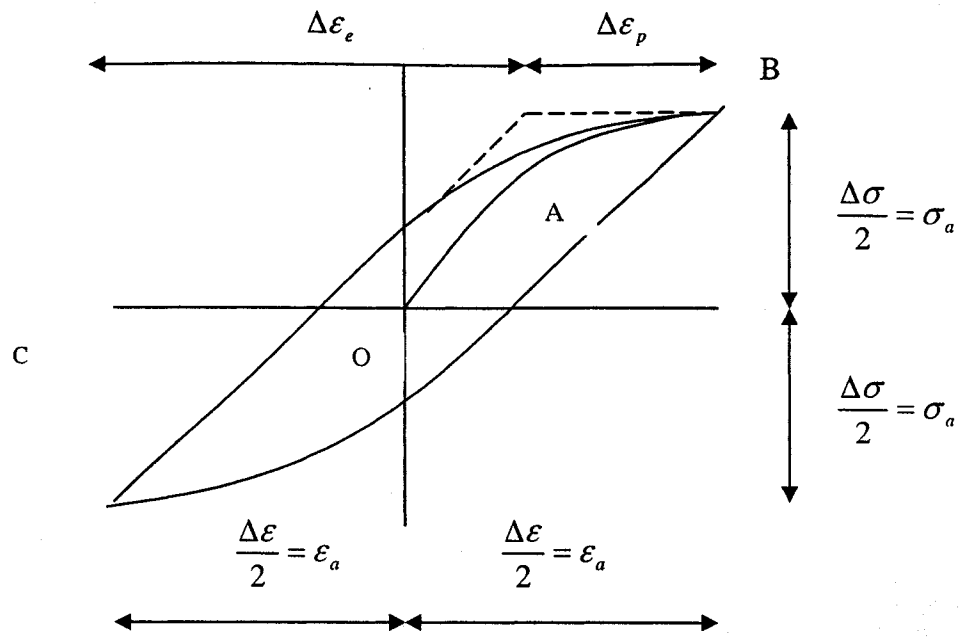

Figure 2.6 Complete stress-strain cycle, hysteresis loop (nCode international, 2001)

Early in life, the stress-strain response of most materials changes significantly with applied cyclic strains. However, after a relatively small number of cycles, typically no more than about 10% of total life, the hysterisis loops tends to stabilize so that the stress amplitude remains reasonably constant over the remaining portion of fatigue life. If the stress, strain coordinates of the tips from stable hysteresis loops, at different strain amplitude, are plotted in stress-strain space, then the locus of these points defines the cyclic stress-strain curve (Bannantine, 1990), as shown in Figure 2.7.

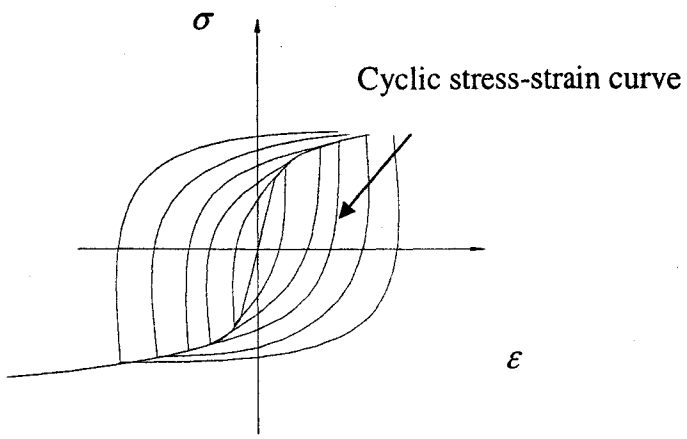

Figure 2.7 Cyclic stress-strain curves obtained by connecting tips of stabilized hysteresis loops (Bannantine, 1990).

Analogous to monotonic stress-strain curve, a log-log plot of completely reversed stabilized cyclic true stress versus true plastic strain can be approximated by a straight line as shown in Figure 2.8:

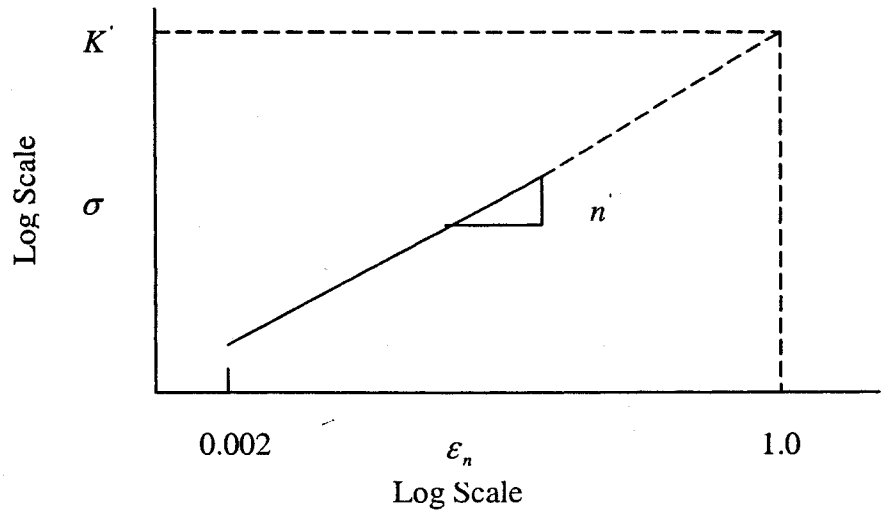

Figure 2.8 Log-Log plot of true cyclic stress versus true cyclic plastic strain (Bannantine, 1990)

A power law function can be deduced:

$$\sigma_a = K'(\varepsilon_p)^{n'} \tag{2.28}$$

where:

σ_a: is the stable stress amplitude and

ε_p :is the stable plastic strain amplitude,

K' : is the strength coefficient and

n' : is the strain hardening exponent

The cyclic stress-strain relation can be written as:

$$\varepsilon_a = \frac{\sigma_a}{E} + \left(\frac{\sigma_a}{K'}\right)^{1/n'} \tag{2.29}$$

Strain-life curve

The stress-life data may be represented by a straight line relationship when plotted using log scales. The relationship was initially given by (Basquin, 1910) as stated in equation (2.2)

$$\sigma_a = \sigma_f'(2N_f)^b \tag{2.30}$$

where:

σ_a: is the true cyclic stress amplitude,

σ'_f : is the fatigue strength coefficient,

$2N_f$: is number of half cycles, reversals, to failure,

b: is the regression slope called the fatigue strength exponent and

σ_f' : is taken approximately equal to the monotonic fracture stress, σ_f

Coefficient *b* varies between -0.05 and -0.12 (Basquin, 1910).

Basquin (Basquin, 1910) equation may be re-written in terms of elastic strain amplitude:

$$\varepsilon_a = \frac{\sigma_a}{E} = \frac{\sigma_f'(2N_f)^b}{E} \tag{2.31}$$

with ε_a is the elastic strain amplitude.

Coffin (Coffin, 1954) and Manson (Manson, 1953) independently proposed that plastic strain component of a fatigue cycle may also be related to life by a simple power law:

$$\varepsilon_p = (2N_f)^c \qquad (2.32)$$

where

ε_p : is the plastic strain amplitude,

ε'_f : is the regression intercept called fatigue ductility coefficient and

$2N_f$: is the number of half cycles, reversals, to failure.

The coefficient ε'_f and c considered to be mathematical properties with the fatigue ductility coefficient being approximately equal to the monotonic fracture strain, ε_f and c varies between -0.5 and -0.7 (Morrow, 1965). Morrow and Socie (Morrow and Socie, 1981) have indicated that the total strain amplitude, that is the sum of the elastic and plastic components, may be better correlated to life. Figure 2.9 illustrates schematically the nature of total strain-life curve.

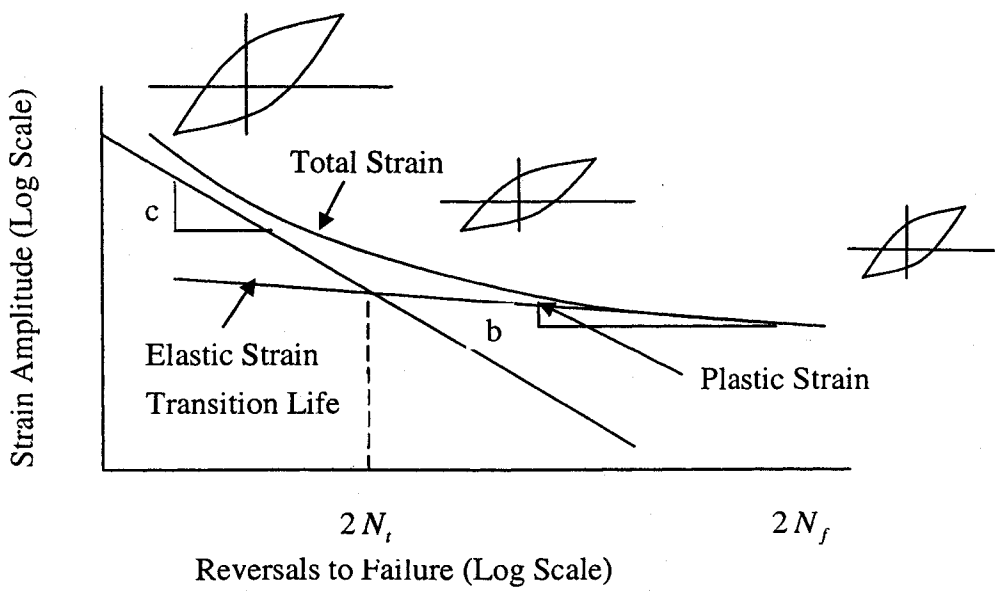

Figure 2.9 Total strain-life curve (Bannantine, 1990)

Mathematically, this curve can be described by summing together the elastic and plastic components:

$$\varepsilon_t = \varepsilon_e + \varepsilon_p \tag{2.33}$$

$$\varepsilon_t = \frac{\sigma_f'(2N_f)^b}{E} + \varepsilon_f'(2N_f)^c \tag{2.34}$$

Determination of cyclic fatigue properties

The fatigue material properties required to define the cyclic stress-strain curve and the strain–life curve are usually determined by carrying out test, under strain control, on a series of smooth highly polished hourglass specimens. Typically, about 15 tests need to be performed at differing strain amplitudes. Fatigue parameters can then be calculated by regression analysis on the following:

k' and n': from a log stress vs. log plastic strain regression,

σ_f' and b: are from a log elastic strain vs. log $2N_f$ regression and

ε_f' and c: are from a log plastic strain vs. log $2N_f$ regression.

2.2.3 Fracture Mechanics Approach

Fatigue life of a component has two stages: initiation, where the damage accumulates locally in the material and propagation stage. The size of the crack at the transition from initiation to propagation is usually unknown and often depends on the analyst point of view and the size of the component being analyzed. The distinction between the initiation life and propagation life is important. At low strain amplitude up to ninety percent of the life may be taken up by initiation, while at high amplitudes the majority of the fatigue life may be spent propagating a crack. Fracture mechanics approaches are used to estimate the propagation life (Bannantine, 1990).

Fracture mechanics approaches require that an initial crack size need to be known or assumed. Alternatively, for an estimate of total fatigue life of a defect-free material, fracture mechanics approaches can be used to determine propagation. Strain-life

approach may then be used to determine initiation life, the total life then is being the sum of these two estimates.

Purpose of fracture mechanics

In general, the possibility of crack like defects being present at the start of service life is to be determined. Even if the component is not cracked, to start with, the remnant life after initiation may be significant or possibly dominant with respect to the total life. Furthermore, for inspection related activities, the remnant life of a component discovered to be cracked during inspection needs to be determined so that the decision regarding serviceability can be supported by reliable predications (nCode, 2001).

The designer must be able to calculate the following criterion to determine crack stability (Figure 2.10):

1- The residual strength as a function of crack size.
2- The crack size that can be allowed at the expected service load (the critical size).
3- How long it takes the crack to grow from a certain size to a critical size.
4- The size of initial flaws that can be tolerated in a new component.
5- The interval between inspections of cracked component.

Fracture mechanics tries to provide tools to answer these questions. This subject includes the materials science studies of fracture process on an atomic scale. This consist of growth of cracks, the analysis of the crack tip stresses and the behavior of cracks in these stress fields, the provision of materials properties by testing, and finally the engineering application of these techniques to the analysis of real structures (Draper, 1999).

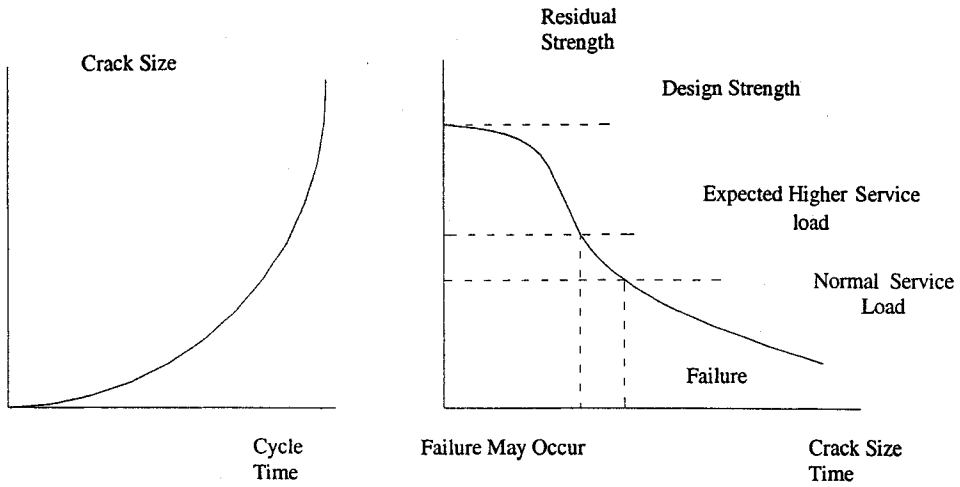

Figure 2.10 Relationship between crack length and failure load (Draper, 1999).

Loading modes

There are generally three modes of loading, which involve different crack surface displacements. These are shown in Figure 2.11:

Mode I: opening or tensile mode (the crack faces are pulled apart);

Mode II: sliding or in-plane shear (the crack surfaces slide over each other);

Mode III: tearing or anti-plane shear (the crack surfaces move parallel to the leading edge of the crack and relative to each other).

Mode I is considered the predominant loading mode in most engineering applications, however, most problems can be addressed by superimposing one or more of these modes.

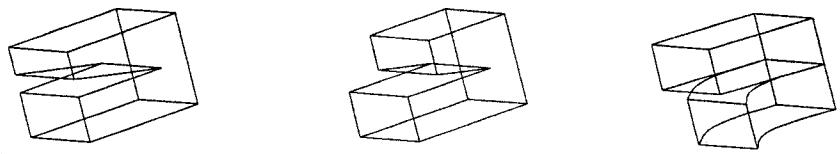

I II III

Figure 2.11 The three crack opening modes (Bannentine, 1990)

Stress intensity factor

The stress intensity factor, K defines the magnitude of the local stresses, around the crack tip. This factor depends on the loading, the crack size, the crack shape, and the geometric boundaries, the general form of the stress intensity factor is:

$$K = f(g)\sigma\sqrt{\pi a} \qquad (2.35)$$

where

σ : is remote stress applied to component.

a : is crack length.

$f(g)$ = correction factor that depends on specimen and crack geometry.

The stress intensity factor solutions are found for a wide variety of problems within LEFM. Stress intensity factors for a single loading mode can be added algebraically. Consequently, stress intensity factors for a complex loading condition of the same loading mode can be determined by superposition.

Plastic zone size

Materials develop plastic strains as the yield stress is exceeded in the region near the crack tip; the amount of plastic deformation is restricted by the surrounding material,

which remains elastic. The size of this plastic zone is dependent on the stress condition of the body. Two types of plastic zone are defined, monotonic and cyclic plastic zone size.

(a) Monotonic plastic zone size

The plastic zone sizes under monotonic loading have been estimated to be:

$$r_y = \frac{1}{2\pi}\left(\frac{K}{\sigma_y}\right)^2 \qquad \text{Plane stress} \qquad (2.36)$$

$$r_y = \frac{1}{6\pi}\left(\frac{K}{\sigma_y}\right)^2 \qquad \text{Plane strain} \qquad (2.37)$$

where

r_y is defined as shown in Figure 2.12 below:

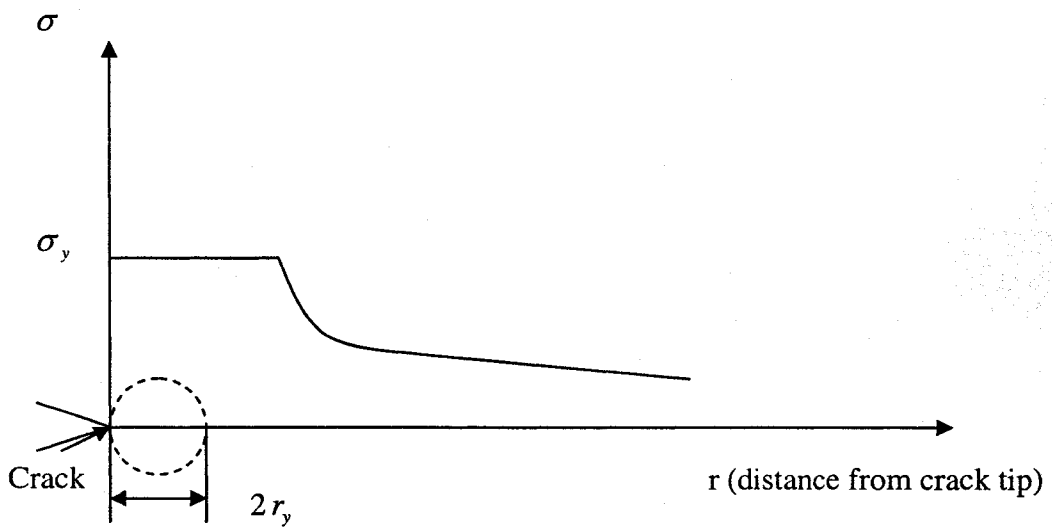

Figure 2.12 Monotonic Plastic Zone Size (Bannantine, 1990)

(b) Cyclic Plastic Zone Size

The reversed or cyclic plastic zone size is four times smaller than the comparable monotonic value. As the nominal tensile load is reduced, the plastic region near the crack tip is put into compression by the surrounding elastic body. As shown in Figure 2.13, the

change in stress at the crack tip due to the reversed loading is twice the value of the yield stress (Bannantine, 1990).

The LEFM concepts can often be used in the analysis of fatigue crack growth problems even in materials that exhibit considerable amounts of ductility. The basic assumption that the plastic zone size is smaller in relationship to the crack and the crack body usually remains valid. Equations 2.36 and 2.37 become:

$$r_y = \begin{cases} \frac{1}{2\pi}\left(\frac{K}{2\sigma_y}\right)^2 = \frac{1}{8\pi}\left(\frac{K}{\sigma_y}\right)^2 \\ \\ \frac{1}{6\pi}\left(\frac{K}{2\sigma_y}\right)^2 = \frac{1}{24\pi}\left(\frac{K}{\sigma_y}\right)^2 \end{cases} \qquad (2.38)$$

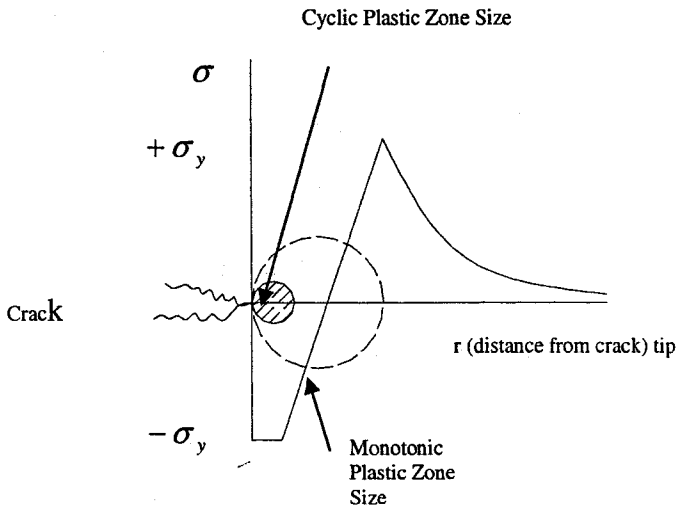

Figure 2.13 Cyclic plastic zone size (Bannentine, 1990)

As the stress intensity factor reaches a critical value, K_c, unstable fracture occurs. This critical value of the stress intensity factor is known as the fracture toughness of the material. The fracture toughness can be considered as the limiting of the stress intensity just as the yield stress might be considered the limiting value of applied stress. Fracture toughness, K_{Ic} is dependent on specimen geometry and metallurgical factors, and it depends on both temperature and the specimen thickness.

Fatigue crack growth

If the crack length, a, is plotted versus the corresponding number of cycles, N, at which the crack is measured, it can be shown that most of the life of the component is spent while the crack length is relatively small. In addition the crack growth rate increases with increased applied stress.

The crack growth rate, $\frac{da}{dN}$, is obtained by taking the derivative of the above crack length, a, versus cycles ,N, curve. Values of the log $\frac{da}{dN}$ can then be plotted versus log ΔK for a given crack length, using the equation:

$$\Delta K = K_{\max} - K_{\min} = f(g)\Delta\sigma\sqrt{\pi a} \qquad (2.39)$$

Plot of log $\frac{da}{dN}$ versus log ΔK, is shown in Figure 2.14.This curve may be divided into three regions. At low stress intensities, Region I, cracking behavior is associated with ΔK_{th} threshold effects. In the mid-region, Region II, the curve is essentially linear, many structures operate in this region. Finally, in region III, at high ΔK values, crack growth rates are extremely high and little fatigue life is involved.

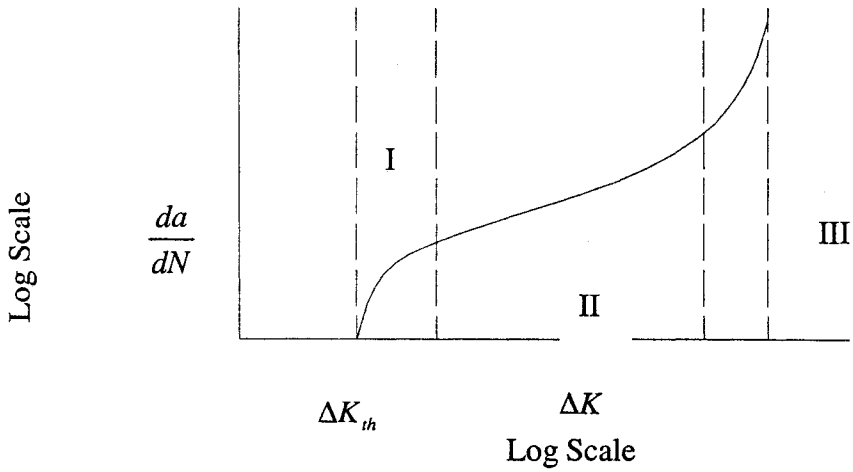

Figure 2.14 Three regions of crack growth rate curve (Bannantine, 1990)

Region II

The LEFM technique tries to estimate crack growth behavior within region II. In this region the slope of log $\frac{da}{dN}$ versus log ΔK curve is approximately linear. Many curve fittings in this region have been suggested; Paris equation is the most widely accepted and it is given in the following equation:

$$\frac{da}{dN} = C(\Delta K)^m \qquad (2.40)$$

where C and m are material constants and ΔK is the stress intensity range $K_{max} - K_{min}$. The crack growth life, in terms of cycles to failure, may be calculated using the equation (2.29). If a_i is the initial crack length and a_f is the final critical crack length, then:

$$N_f = \int_{a_i}^{a_f} \frac{da}{C(\Delta K)^m} \qquad (2.41)$$

Region I

Region I of the sigmoidal crack growth rate curve is associated with threshold effects. Below the value of the threshold stress intensity factor, ΔK_{th}, the fatigue crack growth does not occur or occurs at a rate too slow to be measured. The fatigue threshold decreases with increasing the stress ratio. This threshold also depends on frequency of loading and environment.

Region III

In region III, rapid, unstable crack growth occurs. In many practical engineering situations his region may be ignored because it does not significantly affect the total crack propagation life. The point of transition from region II to region III behavior is dependent on the yield strength of the material, stress intensity factor, and stress ratio.

2.3. Multiaxial fatigue:

In many engineering problems, cyclic loadings that cause complex state of stress and strain are common. Complex state of stress in which the three principal stresses are non proportional or whose directions change during a loading cycle, is usually occurs at geometric discontinuities such as notches or joint connections. Failure under these conditions, termed multiaxial fatigue, is an important design consideration for a reliable operation of components.

Multixial states of stress are very common, and difficult to avoid, for example in a tensile bar components such as crank shaft, rear axels, and bridges are often subjected to combined bending and torsion and both normal and shear stresses can exist. The state of stress in notches is usually multiaxial.

Until 1970s, a limited amount of multiaxial fatigue research had been conducted. This was due, in part, to the difficulties involved in obtaining experimental multiaxial fatigue data. Recently, increased work has been done in this area both experimentally and

theoretically. However, this area continues to be a topic of active research, with theories continuing to be developed and modified. Developments of multiaxial fatigue theories require understanding of two areas:

1- The multiaxial stress/strain state at a point and how this stress/strain changes with respect to time.
2- The damage behavior of the material under multiaxial fatigue loading.

Stress State

The development of multiaxial fatigue analysis methods requires characterizing the stress and strain states in the component being analyzed; this may be sometimes a complex task requiring the use of strain gages to determine the strain experimentally or use of the finite elements methods for the analysis. However, a good understanding is necessary for identifying the parameters that correlate the stress/strain state to the damage developed in the material.

In multiaxial fatigue, the directions of the principle stresses at critical location, often change during the loading cycle and are therefore a function of time. In addition and for some loading cases the three principle stresses can be non proportional. These difficulties complicate the multiaxial fatigue analysis in comparison to the uniaxial loading condition.

Cracking observations

Primary consideration in the development of fatigue analysis methods is the need to reconcile the analytical approaches with the physical observations.

Fatigue crack growth occurs in two distinct phases, which termed as stage I and stage II growth (Bannantine, 1990). Stage I growth includes nucleation and early growth and is spent on shear planes. Stage II is crack growth occurring on planes that are oriented perpendicular to the maximum principle stress range. In fracture mechanics terms, this is often labeled mode I growth.

In nucleation and early growth (stage I) both the shear stresses and strains and the normal stresses and strains on the crack face are the dominant factors (Bannantine, 1990). Normal stresses and strains tend to reduce the amount of stage I growth. In general, the

portion of life spent on stage I or stage II planes has been shown to depend on the material type, loading mode, and strain amplitude. It is interesting to note that even in out-of-phase loading, stage I fatigue crack initiate on the plane of maximum shear strain range which experiences the greatest amplitude of normal strain.

2.4 Multiaxial Fatigue Theories

Early development of multiaxial fatigue theories were based on extensions of static yield theories to fatigue under combined stresses. In 1955, these developments is further extended by Sines, who developed a multiaxial theory that uses the octahedral stress (von Mises) static yield theory combined with hydrostatic stress. In the early 1970s, critical plane multiaxial fatigue theories were developed. These are theories based on the premise that failure occurs due to damage developed on a critical plane, and are based on cracking observations. These approaches are reviewed below and the advantages and disadvantages of each are discussed.

Three main static yield theories are listed in the following section. They are formulated in terms of stresses and strains. Stress-based theories are usually limited to the high cycle fatigue (HCF) regime. In low cycle fatigue (LCF), the stresses and strains are no longer linearly related and the strain-based approach is preferred for this regime.

2.4.1 Equivalent stress/strain theories

Equivalent stress approaches are extensions of static yield criteria to fatigue. The most commonly used equivalent approaches for fatigue are the maximum principal stress theory, the maximum shear stress theory, and the octahedral shear stress theory (von Mises theory).

Maximum principle stress

$$\sigma_1 = \sigma_e \tag{2.42}$$

Maximum principle strain

$$\varepsilon_1 = \varepsilon_e \tag{2.43}$$

Maximum shear stress (Tresca Criteria)

$$\left|\frac{\sigma_1 - \sigma_3}{2}\right| = \tau_e \tag{2.44}$$

Maximum shear strain (Tresca Criteria)

$$\left|\frac{\varepsilon_1-\varepsilon_3}{2}\right|=\frac{\gamma_e}{2}=\frac{(1+\nu)\varepsilon_e}{2} \tag{2.45}$$

Distortion energy (octahedral or von Mises Criteria)

$$\frac{1}{\sqrt{2}}\left[(\sigma_1-\sigma_2)^2+(\sigma_2-\sigma_3)^2+(\sigma_3-\sigma_1)^2\right]^{\frac{1}{2}}=\sigma_e \tag{2.46a}$$

$$\frac{1}{\sqrt{2}}\left[(\sigma_x-\sigma_y)^2+(\sigma_y-\sigma_x)^2+(\sigma_z-\sigma_x)^2+6\left(\tau^2{}_{xy}+\tau^2{}_{xz}+\tau^2{}_{yz}\right)\right]^{\frac{1}{2}}=\sigma_e \tag{2.46b}$$

$$\beta\left[(\varepsilon_1-\varepsilon_2)^2+(\varepsilon_2-\varepsilon_3)^2+(\varepsilon_3-\varepsilon_1)^2\right]^{\frac{1}{2}}=\varepsilon_e \tag{2.47a}$$

$$\beta\left\{(\varepsilon_x-\varepsilon_y)^2+(\varepsilon_y-\varepsilon_z)^2(\varepsilon_x-\varepsilon_z)^2+6\left[\left(\frac{\gamma_{xy}}{2}\right)^2+\left(\frac{\gamma_{xz}}{2}\right)^2+\left(\frac{\gamma_{yz}}{2}\right)^2\right]\right\}^{\frac{1}{2}}=\varepsilon_e \tag{2.47b}$$

$$\beta=\frac{1}{(1+\nu)\sqrt{2}}$$

for an arbitrary ν

for $\nu=\frac{1}{3}$: $\beta=\frac{3}{4\sqrt{2}}$

for $\nu=\frac{1}{2}$: $\beta=\frac{\sqrt{2}}{3}$

$\varepsilon_e,\sigma_e,\gamma,\tau$ are the effective strain, effective stress, shear strain and shear stress, respectively (Fatemi and Socie, 1988).

If the equivalent stress/strain theories [equations 2.42 through 2.47] are used to obtain the torsional strain-life curve in terms of uniaxial fatigue properties. The expression for the strain-life curve for torsional loading is:

$$\frac{\Delta\gamma}{2}=\frac{\tau_f'}{G}(2N_f)^{b_o}+\gamma_f'(2N_f)^{c_o} \tag{2.48}$$

where:

G: is shear modulus

τ_f' : is the shear fatigue strength

γ_f' : is the shear fatigue ductility coefficient

b_o and c_o are shear fatigue strength and shear fatigue ductility exponents, respectively.

The three equivalent stress/strain theories will be used to express the above equation in terms of uniaxial fatigue properties. Using the von Mises theory eq. 2.45 and 2.46 and assuming that parameters b and c remain constant, can be expressed as:

$$\frac{\Delta\gamma}{2} = \frac{\sigma_f'}{\sqrt{3}G}(2N_f)^b + \sqrt{3}\varepsilon_f'(2N_f)^c \qquad (2.49)$$

Using the maximum principle stress/strain theory [eq 2.46 and 2.47] for stress:

In tension: $\sigma_e = \sigma_1$

In torsion: $\sigma_e = \sigma_1 = \tau$

And for strain:

In tension: $\varepsilon_e = \varepsilon_1$

In torsion: $\varepsilon_e = \varepsilon_1 = \frac{\gamma}{2}$

Thus equation (2.48) can be rewritten in terms of uniaxial properties using the maximum principal stress and strain criteria as

$$\frac{\Delta\gamma}{2} = \frac{\sigma_f'}{G}(2N_f)^b + 2\varepsilon_f'(2N_f)^c \qquad (2.50)$$

Using the maximum shear stress or strain (Tresca) criteria [Equation (2.43) and (2.44)] the stress state in tension and torsion are given as $\tau_e = \frac{\sigma_1}{2}$ and $\tau_e = \tau$ respectively.

and $\tau_f' = \frac{\sigma_f'}{2}$

for the strain state in tension

$$\frac{\gamma}{2}=\frac{\varepsilon_1-\varepsilon_3}{2}=\frac{\varepsilon_1-(-\nu\varepsilon_1)}{2}=\frac{(1+\nu)\varepsilon_1}{2}$$

and in torsion

$$\frac{\gamma_e}{2}=\frac{\varepsilon_1-\varepsilon_3}{2}=\frac{\gamma}{2}$$

Therefore,

$$\frac{(1+\nu)}{2}\varepsilon_f'=\frac{\gamma_f'}{2}$$
$$\gamma_f'=(1+\nu)\varepsilon_f'$$

Thus equation 2.48 can be rewritten in terms of uniaxial properties using the maximum shear (Tresca) criteria as

$$\frac{\Delta\gamma}{2}=\frac{\sigma_f'}{2G}(2N_f)^{b_o}+(1+\nu)\varepsilon_f'(2N_f)^{c_o} \qquad (2.51)$$

Substituting in the plastic Poisson's ratio value, $\nu = 0.5$, yields

$$\frac{\Delta\gamma}{2}=\frac{\sigma_f'}{2G}(2N_f)^{b}+(1.5)\varepsilon_f'(2N_f)^{c} \qquad (2.52)$$

In the development above of the equivalent stress/strain theories, general comments can be derived, they are:

1- Of all the equivalent stress/strain approaches the von Mises (distortion energy, octahedral) criteria [equation 2.46 and 2.47] have been shown to have the highest degree of acceptance among researchers, with both conservative and non conservative results reported (Bannantine, 1990).

2- In the Tresca criteria, the value of σ_2 or ε_2 does not affect the equivalent stress or strain value, while the von Mises effective stress or strain varies with σ_2 or ε_2.

3- A discrepancy (often approximately a factor of 2 in strain) generally results when using these equivalent stress/strain criteria to correlate results of axial and torsional tests. For the same plastic strain, torsional loading results in longer lives.

4- Both the Tresca (maximum shear) [equation 2.44 and 2.45] and the von Mises (octahedral or distortion energy) [equation 2.46 and 2.47] criteria do not vary with the application of a hydrostatic stress or strain. However, fatigue failure has been shown to be sensitive to the application of hydrostatic stress (pressure) or strain.

5- Effective stress/strain methods do not account for the fact that fatigue failure is observed to occur on especially oriented planes relative to the principal stress /strain axes. These approaches "average" the stress/strain to obtain a failure criterion with no regard to the direction of crack growth.

6- Equivalent strain approaches do not account for mean stresses. An attempt to rationalize this is based on the argument that at high loads (LCF regime), where equivalent strain approaches are used; mean stresses tend to relax out. In the HCF regime), it has been suggested that mean stresses may be accounted for in the equivalent stress approach by constructing an effective Haigh (modified Goodman) diagram.

7- Significant complications arise in this approach when trying to deal with out-of-phase loading.

Despite of some fundamental problems, equivalent stress/strain approaches are often used. They are easy to implement and may be useful in obtaining a first approximation.

2.4.2 Sines' Model and Similar Approaches

In 1955, Sines (Sines, 1955) reviewed the results of experiments on the effect of different combinations of tensile, compressive, and torsional static (mean) and alternating stresses on fatigue life. He reported that alternation of shear stresses seemed to cause fatigue failure. Because of this, the influence of mean static stresses on the planes of maximum shear alternation was studied.

Sines observed that a torsional mean stress did not affect the fatigue life of a specimen subjected to alternating torsion or bending stresses, and the tensile mean stress reduced the fatigue life of a component subjected to cyclic torsional loading. From the results it is found that the tensile mean stress decreases fatigue life and the compressive mean stress increases fatigue life of a specimen subjected to cyclic uniaxial loading, based on that the following equation has been developed:

$$\frac{1}{3}\left[(\sigma_{a1}-\sigma_{a2})^2+(\sigma_{a2}-\sigma_{a3})^2+(\sigma_{a1}-\sigma_{a3})^2\right]^{\frac{1}{2}}+\alpha(S_x+S_y+S_z)\le A \qquad (2.53)$$

where

the stresses $\sigma_{a1},\sigma_{a2},\sigma_{a3}$ are the amplitude of alternating principal stresses.

S_x,S_y,S_z is orthogonal (any coordinate system) static (mean) stresses.

A is a material constant proportional to reversed fatigue strength.

α is a material constant which gives variation of the permissible range of stress with static stress.

A *and* α are material properties. The first term on the left hand side of equation 2.53 above is the octahedral shear stress, τ_{oct}. Equation 2.53 may be represented graphically by concentric ellipses. The size of the ellipses depends on the sum of the static normal stresses. The larger the sum, representing larger tensile static stresses, the smaller is the ellipse. Any combination of cyclic stresses within the area of the ellipse is safe. A disadvantage of this approach is that it is limited to applications where the principal axes of the alternating stress components are fixed in the body.

2.4.3 Fatigue life prediction by Hoffman and Seeger method

Hoffman and Seeger (Hoffman and Seeger, 1985) proposed two approximations for the proportional loading. In their formulation, the authors use Neuber's rule:

$$\frac{\left(K_1^{eq} S\right)^2}{E} = \sigma^{eq}\varepsilon^{eq} \tag{2.54}$$

Here, the nominal stress S can be defined in any convenient way such that it relates the stress concentration factor to the principal stress.

$${}^{e}\sigma_1 = K_1 s \tag{2.55}$$

The elastic equivalent stress, ${}^{e}\sigma^{eq}$, is computed from the principal strain, the von Mises yield function and the knowledge of the elastic stress ratios.

$${}^{e}\sigma^{eq} = \frac{{}^{e}\sigma_1}{\sqrt{2}}\sqrt{\left(1-\frac{{}^{e}\sigma_2}{{}^{e}\sigma_1}\right)^2+\left(1-\frac{{}^{e}\sigma_3}{{}^{e}\sigma_1}\right)^2+\left(\frac{{}^{e}\sigma_2}{{}^{e}\sigma_1}-\frac{{}^{e}\sigma_3}{{}^{e}\sigma_1}\right)^2} \tag{2.56}$$

an equivalent stress concentration factor, k_t^{eq}, is obtained as:

$$K_t^{eq} = \frac{{}^{e}\sigma^{eq}}{S} \tag{2.57}$$

$$K_t^{eq} = \frac{K_t}{\sqrt{2}}\sqrt{\left(1-\frac{{}^{e}\sigma_2}{{}^{e}\sigma_1}\right)^2+\left(1-\frac{{}^{e}\sigma_3}{{}^{e}\sigma_1}\right)^2+\left(\frac{{}^{e}\sigma_2}{{}^{e}\sigma_1}-\frac{{}^{e}\sigma_3}{{}^{e}\sigma_1}\right)^2} \tag{2.58}$$

The principal stresses can be related to the equivalent stress with the von Mises yield criterion.

$$\sigma^{eq} = \sqrt{\frac{1}{2}\left[(\sigma_1-\sigma_2)^2+\sigma_1^2+\sigma_2^2\right]} \tag{2.59}$$

To obtain the principal stresses and strains, Hoffmann and Seeger suggested the following assumptions:

- The principal stresses and strains are fixed in orientation.
- The ratio of the in-plane principal strains is constant

Once the principal stress and strain are found for the critical locations, the uniaxial strain-life equation can be used to predict fatigue life.

$$\varepsilon_1 = \frac{\sigma_f'}{2}(2N_f)^b + \varepsilon_f'(2N_f)^c \qquad (2.60)$$

Hoffman and Seeger approximation is found quite well in predicting fatigue life cycles for multiaxial proportional loadings (Hoffman and Seeger, 1985). Fatigue life prediction for non proportional loadings using Hoffmann and Seeger method is not suitable as during this type of loading all the simplifying assumptions by Hoffmann and Seeger are violated. In today's applications, it is a general practice to use critical plane approach both for multiaxial proportional and non proportional loading.

2.4.4 Critical plane models

Fatigue crack initiate on planes of maximum shear. The normal stress and strain on these planes have been shown to have an influence on fatigue crack behavior and consequently fatigue life. Critical plane approaches have evolved from experimental observations of the nucleatiation and growth of cracks during loading. Depending on the material, stress-state, environment, and strain amplitude, fatigue life usually will be dominated by crack growth along either shear planes or tensile planes. In this approach, stresses and strains during cyclic loading are determined for various orientations (planes) in the material and the stresses and strains acting on the most severely loaded plane are used to predict fatigue failure (Fatemi and Socie, 1988).

In 1973, Brown and Miller developed a multiaxial fatigue theory which they stated was based on a physical interpretation of the mechanisms of fatigue crack growth. This critical plane approach considered the maximum shear strain plane and the tensile or normal strain acting on it.

$$\frac{\Delta\gamma_{max}}{2} + s\Delta\varepsilon_n = C \qquad (2.61)$$

where

$\frac{\Delta\gamma_{max}}{2}$: is maximum shear strain amplitude.

$\Delta\varepsilon_n$: is the normal strain range on the $\Delta\gamma_{max}$ plane.

S : is material dependent constant that weights the importance of normal strains of different materials.

Critical plane approaches attempt to reflect the physical nature of fatigue damage in their formulation, a common model based on a physical interpretation of fatigue damage is Fatemi-Socie model(Fatemi and Socie, 1988).

Normal strain criterion

In this approach the strain amplitude normal to the critical plane is calculated (nCode International, 2001). Fatigue life is then calculated with the following equation

$$\frac{\Delta\varepsilon_n}{2} = \frac{\sigma_f'}{E}(2N_f)^b + \varepsilon_f'(2N_f)^c \qquad (2.62)$$

where $\frac{\Delta\varepsilon_n}{2}$ is the strain amplitude normal to the critical plane.

Shear strain criterion

In this model shear strain amplitude is calculated along the critical plane (nCode International, 2001). Fatigue life is then calculated with the following equation

$$\frac{\Delta\gamma}{2} = \frac{(1+\nu_e)\sigma_f'}{E}(2N_f)^b + (1+\nu_p)\varepsilon_f'(2N_f)^c \qquad (2.63)$$

Fatemi and Socie model (Fatemi and Socie, 1988)

Critical plane approaches attempt to reflect the physical nature of fatigue damage mechanisms in their formulation. In this model the parameters governing fatigue damage are the maximum shear strain amplitude, $\Delta\gamma_{max}/2$, and the maximum normal stress $\sigma_{n,max}$, acting on the maximum shear strain amplitude plane the physical basis of this model is shown in Figure 2.17 (Fatemi and Socie, 1988).

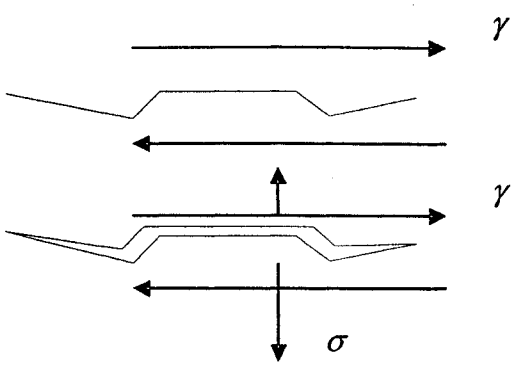

Figure 2.15 Physical basis of the Fatemi and Socie model (Fatemi and Socie, 1988)

Stresses and strains normal to crack plane may have a major effect on the behavior, accelerating the growth if they tend to open the crack. Fatemi and Socie proposed an approach to include the normal strain effect. The proposed model is given by:

$$\frac{\Delta\gamma}{2}\left(1+n\frac{\sigma_{n,\max}}{\sigma_y}\right)=\frac{\tau_f'}{G}(2N_f)^b+\gamma_f'(2N_f)^c \qquad (2.64)$$

where

$\frac{\Delta\gamma}{2}$: is the largest amplitude of the shear strain on the critical plane.

$\sigma_{n,\max}$: is the maximum tensile normal stress acting on the maximum shear strain amplitude plane.

τ_f', b, γ_f', c : are constants found from completely reversed tests in pure shear.

n is an empirical constant, (usually range between 0.6-1.0, depending on the material). (Fatemi and Socie, 1988).

Smith – Watson and Topper (SWT) model

Fatemi-Socie critical plane model has been developed primarily for materials for which the dominant failure mechanism is shear crack nucleation and growth. An alternative damage model is needed for materials that fail predominantly by crack growth on planes of maximum tensile stress or strain. This model includes both the cyclic strain range and the maximum stress. SWT parameter can be used in the analysis of both proportionally and non-proportional loadings applied for materials that fail primarily due to mode I tensile cracking. This approach for multiaxial loading is based on the strain amplitude normal to the critical plane, $\frac{\Delta\varepsilon_n}{2}$ and the maximum normal stress on the critical plane, $\sigma_{n,\max}$.

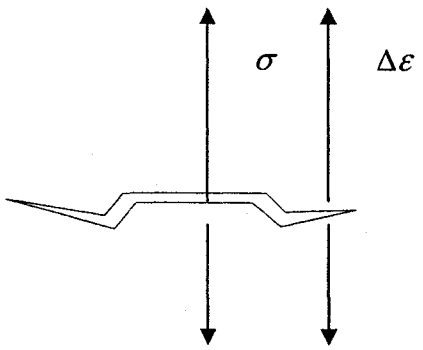

Figure 2.16 Tensile crack growth in SWT model (Smith, 1970)

2.4.5 Vibration fatigue theory

Design of structures can be verified using either tests or analysis. By testing we usually mean the experimental measurement of the stresses or the strains in laboratory or during test track prototype. In automotive industry testing might involve the measurement of noise or vibration rather than stresses, strains and acceleration. By analysis we usually mean the computation of structural response using technique such as ***Finite Element Analysis (FEA).***

In general, there are two alternatives (or domains) which can be used for such testing or analysis. Ideally the analysis is carried out in the ***time domain***, where all inputs loadings and output responses are specified as time dependent. For example, the stress history induced in a critical component of a car chassis while being driven over a road surface might be experimentally measured or estimated at the design stage using appropriate analysis programs and expressed in time domain.

In practical applications, a frequency domain analysis is preferred. In this case all loadings and output stress responses are represented in the frequency domain. ***A Power Spectral Density Function (PSDF or PSD)*** noted here as $S_j(\omega)$ and given by equation 2.66 below, is the most common way of representing the loadings or responses in the frequency domain. The transformation between time domain, i.e., the time history of the loading, and the frequency domain, i.e., PSD is conducted using Fourier transformation and given by an alternative way to specify the time signal. It is obtained by utilizing the ***Fast Fourier Transform (FFT).***

$$S_i(\omega) = \lim_{T\to\infty} \frac{2}{T} \left| \int_0^T e^{-i\omega t} u_i(t) dt \right|^2 \qquad (2.66)$$

Transforming from frequency domain back to the time domain can be derived using the ***Inverse Fourier Transform (IFT)*** see Figure 2.19.

PSD Characteristics

The PSD of a signal represents the mean square amplitude of a random signal and it gives a statistical representation of stationary random process in the frequency domain. The area beneath the PSD represents the mean square amplitude of the random process (MSc.Fatigue manual, 1999).

Mean square (f) = $\frac{1}{2}(amplitude)^2$

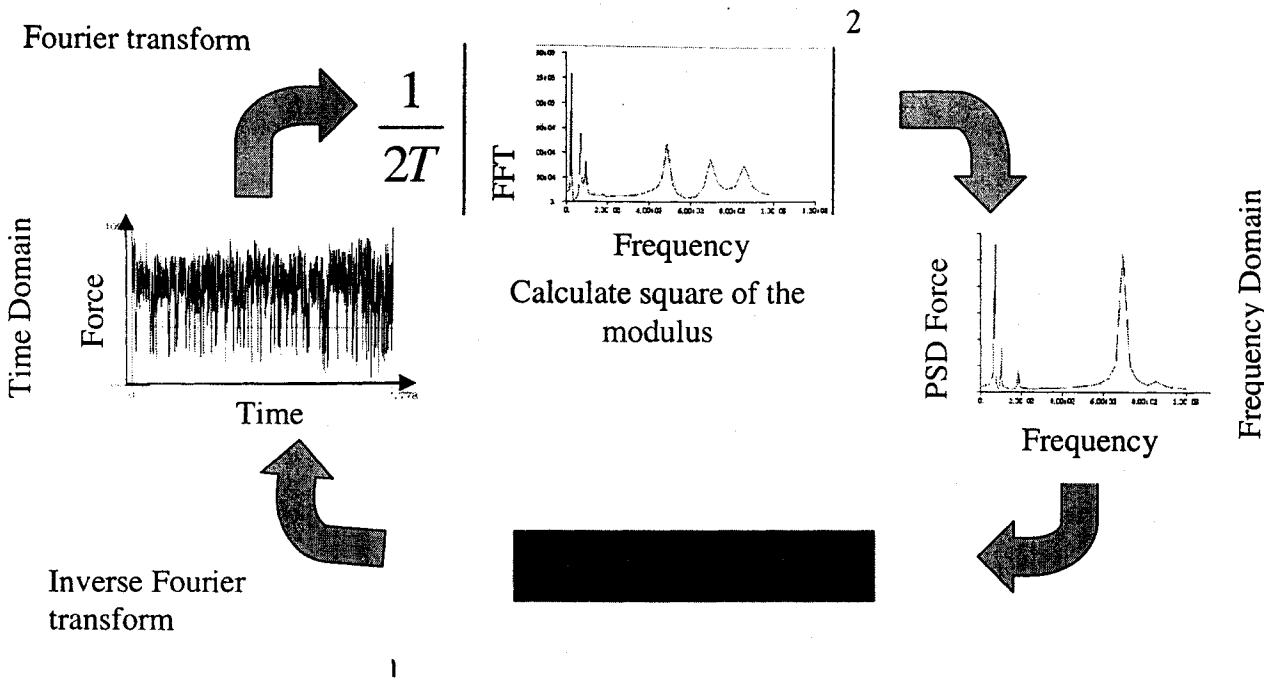

Figure 2.17 Time-Frequency domain transformations (MSC.Fatigue manual, 1999)

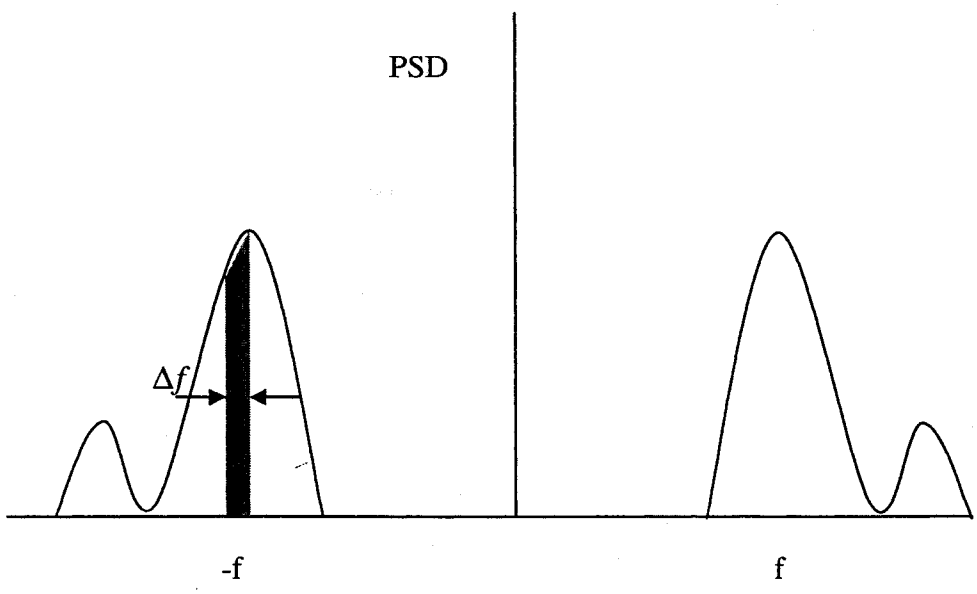

Figure 2.18 Double sided power spectral density (MSC.Fatigue manual, 1999)

$$\Delta f.G(f) = \frac{1}{2}\Delta f^2.|y(f)|^2 \qquad (2.67)$$

From the PSD, one can define a spectral moment of order n, m_n as:

$$m_n(S) = \int_{-\infty}^{\infty} S(f).f^n df \qquad (2.68)$$

Four important statistical parameters can be computed from these moments such as expected number of zeros and peaks per second. From these the irregularity factor, γ, can be computed, as described here, an give an indication of the spread of frequencies present in the signal:

Standard deviation: $\sigma = \sqrt{m_o}$

Expected numbers of zero crossings: $E_o = \sqrt{\frac{m_2}{m_o}}$

Expected numbers of peaks: $E_p = \sqrt{\frac{m_4}{m_2}}$

Irregularity factor: $\gamma = \frac{E_o}{E_p}$

These parameters are important when considering the fatigue assessment. The distinction between narrow and broad banded processes becomes much more apparent from the PSD plots than the time histories.

Vibration fatigue model

Vibration fatigue model in MSC.Fatigue software is based on total life approach and accepts multi-location input files from finite element results. These results can be either a combination of transfer functions (TF) from a frequency response analysis with corresponding loading input PSDs or the output response PSDs from a random vibration analysis.

For random signal which change its amplitudes and characteristics with time an empirical approach is used to calculate the damage caused by stress signals and FEFAT module. is used for the fatigue assessment (MSC.Fatigue manual, 1999):

In FEFAT module the S-N curve equation is expressed as:

$$N^{-b1}.S = SRI1 \tag{2.69}$$

where

$$b = -\frac{1}{b1}$$

$$K = SRI1^{-\frac{1}{b1}}$$

$$b1 = -\frac{1}{b}$$

$$SRI1 = K^{-b}$$

b: is fatigue strength exponent.

b1: is first fatigue strength exponent.

SRI1: is the stress range intercept.

The percentage of damage is calculated using the probability density function (Figure 2.21):

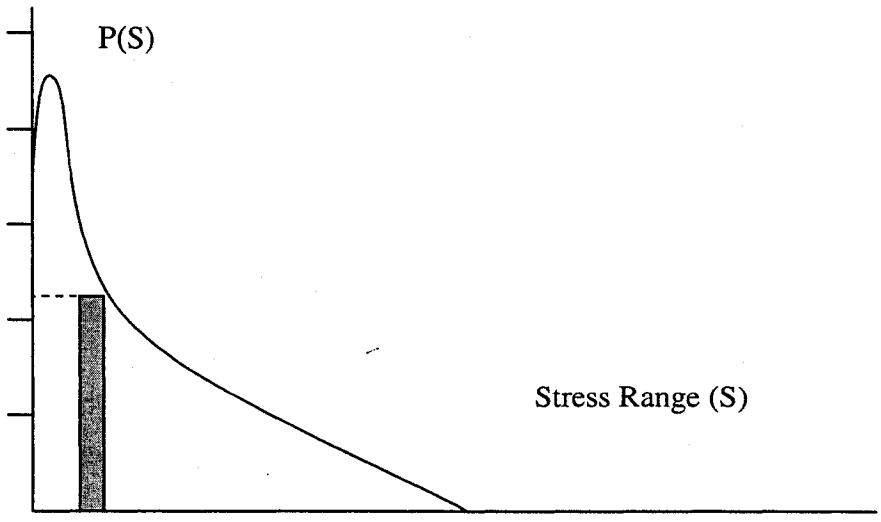

Figure 2.19 Probability density function P(S) (MSC.Fatigue manual, 1999)

The damage is calculated using Palmgren-Miner rule:

$$D = \sum_i \frac{n_i}{N(S_i)} \tag{2.70}$$

n_i: is the actual counted number of cycles

$N(S_i)$: is the number of cycles associated to the stress level(from S-N curve)

$$n_i = \mathrm{P(S)}\ dS.S_t \tag{2.71}$$

$$N(Si) = \frac{K}{S^b} \tag{2.72}$$

S_t: is the total number of cycles in required time

$$D = \sum_i \frac{n_i}{N(S_i)} = \frac{S_t}{K} \int S^b P(S) dS \tag{2.73}$$

This relationship assumes that the damage caused by portion of a stress signal with a particular range can be calculated and accumulated to the total damage separately from that caused by other amplitudes. A ratio is calculated for each stress range, equal to the number of actual cycles at a particular stress range n divided by the allowable number of cycles to failure at that stress N (obtained from the S-N curve). Failure is assumed to occur when the sum of these ratios, for all stress ranges, equals 1.0.

The most convenient mathematical way of storing stress range histogram is in the form of a probability density function (PDF). A typical representation of this function is the diagram in figure 2.21.

Since we are concerned with the structural system analyzed in the frequency domain we require a method for extracting the PDF of rainflow ranges directly from the PSD of stress. The characteristics of the PSD which are used to obtain this information is are the nth moment of the PSD function shown in figure 2.22:

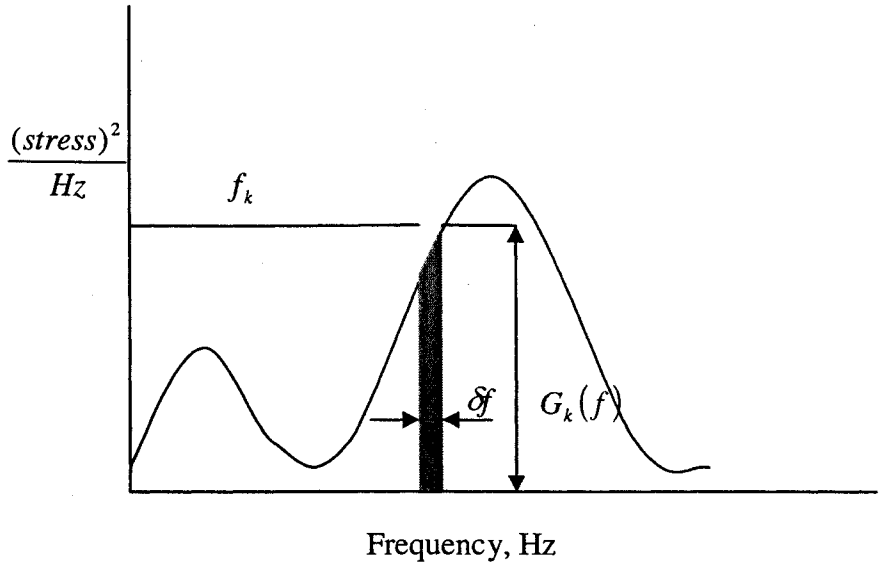

Figure 2.20 Moment from PSD (MSC.Fatigue manual, 1999)

$$M_n = \int G(f)df = \sum_{k=1}^{m} f_k^n Gk(fk)\delta f \tag{2.72}$$

$$E[0] = \left[\frac{m_2}{m_0}\right]^{\frac{1}{2}} \text{ Zero Crossing} \tag{2.73}$$

$$E[P] = \left[\frac{m_4}{m_2}\right]^{\frac{1}{2}} \text{ Peaks} \tag{2.74}$$

$$\gamma = \frac{E[0]}{E[P]} = \left[\frac{m_2{}^2}{m_0 m_4}\right]^{\frac{1}{2}} \text{ Irregularity Factor} \tag{2.75}$$

Expected damage for narrow band can be calculated from the following equation:

Total number of cycles is given by E [P].T in this formula

$$E(D) = E[P]\frac{T}{K}\int S^b P(S)ds \tag{2.76}$$

where S= stress range

$$E[D] = E[P]\frac{T}{K}\int S^{b}\left[\frac{S}{4m_0}e\frac{-S^2}{8m_0}\right]ds \qquad (2.77)$$

Many analysis methods are implemented in MSC.Fatigue software for the vibration module they are mostly suitable for offshore industry, two methods are more appropriate and can be used in automotive industry:

a) **Dirlik method**, Dirlik (Dirlik, 1982) has produced an empirical closed form expression for the PDF of rainflow ranges (eq.2.78), which was obtained using Monte Carlo technique. This method is most suitable analysis method for almost all the cases especially when the signal is wide band and tends to be more conservative when a narrow band signal is used (MSC.Fatigue manual, 1999)

$$P(S) = \frac{\frac{D_1}{Q}e^{\frac{-z}{Q}} + \frac{D_2}{R^2}e^{\frac{-z^2}{2R^2}} + D_3 Z e^{\frac{-z^2}{2}}}{2(m_0)^{1/2}} \qquad (2.78)$$

where:

$$z = \frac{s}{2(m_0)^{1/2}} x_m = \frac{m_1}{m_0}\left[\frac{m_2}{m_4}\right]^{1/2}$$

$$D_1 = \frac{2(X_m - \gamma^2)}{1+\gamma^2}$$

$$D_2 = \frac{\left(1-\gamma-D_1+D_1^2\right)}{1-R}$$

$$D_3 = 1 - D_1 - D_2 Q = \frac{1.25(\gamma - D_3(D_2 R))}{D_1} R = \frac{\gamma - X_m - D_1^2}{1-\gamma-D+D_1^2}$$

b) **Tunna method,** Tunna (Tunna, 1986) predict the fatigue life for steel used in British railways subjected to random load signal. It is used especially when the power in the signal is concentrated at one frequency; this is called narrow-band process.

For a normal, narrow-band random process it is possible to express the probability density function of peaks in the signal by:

$$P(S) = \frac{S}{4\gamma m_0} e^{\frac{-\delta^2}{8\gamma m_0}} \tag{2.79}$$

CHAPTER THREE
FINITE ELEMENT UPDATE USING MEASURED DATA

3.1 Introduction:

Adopting rigorous testing procedures and attention to details can confidently assume that measured data, whether in the time, modal or frequency domain provide true representation of the dynamic behavior of a structure. It is on this basis that we are able to use these data for engineering applications such as product development and design.

In today engineering applications finite element analysis is considered as one of the most powerful tools that is used for design verification and analysis of structures and components. In automotive industry using finite element analysis is essential in design stage to verify the dynamic behavior of the structures and calculate the stress, strains, acceleration, etc in the critical locations and also it save time and money. One of the most important applications in studying the dynamic behavior of structures and components is modal analysis which is conducted in conjunction with finite element technique.

3.2 Objective

Modeling structures and components using finite elements is usually accompanied by approximation; that may leads to some differences between the results obtained from finite element analysis and from those obtained from physical tests.

The analytical models require verification before using them in analysis. The aim of this is to provide a measure of confidence in the dynamic behavior of the structure. The objective of this chapter is to discuss the existing techniques to verify and update the finite element models using test data as a reference.

3.3 Verification of Finite Element model

The work in this field has different levels of ambition (Maia, Silva, 1997); they summarized as:

1) A model which reproduces exactly all the measured modal properties (natural frequencies, mode shape amplitudes for each mode);

2) A model which reproduces all of the measured FRF properties (thereby correctly representing information from the unmeasured modes, as well as those identified explicitly by the modal analysis;

3) A model which is capable of reproducing all of the measured FRFs and /or modal properties (i.e. at points which were not included in the modal test);

4) A model which, in addition to the above requirements, exhibit the correct connectivity;

5) A model which posses all of the correct mass, stiffness and damping elements and which is capable of reproducing all of the dynamic properties, including those not measured.

3.3.1 Factors affecting Finite Element models

It can be seen that each of these criteria discussed above becomes more difficult and elusive to achieve; the problematic area that are associated with the finite element models are summarized by the following:

(i) Approximation of boundary conditions ;
(ii) Discretisation of distributed parameter system;
(iii) Estimation of the physical properties of structural materials;

(iv) Approximation/omission of damping representation, or assumption of proportional damping;

(v) Inadequate modeling of joints;

(vi) Condensation of FE models to make them compatible with the test degrees of freedom.

Most of the time there are some differences arising between the measured results and modal analysis results, therefore in modal updating procedure it is appropriate to mention some potential problem (Maia, Silva, 1997):

(i) The number of measured degrees of freedom is limited and may be different from the analytical model;

(ii) Difficulty of measuring rotational degrees of freedom;

(iii) Limited number of identified mode shapes;

(iv) Complex mode shapes obtained;

(v) Unmodeled errors in measurement (noise, nonlinearity etc.);

(vi) Poor modal analysis of the experimental results ; and

(vii) Some modes not excited or if excited, then not identified;

Conversely, overanalysis leads to false modes occurring.

Although it is important to consider the practical limitations of experimental data, the frequently ignored as the ultimate application of the reconciliation process is often only to replicate the measured or unmeasured characteristics of the experimental model. Accordingly, such procedures to be referred to as correlation, validation or updating methods by assuming that the measured data are correct, which is justifiable given the primary goals of the techniques, but in practice may not be entirely accurate.

However, given that this is the normal application of reconciliation techniques, one still has to judge the success of the updated model relative to its original state and the experimental model.

3.4 Comparison, location and correlation methods:

Reconciliation techniques of the finite element model may be divided into three categories:

(i) Comparison methods: These are used for preliminary assessment of the compatibility of the FE and experimental models. They are limited to give an indication of which modes correspond to each other.

(ii) Location methods: These methods aim to provide information as to where the differences exist between the experimental and the analytical model without describing if they are caused by mass or stiffness irregularities;

(iii) Correlation methods: These methods are the most sophisticated of the three approaches, they attempt to apply localized perturbations to the mass and/or stiffness properties or to the elementary parameters of the FE model, the goal is to achieve a modal and a spatial model which accurately represent the physical characteristics of the real structure.

The logical approach of modal updating which is usually adopted is to apply, in sequence, the comparison, the location and the correlation methods. This is based on the rationale that in order to use location techniques a prior assessment has to be made as to whether they are comparable. Similarly, several correlation methods rely on accurate location of the regions of discrepancy between the FE and experimental models; others, however, incorporate their own idealized locations in order to achieve accurate model updating.

3.5 Incompatibility between measured and FE data:

Inevitably, there will be an incompatibility in the size of the FE model and the the physical part (structure) to be compared to. This difference manifests in two forms, firstly as insufficiency in the number of modes and secondly as a lack of measured DOFs. The first of these difficulties arises from the limited bandwidth of data acquisition and the fact that increased modal density at higher frequencies makes modal extraction problematic beyond moderately low order modes.

The importance of the physical modal test is to acquire more data if the finite element modal analysis reveals quirks or limitations is sufficiently rare not to be relied upon. There is a little that can be done to resolve this after the completion of the test; we simply have to make the best of the available data by meticulous modal identification. It is inevitable that the experimental test will omit some DOFs. However, it is important to ensure that experimental effort is used effectively and the measured data give full modal description (including local modes) across the measured frequency range. Lim (Lim, 1993) suggests an (effective impedance distribution vector) method which defines optimum actuator and response locations by selecting DOFs on the basis of linear modal independence from the other coordinates. Despite this approach, coordinate incompleteness will exist but can be mitigated by adopting the following strategies, either singly or in combination:

(i) The large model could have the non–measured (slave) DOFs condensed out in such a way as not to perturb either the modal or the spatial properties of the system. In practice, this is difficult to achieve as the updating methods generally allow retention of kinetic or potential energy, or compromise both, but system connectivity is unavoidably perturbed;

(ii) The smaller of the two models (the experimental) could be expanded to match its large FE counterpart.

The goal of the updating is to provide a "correct" FE model. It is obviously advantageous that the final model remains in this coordinate system. Although a complete coordinate description of a reduced set of modes can be obtained from the FE model by using Lanczos (Lanczos, 1950) and subspace iteration techniques, there will be always some DOFs that will be unmeasurable (Maia, Silva, 1997).

3.5.1 Finite Element model reduction:

When FE model reduction is unavoidable, this may cause that the spatial information will either be lost or dispersed. These can significantly affect the location or updating method. Guyan`s technique (Maia, Silva, 1997) is the favored as it perseveres the low order modal properties. In many practical situations, such as those using the finite element method, the computational limitations often require the order of the final coupled system be reduced as much as possible. This is achieved by reducing the order (N) of each subsystem model, or in other words, by confining our interest only to a restricted set of coordinates on each subsystem, $n < N$, and/or to only some of the modes ($m < N$).

Where N is the complete DOFs of the system (complete coordinate or all the modes), n is the DOFs of interest or in the subsystem, m some of the modes in the model.

These considerations lead to the formulation of condensed, reduced or incomplete models. The number of DOFs to be retained in the dynamic analysis (at least the DOFs involved in the connection with other components) is specified by the user. In the case of spatial models a transformation matrix relating the remaining DOFs (called secondary or slave coordinates) to those retained (primary or master coordinates) is used to reduce the order of the subsystem. The reduction process is often performed upon a transformation which neglects inertia or static contribution for the eliminated DOFs, and is then used to derive the (n * n) spatial matrices of the condensed system, [M] and [K].

The equilibrium equation of the system after separation of the primary and secondary degrees of freedom (Urgueiva, Lieven, Ewin, 1990) is written as:

$$\begin{bmatrix} [M_{ss}] & [M_{sp}] \\ [M_{ps}] & [M_{pp}] \end{bmatrix} \begin{Bmatrix} \{\ddot{u}_s\} \\ \{\ddot{u}_s\} \end{Bmatrix} + \begin{bmatrix} [K_{ss}] & [K_{sp}] \\ [K_{ps}] & [K_{pp}] \end{bmatrix} \begin{Bmatrix} \{u_s\} \\ \{u_p\} \end{Bmatrix} = \begin{Bmatrix} \{o_s\} \\ \{f_p\} \end{Bmatrix} \tag{3.1}$$

The size of vectors, u_s and u_p, are n_s and n_p respectively. All the coordinates can be related to the primary coordinates by using the following transformation:

$$\begin{Bmatrix} \{u_s\} \\ \{u_p\} \end{Bmatrix} = \underset{(n_p * n_p)}{\begin{bmatrix} [T] \\ [I] \end{bmatrix}}^{(n_s * n_p)} \{u_p\} \tag{3.2}$$

where the matrix [T] is given by:

$$\underset{(n_s * n_p)}{[T]} = (1-\beta)\left[-[K_{ss}]^{-1}[K_{sp}]\right] + \beta\left[-[M_{ss}]^{-1}[M_{sp}]\right] \tag{3.3}$$

β being a reduction coefficient whose limits are β= 0 for static reduction (Guyan, 1965) and β =1 for dynamic reduction.

for β = 0:

$$\underset{(n_s * n_p)}{[T]} = -[K_{ss}]^{-1}[K_{sp}] \tag{3.4}$$

The matrices describing the reduced spatial model are given as:

$$\underset{(n_p * n_p)}{[M^R]} = \underset{(n_p * N)}{\left[[T]^T \vdots [I] \right]} \underset{(N*N)}{\begin{bmatrix} [M_{ss}] \vdots [M_{sp}] \\ [M_{ps}] \vdots [M_{pp}] \end{bmatrix}} \underset{N * n_p}{\begin{bmatrix} [T] \\ [I] \end{bmatrix}} \tag{3.5}$$

$$\underset{(n_p * n_p)}{[K^R]} = \underset{(n_p * N)}{\left[[T]^T \vdots [I] \right]} \underset{(N*N)}{\begin{bmatrix} [K_{ss}] \vdots [K_{sp}] \\ [K_{ps}] \vdots [K_{pp}] \end{bmatrix}} \underset{N * n_p}{\begin{bmatrix} [T] \\ [I] \end{bmatrix}} \tag{3.6}$$

System equivalent reduction technique (SEREP):

This technique derived by O'Callahan (Callahan, Avitable, Riemer, 1989), it is based on mapping the complete FE eigenvectors onto the experimental slave DOFs by means of the following transformation matrix:

$$[T] = \begin{bmatrix} [\phi_{AP}] \\ [\phi_{AS}] \end{bmatrix} \left[[\phi_{Ap}]^T [\phi_{Ap}]^{-1} \right] [\phi_{AP}]^T \qquad (3.7)$$

Where $\left[[\phi_{Ap}]^T [\phi_{Ap}]^{-1} \right] [\phi_{AP}]^T$ is the moore-Penrose pseudo–inverse $[\phi]$ and the subscript A, P and S refer to the analytical model, master (primary) and slave (secondary) DOFs respectively.

The reduced system matrices are then obtained by substituting the transformation matrix into equations 3.5 and 3.6 (with the addition of the identity matrix). The main advantages of this method are:

(i) The reduced model has exactly the same frequencies and mode shapes as the full system for the selected modes of interest;

(ii) The quality of the results is insensitive to the selection of the full system DOFs that are kept in the reduced model.

3.5.2 Expansion of measured modal data:

These methods reflect the relative value of having modal completeness for modal reconciliation. In addition, Gysin (Gysin, 1990) demonstrated that the effectiveness of the expansion methods has a significant influence on the overall location and updating procedure.

Four approaches of expansion methods exist which have a varying dependency on the FE model are:

(i) Analytical eigenvector substitution. This method directly substitutes the analytical slave DOFs for the unmeasured data, without using the available measurements;

(ii) Direct data generation using the FE model and experimental data. The SEREP method (discussed above) and the modal projection techniques create a transformation matrix from the master DOFs to the complete FE coordinate system. Kidder's method (Kidder, 1973) create a spatial transformation formulated using the analytical mass and stiffness matrices and partitioning the generalized eigenvalue problem ;

(iii) Indirect data generation using the FE model. A geometric fit of the experimental data is enhanced by knowledge acquired from the FE model, this done by Waters (Waters, Lieven, 1995);

(iv) Expansion of the experimental data in isolation. These methods interpolate the experimental data by fitting a continuous function though the data by means of cubic splines (Ng'andu, Williams, 1995), surface splines (Harder, Desmarias, 1972) or polynomial fits (Williams, Green, 1990).

Kidder's method (Kidder, 1973):

This is the most commonly used expansion method, which is derived from an inverse Guyan reduction. Starting from the partitioned eigenvalue problem

$$\left[\begin{bmatrix}[K_{pp}][K_{ss}]\\ [K_{sp}][K_{ss}]\end{bmatrix} - \omega_r^2 \begin{bmatrix}[M_{pp}][M_{ps}]\\ [M_{sp}][M_{ss}]\end{bmatrix}\right]\begin{Bmatrix}\{\phi_p\}\\ \{\phi_s\}\end{Bmatrix} = \begin{Bmatrix}\{0\}\\ \{0\}\end{Bmatrix} \qquad (3.8)$$

Where the subscript, r, corresponds to the r^{th} mode. From eq.3.8, it can be shown that by substituting the measured eignvalues and mode shapes, the expanded slave DOFs are given by:

$$\{{}_x\phi_s^E\} = -[[K_{ss}] - \omega_r^2[M_{ss}]]^{-1}[[K_{sp}] - \omega_r^2[M_{sp}]]\{{}_x\phi_p\}_r \qquad (3.9)$$

This method has the advantage that by using the partitioned unreduced analytical system matrices, the physical connectivity properties are consistent with the structure of the final model. The implication of this is that the expansion depends of the basic form of the original FE model.

Expansion using analytical modes:

Although missing DOFs in the measured data can be directly replaced by substituting corresponding analytical data, this may cause discontinuities in the resulting mode shape vector. A solution for this problem is suggested by Lipkines (Lipkines, Vandeurzen, 1987); their approach uses the eignsolution from the FE model to expand the measured modes. The complete coordinates in the experimental model are generated by assuming that each mode is constructed from a linear combination of the analytical models. The full analytical model can be partitioned:

(i) by rows into n master and N-n slave DOFs; and

(ii) by columns into m chosen and N-m discarded modes.

$$\left[\underset{(N*N)}{\phi_A}\right] = \left[\begin{array}{cc} [{}_A\phi_{11}] & [{}_A\phi_{12}] \\ \underbrace{[{}_A\phi_{21}]}_{m} & \underbrace{[{}_A\phi_{22}]}_{N-m} \end{array}\right] \qquad (3.10)$$

where, ${}_A\phi$, is the analytical mode.

Then the expanded experimental modes, ${}_X\phi^E$, can be constructed from a linear combination of the chosen analytical modes by setting

$$\begin{Bmatrix} \{{}_x\phi_1^E\} \\ \{{}_x\phi_2^E\} \end{Bmatrix} = \begin{bmatrix} [{}_A\phi_n] \\ [{}_A\phi_{2i}] \end{bmatrix} \{\upsilon\} \tag{3.11}$$

$\{\upsilon\}$: is set of unknown coefficients.

And:

$$\{{}_x\phi_1^E\} = [{}_A\phi_{11}]\{\upsilon\} \tag{3.12}$$

$$\{{}_x\phi_2^E\} = [{}_A\phi_{21}]\{\upsilon\} \tag{3.13}$$

Where

$$\{\upsilon\} = [{}_A\phi_1]^x \{{}_x\phi_1\} \tag{3.14}$$

Note that:

(i) If n = m, the pseudo-inverse in (eq.3.14) becomes the standard inverse and $\{{}_x\phi_1^E\} = \{{}_x\phi_1\}$. This means that the expanded mode fits the experimental data exactly;

(ii) If n > m, a linear combination of analytical modes is found that fits the experimental data in a least squares sense. Consequently, $\{{}_x\phi_1^E\}$ is a smoothed counterpart of $\{{}_x\phi_1\}$;

(iii) if n < m, then the pseudo-inverse in the above equation is rank deficient and the solution is likely to be physically meaningless

The success of this modal projection approach is critically dependent on the selected set of analytical modes which must include a reasonable counterpart to each experimental mode.

3.6 Comparison techniques:

The first stage of any reconciliation exercise is to determine how closely the experimental and analytical models correspond. This is usually achieved in the modal domain, which presents a medium between the raw state of the experimental data time domain

information and that of the analytical model (the system matrices). Note that before the comparison of the data sets can be achieved, the issue of the coordinate incompleteness has to be resolved.

Comparison techniques are to a greater or lesser extent based on the orthogonality conditions

$$[\phi]^T [M][\phi] = [I] \qquad \text{and} \qquad [\phi]^T [K][\phi] = [\omega_r^2] \tag{3.15}$$

Where $[\phi]$ represent the mass normalized eigenvectors, either from test or analysis, and [I] and [ω] are the diagonal identity and eigenvalue matrices respectively. Note that using the experimental eigenvector matrix which inevitably will differ from the produced by the analysis will cause the condition of orthogonality to be contravened.
This will result in an off-diagonal terms away from their predicted values. Taking the mass orthogonal condition, as this is the one most commonly used; one can identify correlated modes by values of near unity and their degree of correlation by their deviation from this value.

3.7 Location techniques:

Detecting the locations of the differences between the test structure and the FE models is the most exacting task in the correlation procedure and it simply indicate the region(s) of difference. It is relatively easy task to rectify anomalies if we know where they exist. Research in the area of fault or damage detection has shown that detecting these regions present a considerable challenge.

Perhaps the most directly informative technique to identify errors is to compare mode shape animations. Frequently this trivial activity is bypassed in order to explore more glamorous approaches. It is far better to eradicate the mundane sources of difference by observation. The test errors must be identified and corrected early in the reconciliation

process when the physical modal test is not good to be relied upon in the design stage. Few algorithms have been developed specifically for this task.

3.8 Correlation techniques:

An accurate finite element model can only be achieved through the correlation process which can be categorized into different methods:

3.8.1 Least-Square updating:

Theoretical development in the frequency domain:

The general dynamic equation in the frequency domain is:

$$[[K]-\omega^2[M]+i[D]]\{\overline{X}\}=\{\overline{F}\} \tag{3.16}$$

If the modal model is to be converted into the response model which is required by the FRF coupling method then:

$$[\alpha(\omega)]^{-1}\{\overline{X}\}=\{\overline{F}\} \tag{3.17}$$

where, $\alpha(\omega)$, is the response of the system.

The orthogonal property of the modal matrix is:

$$[\phi]^T[M][\phi]=[I] \tag{3.18}$$

therefore:

$$[\phi]^T[[K]+i[D]][\phi]=[\lambda_r^2]=[\omega_r^2(1+i\eta_r)] \tag{3.19}$$

$$[\phi]^{-T}[\omega_r^2(1+i\eta_r)][\phi^{-1}]=[K]+i[D] \tag{3.20}$$

From the above equations, Maria (Maria, Silvia, 1997) derived the following equation for the response:

$$[\alpha(\omega)] = [\phi][\omega_r^2(1 + i\eta_r - \omega^2)]^{-1}[\phi]^T \quad (3.21)$$

If the structure is modeled using FE and by applying some unknown parametric changes an updated FE model can be derived that mimics the measured response of the structure. Then by applying a single input force to both the updated and original FE models gives:

$$[Zu(\omega)]\{\alpha_x(\omega)\} = \{f\} = [Z_A(\omega)]\{\alpha_A(\omega)\} \quad (3.22)$$

The above equation can be rearranged to in the form:

$$[\Delta Z(\omega)]\{\alpha_x(\omega)\} = \{I\}_j - [Z_A(\omega)]\{\alpha_x(\omega)\} \quad (3.23)$$

Where, $\Delta Z(\omega)$, is the error in the dynamic stiffness matrix, $\{I\}_j$, denotes the j^{th} column of the identity matrix and, j, indicates the location of the input force. The right hand side of the equation 3.23 referred to as the input error, is inherently ill conditioned, the remedy for that is by premultiply equation 3.23 by the analytical FRF matrix:

$$[\alpha a(\omega)][\Delta Z]\{\alpha_x(\omega)\} = \{\alpha_A(\omega)\}_j - \{\alpha_x(\omega)\} = \{\Delta\alpha(\omega)\} \quad (3.24)$$

The right hand side of equation 3.24 is the disparity between the analytical and experimental FRFs, or output error; to proceed towards a solution for the system error matrix we must assume a form for the errors. This is achieved by selecting a set of N_p design parameters to vary, $\{\dot{P}\}$, to account for the discrepancy in the response between experiment and analysis. It is convenient to non dimensionalise the updating parameter as follows:

$$\dot{P}_i = \frac{(\dot{P}_i - \dot{P}_i^\circ)}{\dot{P}_i^\circ} \quad (3.25)$$

Where, $\dot{P}$, is the parameter value for the original FE model. The nondimensionalised updating parameter or (P values) represent the fractional changes in the design variables.

The dynamic stiffness matrix for the updated FE model, [Zu], is a function of {P} and can be expressed as a Taylor expansion about the dynamic stiffness matrix for the original FE model, [Za],

$$[Zu]=[Z_A]+[\Delta Z]=[Z_A]+\sum_{i=1}^{N_p}\frac{\partial[Z]\dot{P}_i+O(\dot{P}_i^2)}{\partial\dot{P}_i} \tag{3.26}$$

$$[Z]=\sum_{i=1}^{N_p}\frac{\partial[Z]\dot{P}_i}{\partial\dot{P}_i}$$

$$[S(\omega)]\{\dot{P}\}=[\Delta\alpha(\omega)] \tag{3.27}$$

Each row of the sensitivity matrix, [S]; define the sensitivities of the response at a particular DOF to the set of $\dot{P}$-values.

Updating using modal sensitivity:

The modal and the FRF sensitivity methods are analogous approaches set in different response domains. Both methods treat the experimental model as a perturbation in design parameters about the original FE model. From estimate of the sensitivity of the dynamic response or modes of vibration to parameter variations, a combination of changes is found that accounts for the disparity between analytical and experimental values.

Theory of modal sensitivity:

This approach discusses the sensitivities of the eigenvalues and eigenvectors with respect to changes in specified design parameters.

If $(\omega_A)_r^2$ and $\{\phi_A\}$, are the eigensolution to the eigendynamic equation for the undamped analytical model, so

$$[K_A]\{\phi_A\}_r=(\omega_A)_A^2[M_A]\{\phi_A\}_r \tag{3.28}$$

If {p} is a set of N_p updating parameters that are assigned to design variables of the FE model. Then $(\omega_A)_r^2$ and $\{\phi_A\}_r$ are functions of $\{\dot{P}\}$. Now suppose that the correlation of the experimental eigenpair (ω), {φ} has been found to correspond to the analytical eigensolution, (ω), {φ}. Then the experimental eignsolution can be expressed as a Taylor expansion in terms of the updating parameters about the analytical eigensolution (Maia, Silva, 1997):

$$(\omega_x)_r^2 = (\omega_A)_r^2 + \sum_{i=1}^{N_p} \frac{\partial(\omega_A)_r^2 \dot{P}_i}{\partial \dot{P}_i} + O(\dot{P}_i)^2$$

(3.29)

$$(\phi_x)_r = (\phi_A)_r + \sum_{i=1}^{N_p} \frac{\partial(\phi_A)_r \dot{P}_i}{\partial \dot{P}_i} + O(\dot{P}_i)^2$$

Assuming that required changes in the updating parameters are small, can be linearized and rearranged to give:

$$\Delta(\omega)_r^2 = \sum_{i=1}^{N_p} \frac{\partial(\omega_A)_r^2 \dot{P}_i}{\partial \dot{P}_i} \tag{3.30}$$

$$\Delta(\phi)_r = \sum_{i=1}^{N_p} \frac{\partial(\phi_A)_r \dot{P}_i}{\partial \dot{P}_i} \tag{3.31}$$

The sensitivity of the eigenvalues can be expressed as:

$$\frac{\partial(\omega_A)_r^2}{\partial P_i} = \{\phi_A\}_r^T \left[\frac{\partial[K_P]}{\partial P_i} - (\omega_A)_r^2 \frac{\partial[M_a]}{\partial P_i} \right] \{\phi_A\}_r \tag{3.32}$$

The sensitivity of the eigenvectors can be expressed as:

$$\frac{\partial\{\phi_A\}_r}{\partial P_i} = \sum_{j=1, j\neq r} \frac{\{\phi_A\}_j \{\phi_A\}_j^T}{(\omega_A)_r^2 - (\omega_A)_j^2} \left[\frac{\partial[K_A]}{\partial P_i} - (\omega_A)_r^2 \frac{\partial[M_A]}{\partial P_i} \right] \{\phi_A\}_r$$
$$-\frac{1}{2}\{\phi_A\}_r \{\phi_A\}_r^T \frac{\partial[M_A]}{\partial P_i}\{\phi_A\}_r \qquad (3.33)$$

Experimental sensitivities:

When large discrepancies exist between the experimental and analytical models, the validity of the Taylor series truncations discussed above are undermined and the iterative process is prone to divergence. A modification to the modal sensitivity method that enables convergence for larger magnitudes of FE modeling errors achieved by using both analytical and experimental modal data in the formulation of the eignsensitivities. Lin (Lin, Lim, 1995) derived the following equations from equations 3.32 and 3.33:

$$\frac{\partial(\omega_A)_r^2}{\partial \dot{P}_i} = \{\phi_A\}_r^T \frac{\partial[K]}{\partial \dot{P}_i}\{\phi_x\}_r - (\omega_x)_r^2 \{\phi_A\}_r^T \frac{\partial[M_A]}{\partial \dot{P}_i}\{\phi_x\}_r \qquad (3.34)$$

$$\frac{\partial\{\phi_A\}}{\partial \dot{P}_i} = \sum \frac{\{\phi_A\}_j \{\phi_A\}_j^T}{(\omega_x)_r^2 - (\omega_A)_j^2} \left[\frac{\partial[K_A]}{\partial \dot{P}_i} - (\omega_x)_r^2 \frac{\partial[M_A]}{\partial \dot{P}_i} \right] \{\phi_x\}_r$$
$$-\frac{1}{2}\{\phi_A\}_r \{\phi_A\}_r^T \frac{\partial[M_A]}{\partial \dot{P}_i}\{\phi_x\}_r \qquad (3.35)$$

As a result of this modification:

(i) When there is a large disparity between experimental and analytical modes, the sensitivities are not calculated exclusively on the basis of the incorrect analytical modes. This enables convergence for a wider domain of updating problems ;and

(ii) Calculations of the experimental eignsensitivities require measured modal displacements at every DOF in the FE model, causing coordinate incompleteness in all practical cases.

3.8.2 Modes or FRFs for correlations:

Unfortunately it is impossible to give hard and fast rules as to indicate weather modal or frequency domain data are more appropriate for correlation. Some of the issues which need to be considered when adopting particular approach are;

(i) Modal extraction is subject to errors and omission, a problem exacerbated by increased modal density at high frequencies;

(ii) Although FRFs gives more equations, the only new information occurs due to the residual terms outside the measurement bandwidth;

(iii) Modal parameters need weighting between the natural frequencies and the mode shapes. Natural frequencies are more reliable and sensitive to parametric changes. However, excessive weighting towards natural frequencies will cause mode shape information to be lost, this cause the updating problem become ill-conditioned;

(iv) For FRFs the weighting is implicit and depends on the proximity of the chosen frequency points to resonance, weighting is therefore is less controllable;

(v) FRFs are more appropriate for the updating of damping due to the variation of phase over the measured bandwidth. However this asset can be a problem for updating undamped models.

Increasing the number of updating parameters including damping means that overditermination of the problem to combat ill-conditioning and noise effect will dictate

an increased data requirements, currently only available in the frequency domain. This inevitably will require measurements over a higher frequency bandwidth, making modal extraction problematic in regions of high modal density.

Coordinate incompleteness:

The FRF sensitivity approach to model updating requires measured response data at every DOF in the FE model, resulting in coordinate incompleteness in all practical cases. One approach is to complete the experimental response vector by adopting analytical counterparts at slave DOFs which is effectively a very simple form of FRF expansion. When the divergence between the experimental and the analytical models are large, it is better to use the reduction of the FE model to overcome the coordinate incompleteness.

3.8.3 Direct optimization:

Considerable efforts have been expended trying to minimize the norm between two vectors using the least square approach. This approach can be interpreted task form of optimization. Many optimization techniques were developed , some of are discussed here. For the case of this research *The Modified Feasible Direction algorithm in MSC.Nastran* is used.

Direct updating methods:

It is based on the assumption that the mass matrix is correct and minimized the difference between the original and updated FE models is defined by the Euclidean norm,

$$\varepsilon = \left\| [M_A]^{\frac{1}{2}} [[K_x] - [K_A]] [M_A]^{\frac{1}{2}} \right\| \tag{3.36}$$

(i) [K] is symmetric

$$[K_x] = [K_x]^T \tag{3.37}$$

(i) Orthogonality condition

$$[\phi_x]^T [K_x][\phi_x] = [\omega_x^2] \tag{3.38}$$

Equation (3.36) is minimized using Lagrange multiplier (Maia, Silva, 1997) to give the following expression for the stiffness error matrix:

$$[\Delta K] = -[K_A][\phi_x][\phi_x]^T [M_A] - [M_A][\phi_X][\phi_X]^T [K_A] + [M_A][\phi_X][\phi_X]^T [K_A][\phi_X] \tag{3.39}$$
$$[\phi_X][M_A] + [M_A][\phi_X][\omega_X^2][\phi_X]^T [M_A]$$

Similar approach was used to update the mass matrix

The Modified Feasible Direction algorithm in MSC.NASTRAN:

Solving approximate problem in MSC.NASTRAN $F\left(\vec{x}\right)$ and constraint $g_j(x) \le 0$, j=1, 2,...., n_g

The general problem is defined by the equations:

Minimize	$F\left(\vec{x}\right)$		Objective	(3.40)
Subject to	$g_j(x) \le 0$	j=1, 2,...., n_g	Inequality constraint	(3.41)
	$x_i^l \le x_i \le x_i^u$	i=1, 2,...., n	Side constraints	(3.42)
where $\vec{x} = \{x_1, x_2, ..., x_n\}$			Design Variables	(3.43)

The overall optimization process is described in steps below:

1. Start q=0 , $\vec{x} = \vec{x}$
2. q=q+1
3. Evaluate $F(\vec{x})$ *and* $g(\vec{x})$ where J=1, 2,...., n_g
4. Identify the set of critical and near critical constraint J

5. Calculate $\nabla F\left(\vec{x}\right)$ *and* $\nabla g_j\left(\vec{x}\right)$ *for all* $j \in J$

6. Determine the usable-feasible search direction vector $\vec{S}^q$

7. Perform a one dimensional search to find α^*

8. Set $\vec{x}^q = \vec{x}^{q-1} + \alpha^* \vec{S}^q$

9. Check for convergence to the optimum. If satisfied, exit. Otherwise go to step 2.

The critical parts of the optimization task consist of the following:

1. Finding a usable-feasible search direction, $\vec{S}^q$
2. Finding the scalar parameter α^* that will minimize $F\left(\vec{x}^{q-1} + x^* \vec{S}^q\right)$ subject to the constraints.
3. Testing the convergence to the optimum $\vec{x}^*$, and terminating if convergence achieved.

CHAPTER FOUR

EXPERIMENTAL TESTS AND DATA ACQUISITION

4.1 Introduction

The experimental study of structural dynamics has always provided a major contribution to understand and to control the vibration phenomena encountered in practice. Experimental observations are necessary for verifying the theoretical models and predictions of the various dynamic phenomena which are collectively referred to as "vibration".

4.2 Fatigue assessment methodology

As discussed in chapter one, there were a vast difference between the fatigue life assessment of the FE model and the physical life of the real component predicted from tests. Therefore, a need to conduct physical tests and use their results to update the FE model is essential before using the FE model for an accurate fatigue assessment. Fatigue assessment methodology diagram and uncertainties in the finite element analysis are shown in figure 4.1 and 4.2, respectively.

There exist three types of physical tests:

1. Modal test, it is the processes involved in testing components or structures with the objective of obtaining a mathematical description of their dynamic or vibration behavior. The approximation in the FE model mentioned in chapter three, leads to differences between the FEA results and test results which means that the dynamic behavior of the FE model is different than that of the actual component. Therefore, a full scale modal test was essential to capture modes of vibration of the real component. Then a need to compare the test results with the FEA results and correlate the latter modes with the real component modes to come up with an FE model observe the physical behavior of the actual component.

2. Durability test on a shaker table, using random excitation signal as an input load history in X and Z directions separately to find out the component fatigue life, the crack locations, and the strain values in the critical locations. The real test results can be used to compare with the FEA results and to update the FE model.

3. Bushings stiffness test, at this stage there is no accurate number or range for bushings stiffness that can be used as an input for the bushings elements properties in the analytical model, therefore, a simple uniaxial stiffness test for the real bushing were conducted to give an idea about the stiffness in x-direction of this bushing.

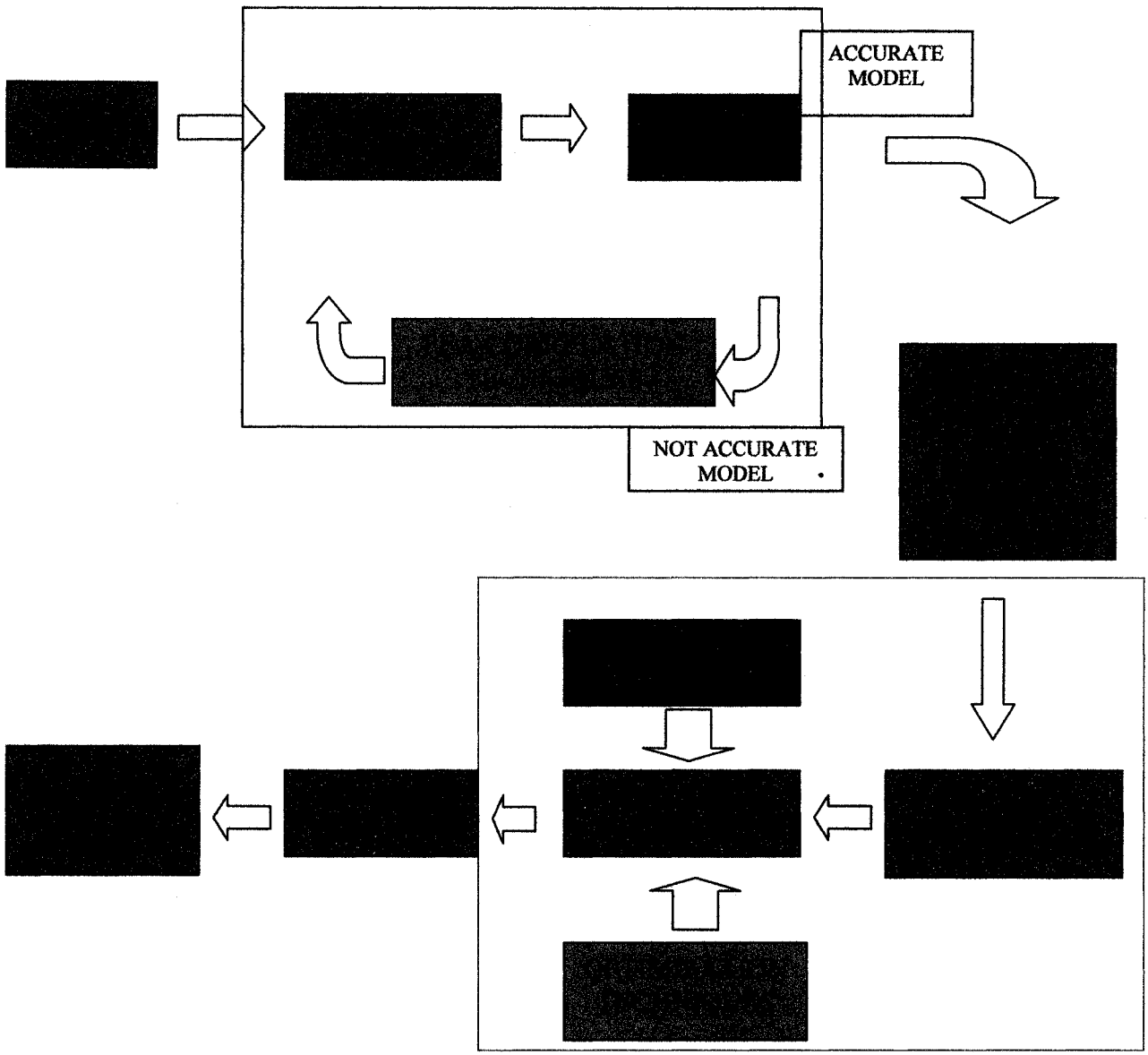

Figure 4.1 Methodology procedure diagram for accurate fatigue life assessment

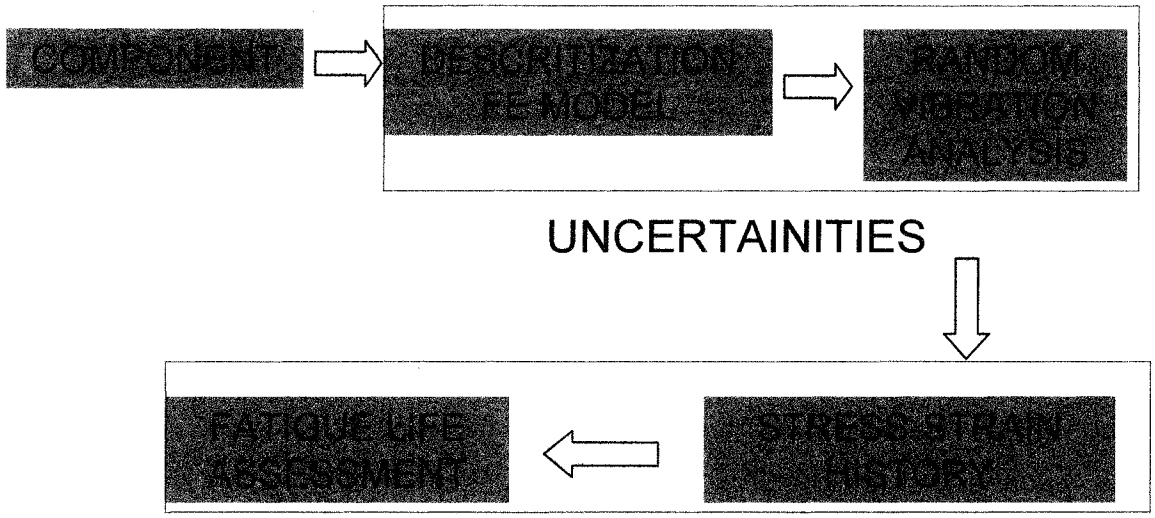

Figure 4.2 Uncertainties in the FEA

4.3 Durability test criterion:

Durability test criterion for the ABS-bracket required that the bracket pass a durability test on shaker table using random vibration signal PSD in X,Y and Z directions separately for a time more than target life time in each excitation axis with no failure or crack occurred (the above PSD's load history are shown in Table 1.1). These three axes represent the real component axis in the car; X, Y, and Z represent the longitudinal, the lateral, and the vertical direction in the car, respectively.

4.4 Sensitivity analysis

As discussed in chapter one, the actual bracket passed the physical test on shaker table with no failure or cracks occurred, therefore, there is no idea about the fatigue life of this

bracket, and there is no physical fatigue life number can be used to compare with the FEA fatigue simulation results or to correlate the latter.

For the above reason there was a need to scale-up the mass (ECU) which is weighted originally to 3.15 kg to a bigger mass that make the bracket fail during durability test in a time less than target hrs, in this case fatigue life for the bracket with the modified mass can be measured and used to compare and/or update the FE model. Sensitivity analysis, as discussed in chapter three, were conducted to help making a decision about the value of the modified mass that will be used, and give an idea about the sensitive parameters in the FE model and which one is affecting the dynamic behavior of the component, the stresses, the strain and the fatigue life.

Four types of sensitivity analysis are conducted:

1. Mass-stress sensitivity
2. Mass-fatigue life sensitivity
3. Stiffness sensitivity
4. Damping sensitivity

4.4.1 Mass-stress sensitivity

The original mass (3.15 kg) was scaled-up to (4.0, 4.5, 5.0 kg). For each mass, the stresses, and there critical locations were calculated using MSC.Nastran software in each excitation axis. The critical stresses and their locations are found. It is shown clearly that X-direction is the most damaging axis; the results are shown in Figure 4.3. Care should be taken when choosing mass values because bigger mass value may lead to a very high stresses causing the bracket fail very fast in test, this may make it difficult to capture some important information like the strain or the life time that needed in the proposed methodology to correlate the FE model.

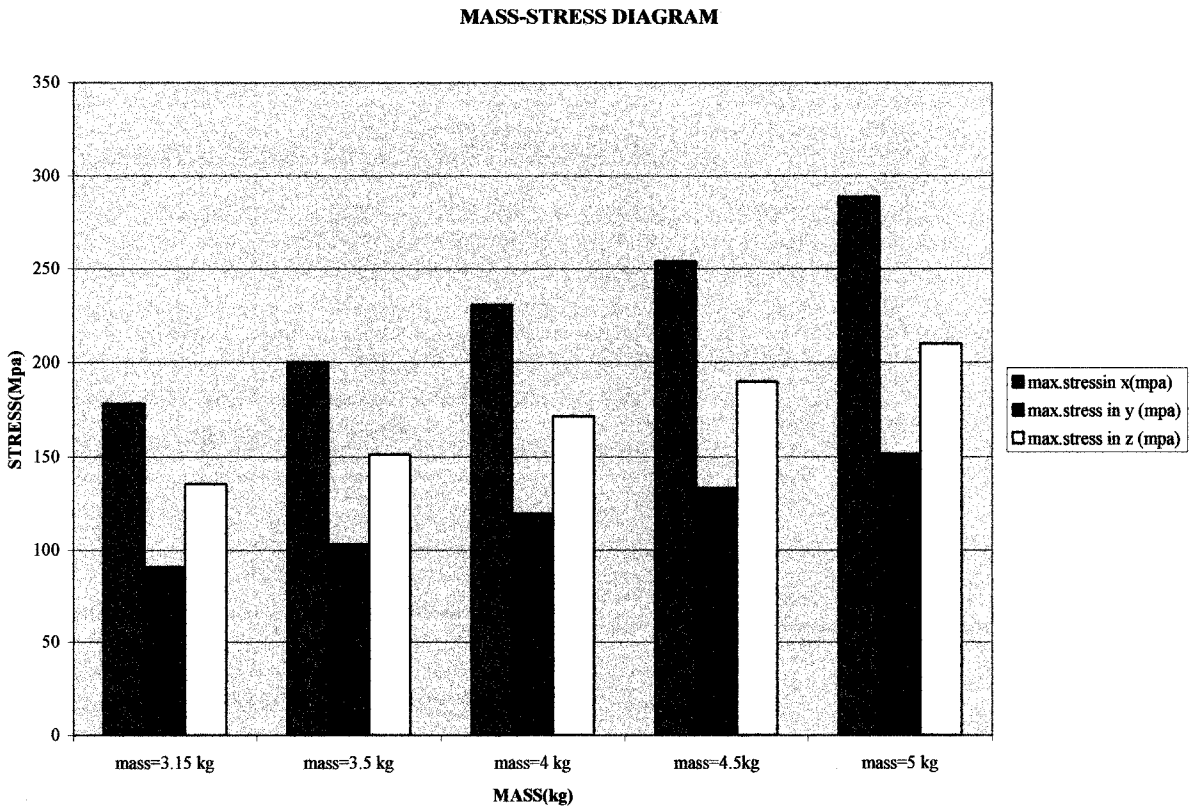

Figure 4.3: Mass-Stress sensitivity using (X, Y, Z) excitation PSD and five mass values

(Scaled for Confidential Purposes)

4.4.2 Mass-fatigue life sensitivity

The calculated stresses for each mass from the mass sensitivity analysis are used to conduct fatigue assessment using MSC.Fatigue software as mentioned before. The fatigue life and damage ratio for each mass in each of the three axes is calculated in all nodes of interest. Based on these results a decision were made to choose a 4.5 kg mass to make the bracket fail in less than target hrs in the most damaging excitation axis (X-axis).

Figure 4.4 (a, b, and c) show the fatigue life for different mass values in three axes X, Y and Z respectively at different nodes in the bracket.

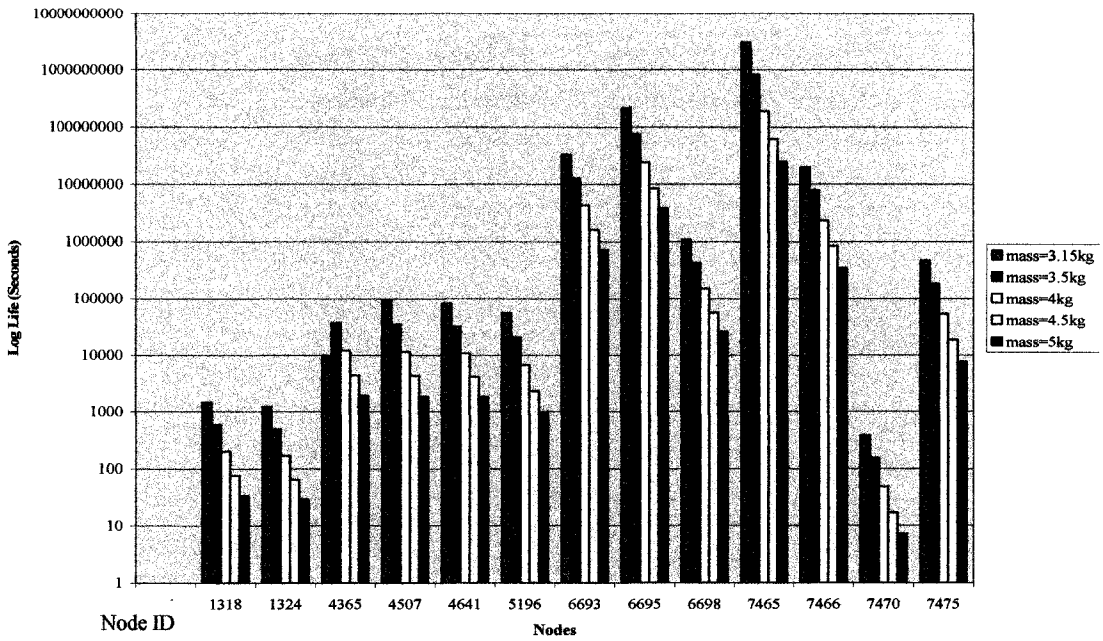

Figure 4.4(a) Mass-Life sensitivity in using PSD in X-direction in critical nodes location

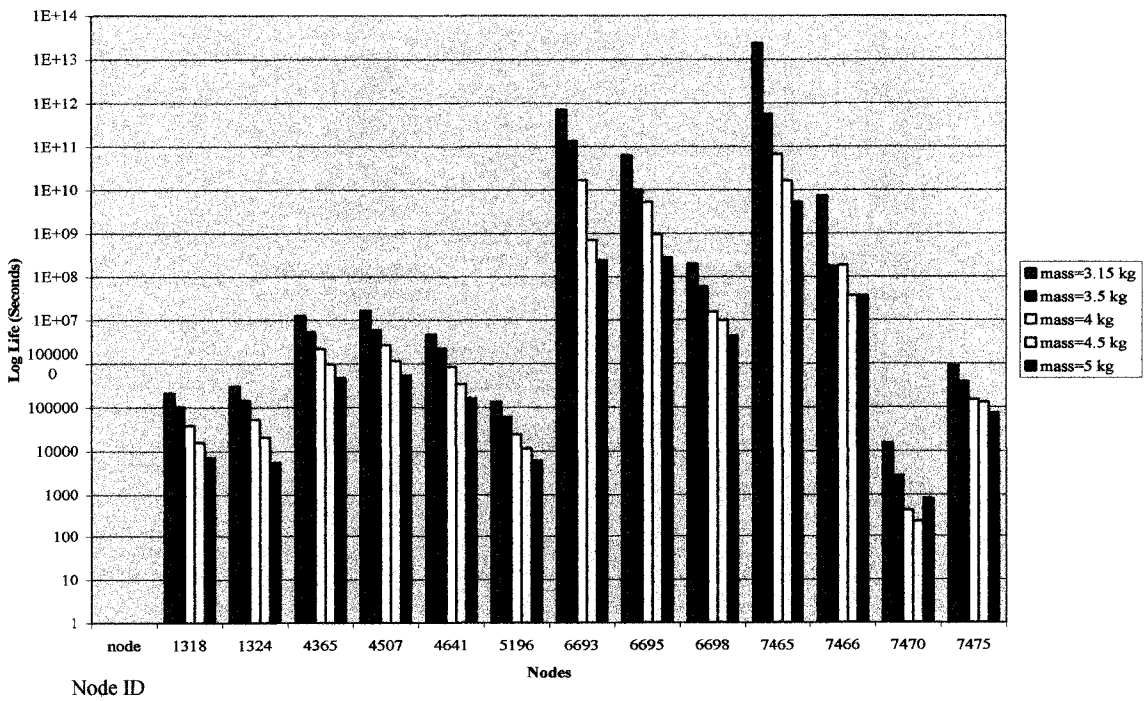

Figure 4.4(b) Mass-Life sensitivity using PSD in Y-direction in critical nodes location

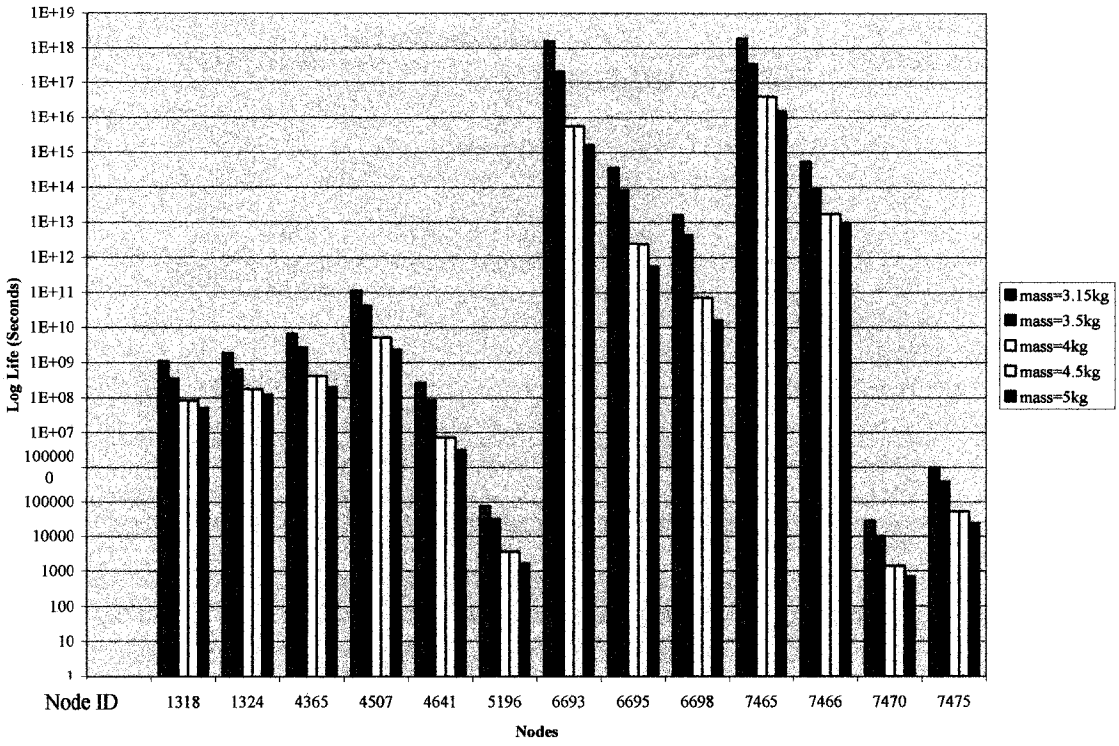

Figure 4.4(c) Mass-Life sensitivity using PSD in Z-direction in critical nodes location

Note: Figure 4.4(a,b,c are scaled for confidential purposes)

4.4.3 Stiffness sensitivity

Bushings stiffness is very difficult to predict and model in FE and they have a great effect on the dynamic behavior of the model. Sensitivity analysis is conducted for the above reason to give a better picture of their effect on the structure behavior.

Bushings stiffness are changed based on a realistic range of values for the translational stiffness (X, Y and Z) between (60-1500) N/mm and rotational stiffness between (2000-200000) N.mm/rad. These values are used to define bushings properties and conduct modal analysis, frequency response analysis and RMS analysis in MSC.Nastran and MSC.Random software. The bushings stiffness sensitivity to the modal analysis, the dynamic behavior of the structure, the stresses and finally the fatigue life are found. Table 4.1 shows the effects of bushings stiffness on the modes of vibration of the FE model.

Table 4.1 Bushings stiffness sensitivity analysis results (scaled for confidential purposes)

NORMAL MODES SENSTIVITY(Hz) FOR VARIOUS BUSHINGS STIFFNESS FOR ABS-BRACKET AND ECU (T,TRANSLATION STIFFNESS,"N/mm" ,R, ROTATIONAL STIFFNESS,N*mm/rad)								
T 500, R 5000	T 1500, R 5000	T 1500, R 70000	T 2000, R 50000	T 2000, R 75000	T 2500, R 50000	T 2500, R 150000	T 5000, R 50000	T 5000, R 200000
53.40	55.03	55.28	55.91	56.13	56.55	57.68	57.92	58.87
135.07	152.00	152.55	155.29	156.03	157.61	160.30	162.47	166.26
147.99	181.94	184.63	197.70	200.15	210.79	220.49	250.66	260.59
210.92	258.30	260.16	271.97	273.88	281.47	290.76	306.58	319.41
215.32	325.76	326.62	363.76	364.60	394.32	400.00	491.84	499.17
386.70	627.30	628.50	712.90	714.03	786.84	791.61	1063.65	1068.93
1027.99	1432.05	1440.19	1548.50	1559.08	1626.99	2093.33	1793.08	1909.13
2030.60	1788.84	1784.85	1935.29	1938.46	2080.46	2614.29	2706.98	2715.57
1814.11	2136.16	2138.42	2386.62	2388.31	2607.54	3530.03	3414.93	3421.37
	1240.47	3361.82	3471.58	3475.80	3522.22	3988.74	3664.52	3670.13
	3376.83	3583.71		3736.96	3930.72			

4.4.4 Damping sensitivity

Structural damping is one of the big issues in modeling structures, because of its complexity. Different structures reflect different structural damping ratio which varies in the range of (1%-8%) and some times even more depending on many geometric characteristics and material properties.

Various frequency response and random vibration analysis for the ABS-bracket supporting the assumed mass are conducted using various structural damping ratios (1, 2, 3, 4 and 5%), the stresses are calculated and used in fatigue life prediction, the results are shown in Figure 4.5 a and b for the critical node.

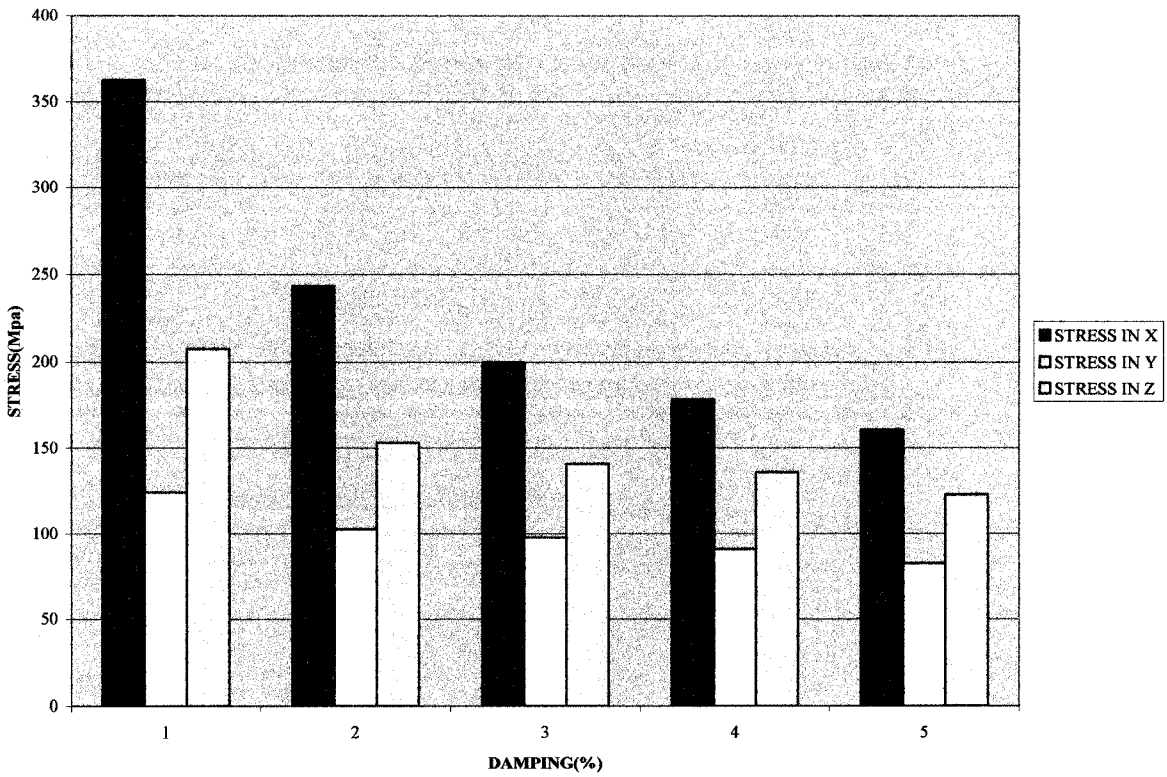

Figure 4.5 (a) Damping-Stress sensitivity for the most damaged node (node 1318) in X, Y and Z (Scaled up for confidential purposes)

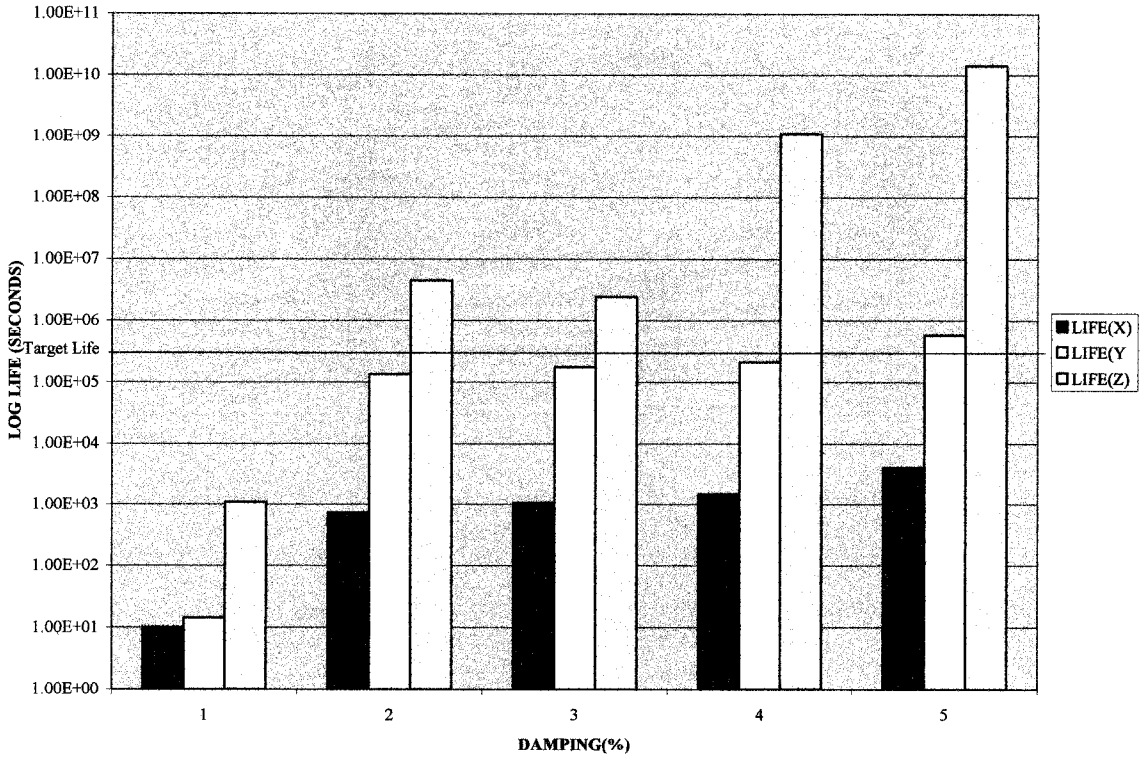

Figure 4.5 (b) Damping-Life sensitivity for 4.5 kg mass in the most damaged node (node 1318) in X, Y and Z (Scaled up for confidential purposes)

4.5 Mass creation

Based on the mass and fatigue sensitivity analysis conducted above, a decision is made to use a 4.5 kg mass to be mounted on the bracket in durability test as mentioned before. This mass is made of steel and designed in shape to keep the same center of gravity for the original (ECU) using CATIA & MSC.Patran softwares. This mass is shown in Figure 4.6.

Six components moments of inertia for the assumed mass are calculated using the above software. The results are shown in Table 4.2:

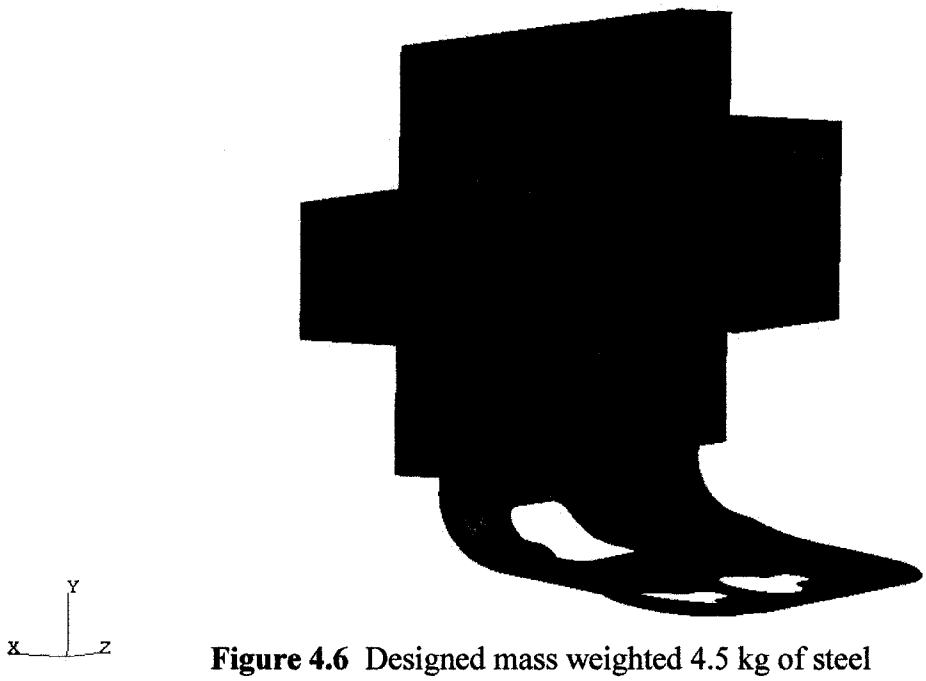

Figure 4.6 Designed mass weighted 4.5 kg of steel

Table 4.2 Manufactured mass properties and center of gravity

(Scaled up for confidential purposes)

Manufactured Mass	
center of gravity (mm)	
X	2067.152
Y	-731.117
Z	1494.167
moment of inertia mm ^{4}	
XX	24.148
YY	16.640
ZZ	11.489
XY	0.217
YZ	-0.113
ZX	0.282
mass (Kg)	
Aluminum	7.545
steel	1.363
plastic	0.506
Total Mass	9.414

4.6 Modal tests

Two modal tests were conducted. First one is a hammer modal test for the actual component (ECU) supported on the bracket, the second one is three axes shaker table modal test for the assumed mass (4.5 kg) mounted on the bracket, both tests are described here;

4.6.1 Hammer table modal test:

Is one of the wide and oldest methods used to assess modes of vibration of structures and components.

4.6.1.1 Hammer table FE model:

The real hammer table were measured and modeled in FE; modes of vibration were calculate using modal analysis to find the dominant frequencies and their ranges compared with the component frequencies to ensure test accuracy. The FE model and the FEA results are shown in Figure 4.7 and Table 4.3 respectively.

4.6.1.2 Hammer table test

A Hammer table test for the real component supported by the bracket was conducted using one accelerometer mounted in different locations to measure acceleration and then transfer the response to frequency domain using Fourier transfer functions. PUMA analyzer and STARC software's were used for this transformation purposes. Modes of vibration are shown in Table 4.4.

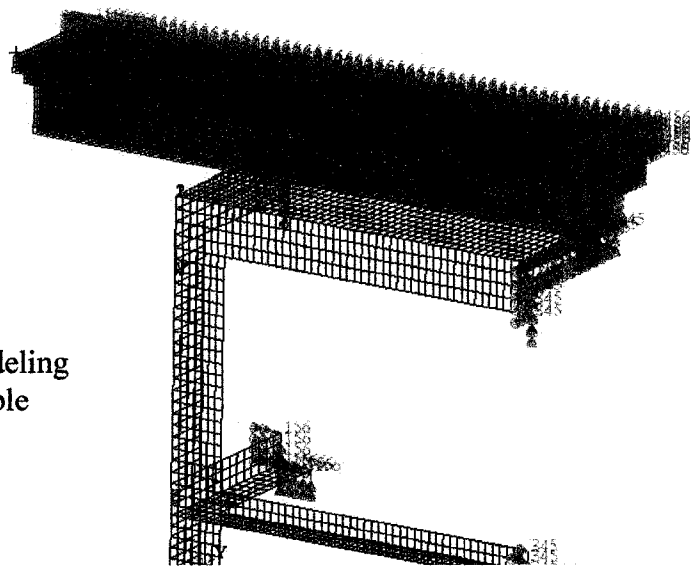

Figure 4.7 FEA modeling of the hammer table

Table 4.3 Hammer table modes of vibration in FEA

(Scaled up for confidential purposes)

Modes Frequency(Hz)
199.16
277.41
296.37
341.42
379.36
424.41
609.35
673.36
711.30
829.85

Table 4.4 Hammer modal test for the ABS-bracket and ECU

(Scaled up for confidential purposes)

MODES Hz
59.986
156.249
197.030
310.601
360.155
1325.389
1970.894
4630.563

4.6.2 Three-axes shaker table modal test:

Modes of vibration which represent the dynamic behavior of the structure are very important in the FE correlation procedure and curve fitting, therefore, capturing all or most of the modes is a challenging issue, because some of the modes may show up in one direction and doesn't in other, or may an excitation signal in one axis doesn't excite one or more of the modes in the range of interest. Many factors affecting the accuracy of the real test, are: the fixture, how to input the excitation load, how many accelerometers are needed, where the response measurements points (accelerometers location) are, and how the structure is mounted on the table.

To model the test accurately, an aluminum cube were designed and manufactured to support the bracket on the shaker table. Three faces of the bracket are inclined by an angle to represent the real bracket orientation axis in the car (X, Y, and Z) as shown in Figure 4.8.

Modal test are conducted for the above reason on shaker table to capture essential modes in three excitation axes X,Y, and Z directions. Three accelerometers are used in different locations, two accelerometers are mounted on the bracket, first one on the top left side of the bracket web, the second were mounted on the bottom right side of the web, and the third accelerometer mounted on the mass as shown in Figure (4.9 a, b and c respectively). The results are shown in Figure (4.10 a, b, c) for X, Y and Z direction respectively and Table 4.5.

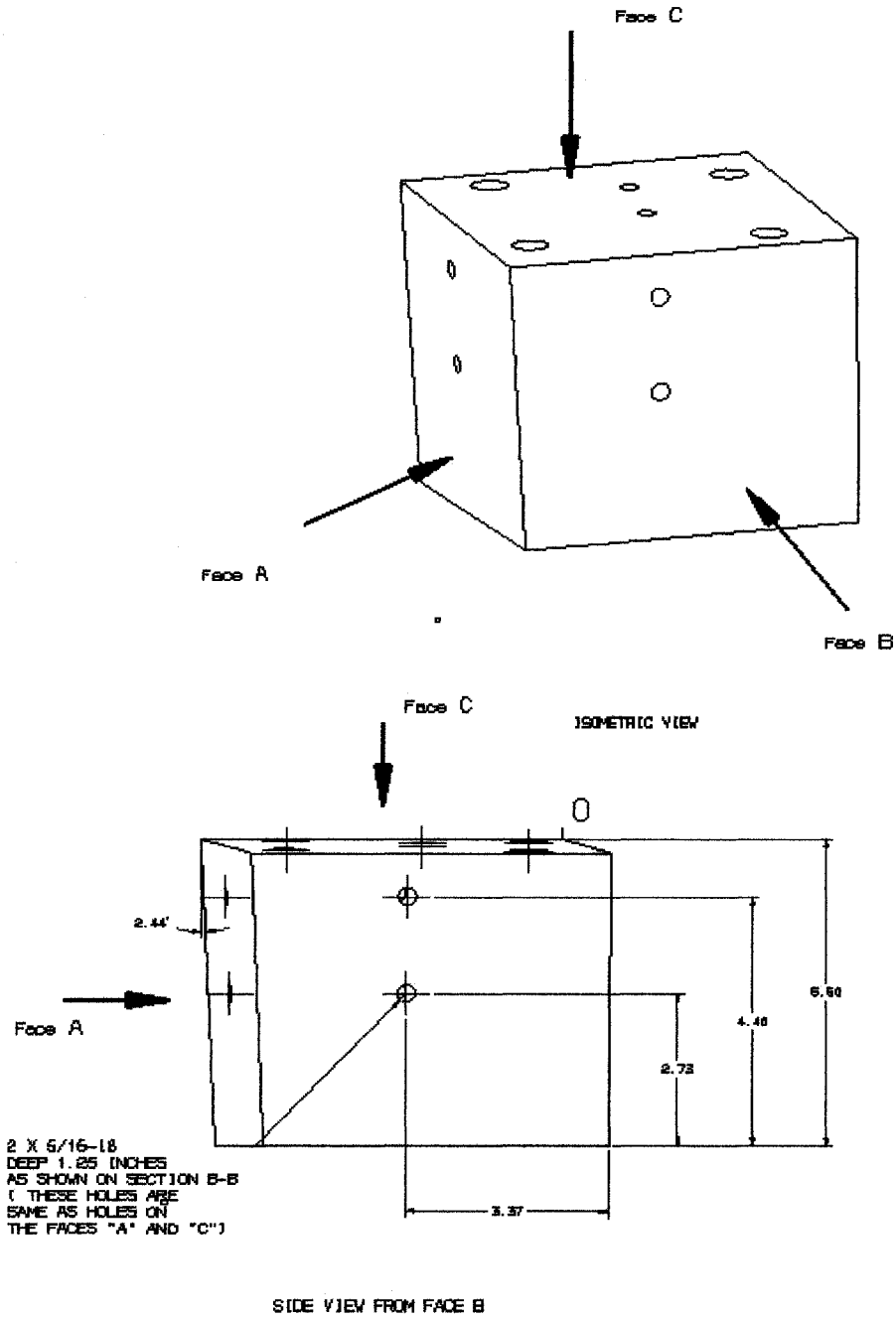

Figure 4.8 Aluminum cube mass used as a fixture to mount the ABS-bracket with the same angle of inclination in the car to simulate the real excitation direction in the car

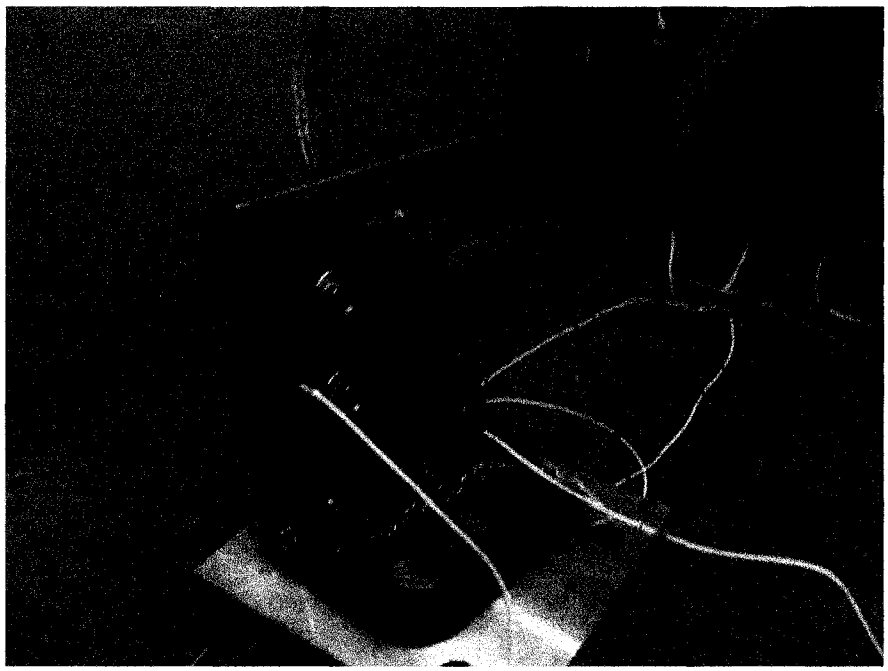

Figure 4.9 (a): Modal test of the bracket supporting dummy mass on shaker table in Z-direction

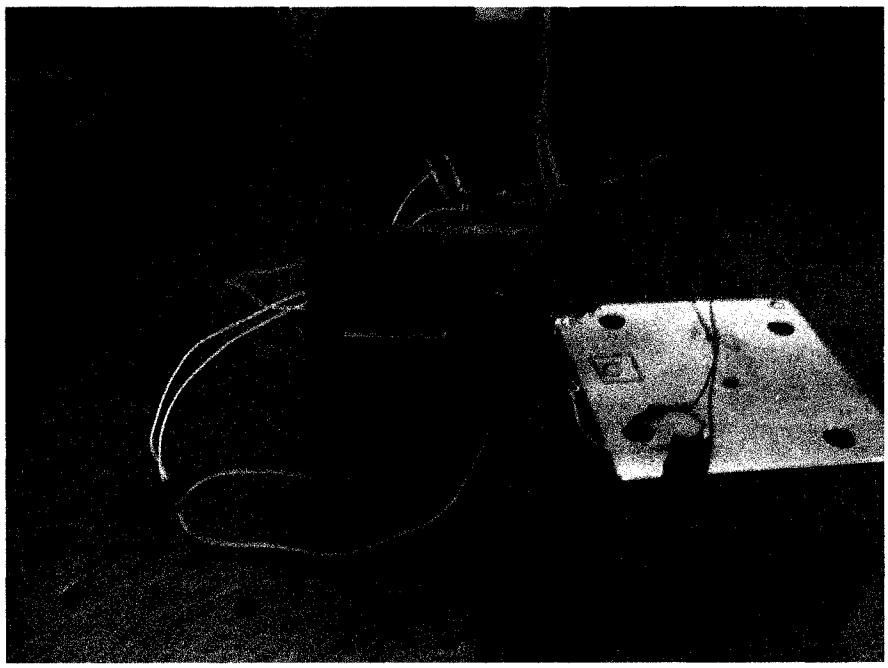

Figure 4.9 (b): Modal test of the bracket supporting dummy mass on shaker table on shaker table in X-direction

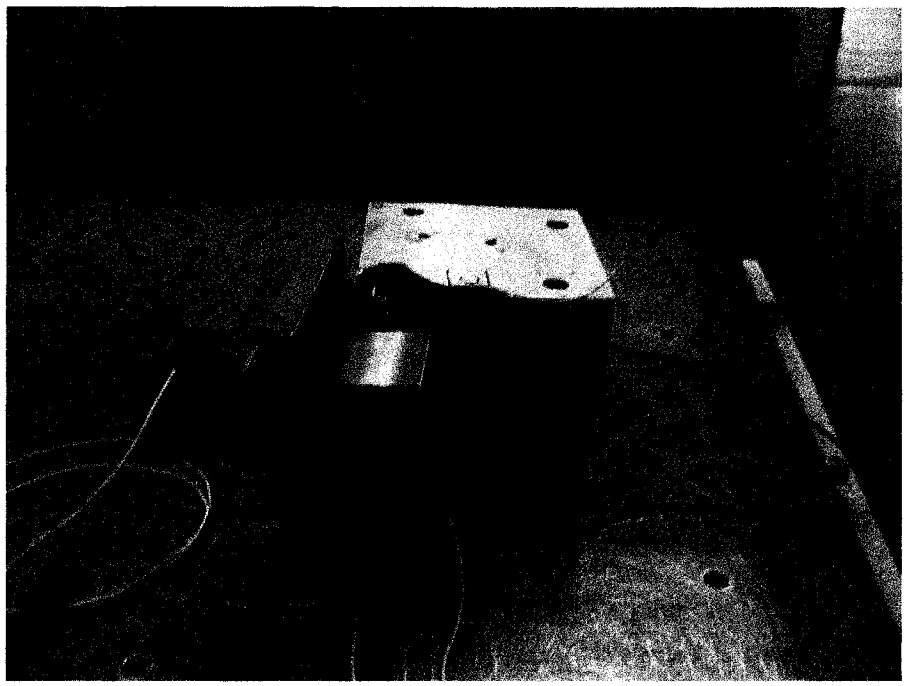

Figure 4.9(c): Modal test of the bracket supporting dummy mass on shaker table in on shaker table in X-direction

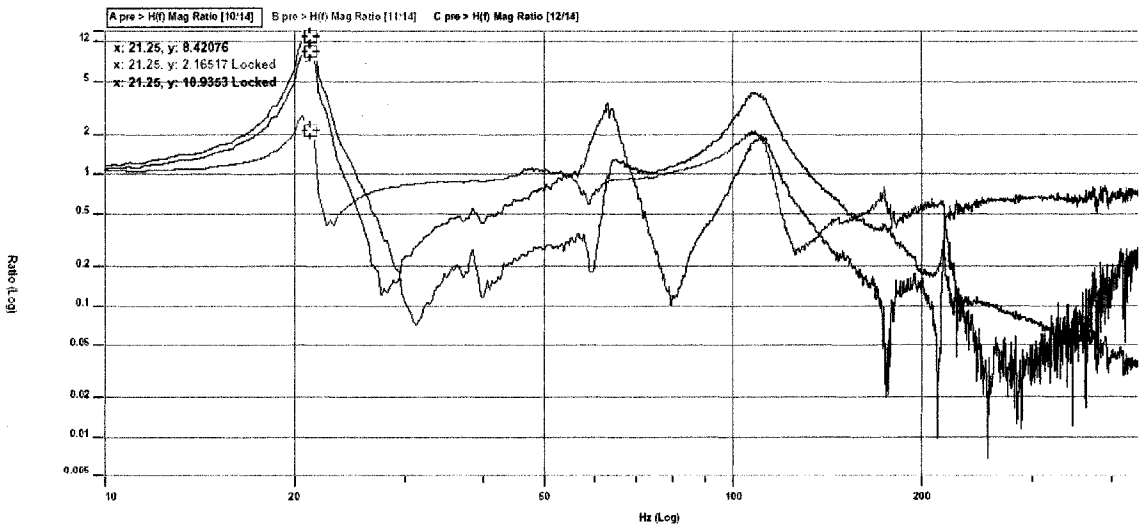

Figure 4.10 (a): Transfer function results on shaker table (X-direction)

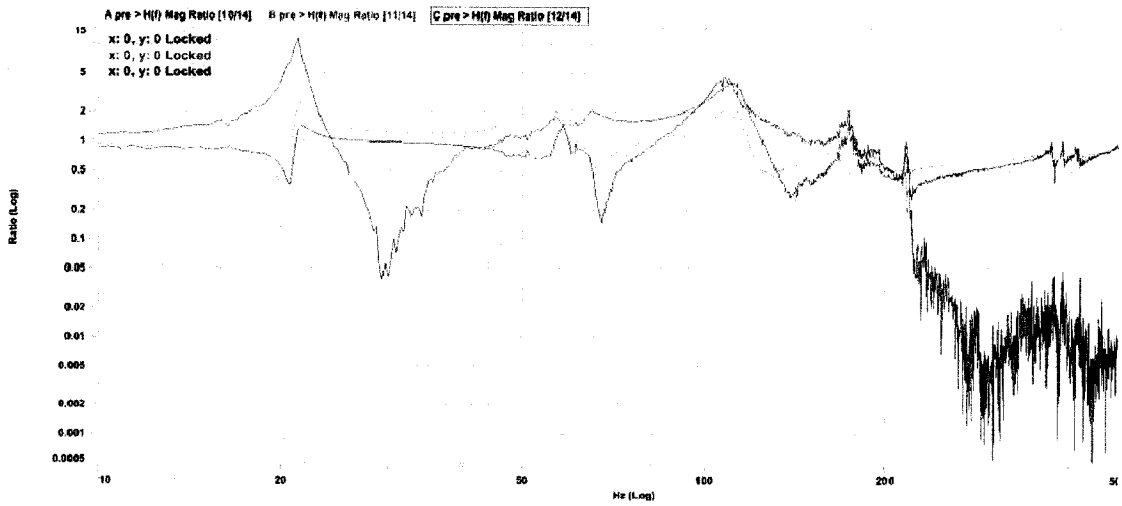

Figure 4.10 (b): Transfer function results on shaker table (Y-direction)

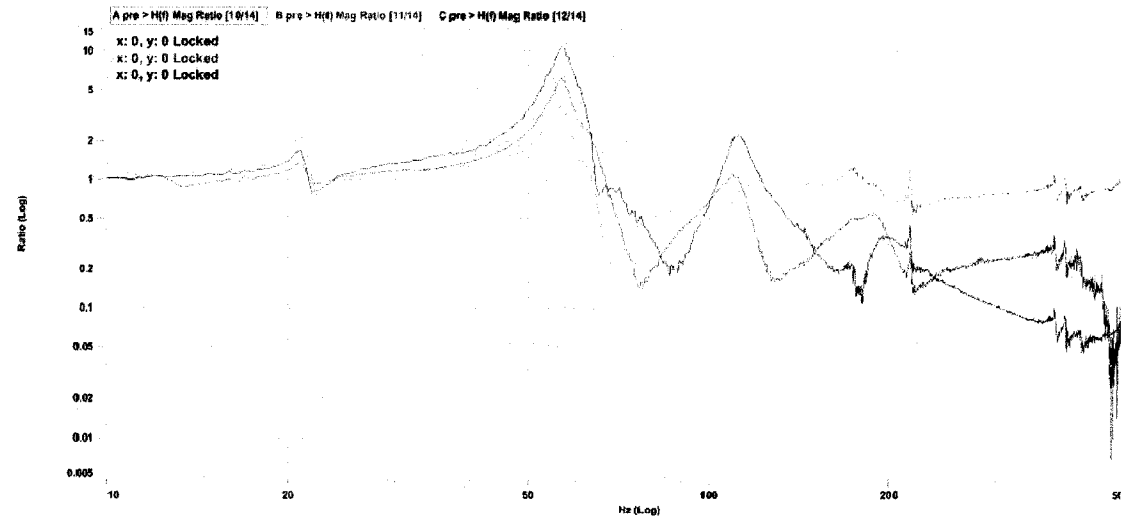

Figure 4.10 (c): Transfer function results on shaker table (Z-direction)

Table 4.5: Modes of vibration of the bracket supporting dummy mass recorded from the three axis modal test on shaker table (scaled for confidential purposes)

THREE AXES MODAL TEST ON SHAKER TABLE (Hz)		
X-DIRECTION	Y-DIRECTION	Z-DIRECTION
48.843	48.131	50.384
90.098	113.808	135.147
143.683	148.188	256.068
250.615	237.811	412.554
411.369	403.070	512.136
512.136	512.136	891.496
889.125	889.125	927.061
924.690	927.061	976.852
974.481	974.481	1145.193
	1161.790	

4.7 Durability test

Durability test using shaker table in most damaging axes (X and Z directions) are conducted separately to find the fatigue life and the strain history at critical locations.

4.7.1 Test setup

The purpose of this test is to calculate the fatigue life and to measure the strain to compare this results with the FEA results and correlate the FE model as mentioned before.

Several steps have to be done before starting the actual test:

1. Two sensitive wiring loops are fixed, one on each face of the bracket base passing through the critical locations for high stresses and expected cracks locations (these locations are predicted from the FEA previous results). These wiring loops are connected to a trigger on the shaker table to shutoff the test automatically when a crack is detected.

2. Two strain gages are fixed near the critical locations at the bottom face of the bracket. One is a Rosette strain gage, the other is a uniaxial strain gage, and both connected to a data acquisition system as shown in Figure 4.11.
3. Setup the PSD input load in X-direction as described in Table (1.1), then a full scale test on shaker table is conducted until a failure occurred in the bracket in an estimate time less than target time. The bracket found to be failed under the real test after 67 hours and 15 minutes (242100 sec.), Figure 4.12 a and b.
4. Durability test using excitation PSD in Z-direction were conducted. The bracket life found to be over target life with no failure occurred in the bracket or observation of crack.

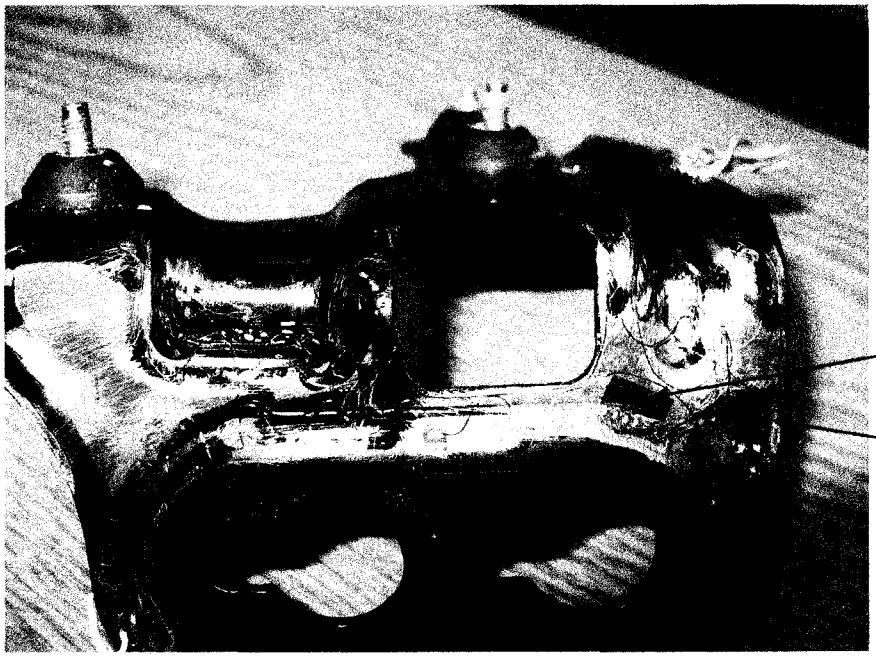

Figure 4.11: Two strain gages fixed on the rear face of the bracket near the critical areas

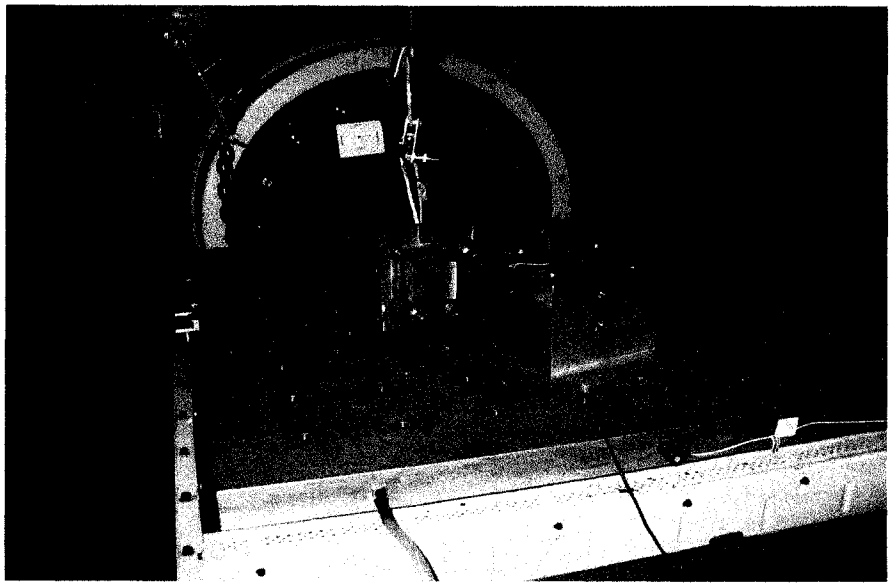

Figure 4.12(a): Durability test for the bracket and mass in X-direction

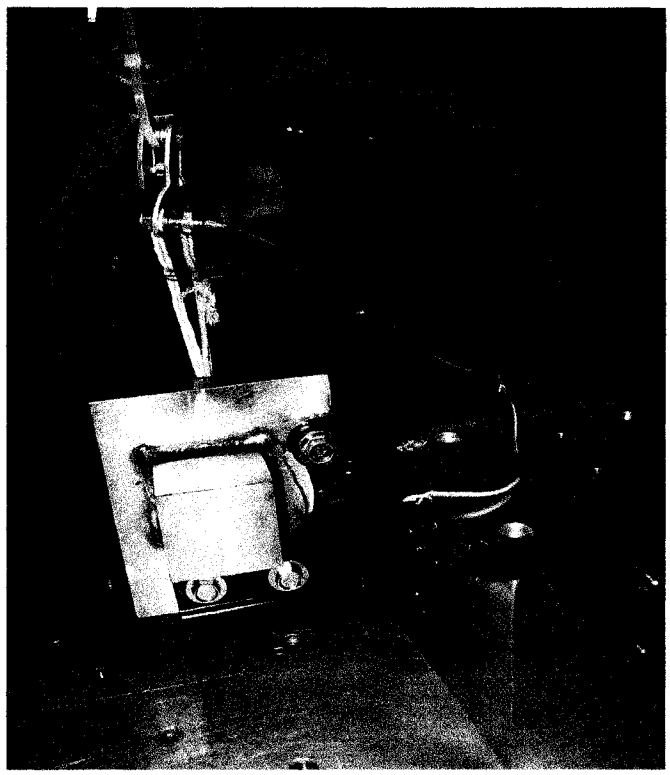

Figure 4.12 (b): Durability test for the bracket and mass in X-direction

4.7.2 Post processing the results

The strain gages measurements records are used for fatigue life assessment and to get statistical information using RPC-PRO as post processor software. The obtained results are used to compare and correlate the FE model; the results are shown in Table 4.6 below:

TABLE 4.6: Statistical report for the ABS-bracket using post processor RPC-PRO (scaled for confidential purposes)

STATISTICAL REPORT OF THE ABS-BRACKET IN X-DIRECTION DURABILITY TEST AFTER 9 hrs WITH 1000 SAMPLES/SECONED												
CHANNEL	FULL SCALE	UNITS	MAXIMUM	MINIMUM	MEAN	VARIANCE	STD.DEVIATION	RMS	CREST	SUM	KURTOSIS	SKEW
32.000	2450.300	uE	284.876	-329.577	-0.982	1206.990	53.496	53.505	14.564	-3575719.33	0.982	-0.487
33.000	2438.600	uE	3580.760	-3644.846	10.978	265005.010	792.671	792.747	10.935	39950567.57	-0.156	-0.099
34.000	2450.300	uE	3374.350	-3400.427	8.651	250908.467	771.300	771.348	10.480	31483513.18	-0.284	-0.094
35.000	2468.000	uE	2196.827	-2182.712	0.515	110835.027	512.630	512.630	10.158	1875296.216	-0.343	-0.049

In the above table channels 32,33 and 34 represent the rosette strain gage. Channel 35 represents the uniaxial strain gage. These results helped to verify the accuracy of the FE model by correlating the strain gage measurements in the same location of the bracket with its corresponding result from the FE model. Correlating the RMS from test with the FEA model results and plot the response of PSD from the test to verify the signal type (narrow or wide band)

CHAPTER FIVE

FINITE ELEMENT CORRELATION

5.1 Introduction

In the previous chapters, a methodology for modeling, analysis, testing and acquisition of structures for the purpose of modal analysis, frequency response, random analysis and fatigue assessments were established and shown that they were neither trivial nor straightforward. However, adopting rigorous testing procedure and attention to detail can confidentially assume that the measured data whether in the time, modal or frequency domain provide a truer representation of the dynamic of structure and can be used for engineering applications.

An application of the modal analysis is finite element (FE) model updating which based on the use of the results from physical tests to correlate the analytical model to come up with a model reflects the real component dynamic behavior, or correlate the FEA model results to be closer to the physical test results.

5.2 Finite element modeling

Finite element model is usually influenced by many parameters due to the discritization and uncertainties as described in chapter three; however, sensitivity analysis were conducted to predict the sensitive parameters in the FE model. Therefore, care should be taken in each step of the finite element modeling to decrease the percentage error and model the component to be close to the reality.

5.2.1 Meshing the bracket

The bracket is meshed using shell elements QUAD 4 as discussed in chapter one because the t/l ratio (thickness/length) is less than 5%.

5.2.2 Boundary condition modeling

Modeling the boundary conditions in finite element is considered one of the most sensitive parameters that may cause significant changes in the FE model behavior and results. For this reason modeling the connection between the base of the ABS-bracket and the body of the car needs to be as accurate as to the real component connection. This is a challenging step because of its effect on the stresses in the critical locations. Some relief in the base constraint is given when modeling the base bolts in FE to represent the real constraint. This is achieved by modeling the connections at the base using thirty two bushings elements around the bolts holes in two rows for each hole to represent the bolt and the washer effect on the base in the connection area.

5.2.3 MSC.Nastran bushings elements

A generalized spring and damper element with six stiffness components ($K_X, K_Y, K_Z, K_{\theta X}, K_{\theta Y}, K_{\theta Z}$) at each end is used to model the bushings as discussed before.

This bushing element is used to model connection between the ECU and the bracket using three bushing elements as in the reality and thirty two bushings elements to model the base connection to the car body.

5.2.4 Modeling the mass

To model the ECU, a mass element is created at the same center of gravity of the mass which is calculated in chapter four, and used as input node for the weight of the assumed mass (4.5 kg) in the FE model. The material properties, Young modulus of elasticity, Poisson's ratio and density for steel are 207000 MPa, 0.29, and 7860 kg/m^3 respectively. The six components of the mass moment of Inertia are shown in Table 4.2. Bushings

stiffness is to be calculated from the optimization techniques as in section 5.3.1 and Table 5.1. Figure 5.2 shows the final finite element model of the bracket and the mass.

5.2.5 Loading history input

A base input node is created below the base of bracket and connected to the bracket by multi-point constraint elements MPC's to model a rigid connection and it is used as an input node for the acceleration load history PSD in the FEA. Three excitation PSD are used, one for each direction as shown in Table (1.1).

5.2.6 Finite element analysis

After completing the FE model, finite element analysis is conducted, in three steps for the analysis and fatigue assessment:

1. Modal analysis.
2. Frequency response and random vibration analysis.
3. Fatigue assessments and life estimation.

5.3 Finite element correlation methodology

Updating the FE model to act as close as the real component using the techniques discussed in chapter three. This is to be done carefully and to be applied to all the sensitive parameters in the FE model to updating them and come up with an accurate FE model. This consists of three steps:

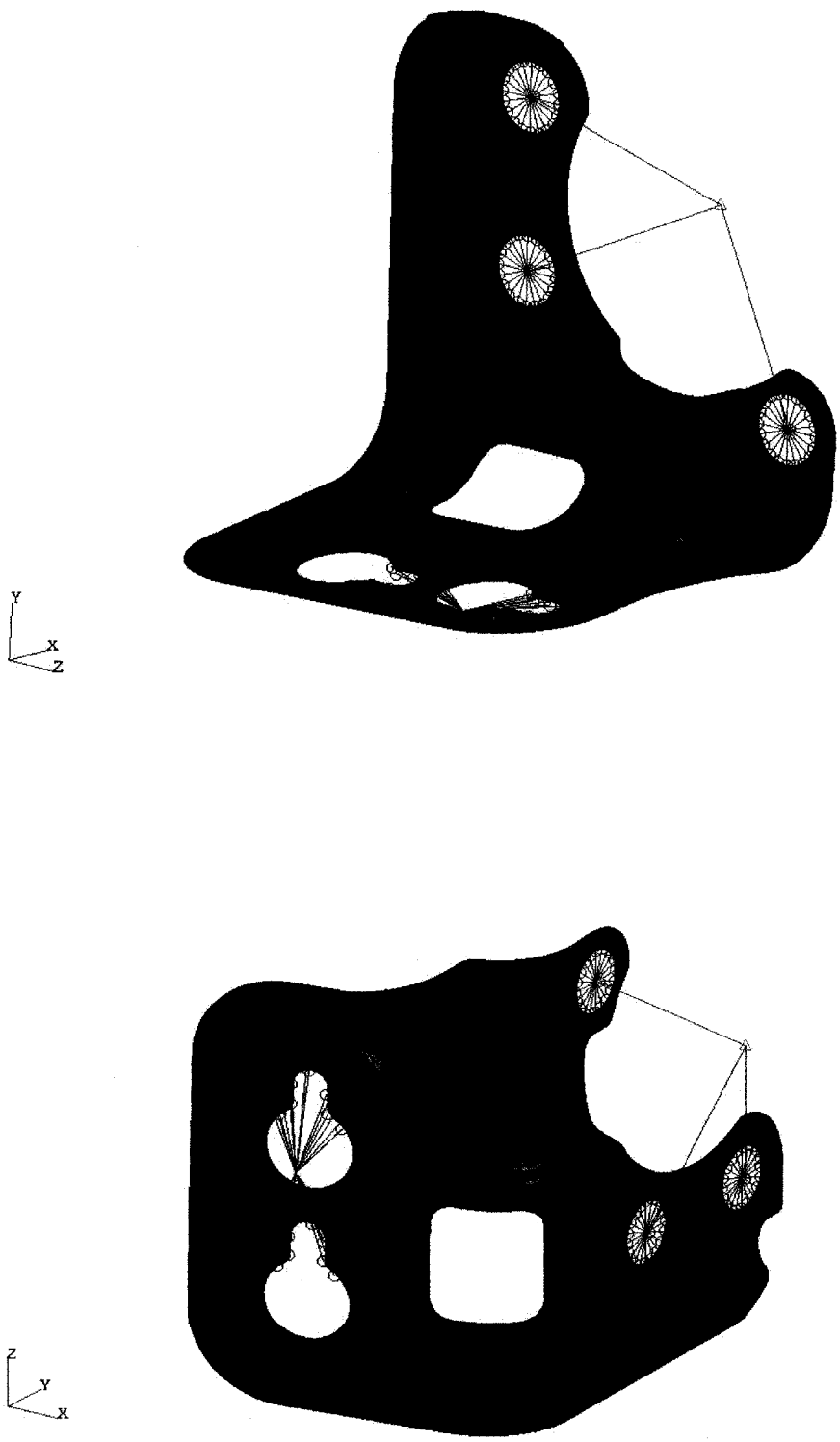

Figure 5.1 Finite element model of the ABS-bracket and ECU with bushings elements to support the unit at the web of the bracket and to connect the bracket with the base

5.3.1 Optimization techniques

As mentioned in chapter three, this technique is done by using the algorithm implemented in MSC.Nastran software (SOL 200):

1. From the conducted sensitivity analysis, it is obvious that the bushings stiffness is dominating the dynamic behavior of the component, modes of vibration, stress-strain relation and fatigue assessment. For this reason a decision is made to use these twelve bushings stiffness components as modal variables in the optimization procedure.
2. Minimize the component weight.
3. To get an accurate model the first four modes in the FE model are chosen to be correlated with the real component modal test results, this is achieved by constraining the first six modes (between 0-230 Hz) in the optimization procedure.
4. Using MSC.Nastran software (SOL 200) to find an optimum values of the bushings stiffness that correlate the FE model with the constraint modes.

Many optimization solutions are conducted and the results are listed in table 5.1 below:

Table 5.1 optimization results

OPTIMIZATION_RESULTS														
job	constraint	BUSHINGS STIFFNESS, TRANSLATIONAL N/mm, ROTATIONAL N*mm/rad												
		K1	K2	K3	K4	K5	K6	K7	K8	K9	K10	K11	K12	modes
optim_1	40-60	583.8	413.7	407.4	189000	189000	189000	1404900	1677900	1677900	23163000	16380000	29820000	46,88,120,134,170,198,872
	60-80													
	96-110													
optim_2	40-48	840	426	489	117621	207900	207900	1404060	1677900	1677900	23163000	16380000	29820000	46,92,120,138,190,198,884
	60-80													
	116-130													
optim_3	40-48	840	431	480	146460	230643	197471	1404060	1677900	1677900	23163000	16380000	29820000	46,82,120,128,176,198,872
	60-80													
	116-136													
optim_4	40-48	840	426	581	40026	207900	207900	5394270	3780840	3955560	23163000	16380000	29820000	46,80,118,162,182,860
	60-80													
	116-126													
optim_6	40-48	567	330	321	189000	189000	189000	1404900	1677900	1677900	23163000	16380000	29820000	44,72,100,106,136,178,758
	60-74													
optim_7	40-48	126	166	132	48105	207704	207900	105000	2863350	1050000	23163000	16205070	29820000	36,50,66,78,92,104,524,994
	60-74													
	380-450													
optim_8	40-48	567	329.7	321.3	189000	189000	189000	1404900	1677900	1677900	23163000	16380000	29820000	44,72,100,106,136,158,758
	60-74													
	100-112													
optim_9	40-48	449.4	535.5	268.8	189000	189000	189000	1404900	1677900	1677900	23163000	16380000	29820000	43,74,102,106,138,162,718
	60-74													
	98-104													
	106-115													
optim_10	40-48	367.5	785.4	165.9	189000	189000	189000	1404900	1677900	1677900	23163000	16380000	29820000	42,66,98,108,132,180,688
	60-74													
	98-102													
	106-112													
	120-132													

Table 5.1 optimization results continued

optim_11	40-48	367.5	787.5	165.9	189000	189000	189000	1404900	1677900	1677900	23163000	16380000	29820000	42,64,100,108,132,180,688
	60-74													
	98-102													
	106-120													
	120-132													
optim_12	40-48	186.9	837.9	457.8	315000	148789.2	248157	31000200	23360400	16894500	23163000	28240800	45511200	40,78,94,104,140,192,604
	60-74													
	98-102													
	106-112													
	120-132													
	198-220													
optim_13	40-48	300.3	840	281.4	735000	203987.7	193872	29855700	7887600	16447620	23163000	29761200	48363000	40,78,98,114,134,192,646
	60-74													
	98-102													
	106-110													
	120-132													
	198-220													
optim_14	40-48	840	840	840	9989.7	18167.1	20764.8	18900000	13815060	10833480	23163000	21905100	31500000	46,92,118,150,180,210,886
	60-80													
	120-134													
	200-220													
optim_15	40-48	840	840	840	9380.7	140603.4	315000	29093400	17048640	13519800	23163000	24786300	46460400	45,92,118,150,192,210,888
	60-80													
	120-130													
	198-240													
optim_16	40-48	840	840	478.8	4200	315000	120823.5	1050000	1050000	1050000	23163000	16354800	29794800	46,88,120,134,170,196,872
	60-80													
	120-130													
	140-170													
optim_17	40-48	840	619.5	840	4200	181440	401310	1242570	1050000	8171100	23163000	1050000	34526310	48,92,120,138,190,198,884
	60-80													
	120-138													
	140-170													
	200-230													
optim_18	40-48	840	619.5	346.5	5334	315000	315000	2091600	1050000	1104180	23163000	16338000	29807400	46,82,120,128,176,198,872
	60-80													
	120-130													
	132-160													

Table 5.1 optimization results continued

optim_19	40-48	840	539.7	821.1	194997.6	378000	340389	1405425	1677900	1677900	23163000	16380000	29820000	48,92,126,134,186,196,890
	78-92													
	120-130													
	134-160													
	180-192													
optim_20	40-48	833.7	787.5	636.3	57909.6	244335	306810	1400700	1677900	1677900	23163000	16380000	29820000	46,92,120,140,182,200,880
	79-92													
	120-130													
	134-154													
	180-192													
	200-230													
optim_21	40-48	833.7	535.5	840	336000	161700	474264	1050000	1050000	1050000	23163000	1050000	1050000	48,94,120,134,194,202,882
	78-92													
	120-130													
	134-154													
	200-230													
optim_22	40-48	840	420	840	735000	105640.5	596400	1050000	1050000	1050000	23163000	16345560	29761200	48,94,120,124,198,208,882
	76-92													
	120-130													
	200-230													
optim_23	40-48	678.3	497.7	840	735000	4200	695100	1050000	1497300	1780590	23163000	16380000	29813700	48,92,110,130,200,204,840
	80-94													
	120-140													
	200-230													
optim_24	40-50	762.3	501.9	840	634200	117600	871500	2228100	2186100	2045400	23163000	16380000	29832600	48,94,120,130,200,216,880
	80-96													
	116-120													
	116-150													
	200-230													
optim_25	40-50	840	840	840	945000	160020	945000	9754500	1050000	6846000	23163000	15844500	31080000	50,104,124,150,218,200
	80-96													
	116-120													
	124-138													
	200-230													

Table 5.1 optimization results continued

optim_26	32-34	407.4	798	840	31668	13872.6	16959.6	1050000	1470000	1640499	23163000	16375800	29815800	48,86,140,248,450,571,889
	82-90													
	120-130													
	140-160													
	200-220													
optim-27	34-36	371.7	840	829.5	26630.1	32142.6	42000	1404900	1677900	1677900	23163000	16380000	29820000	49,90, 144, 252,415,520,889
	72-82													
	120-130													
	204-220													

5.3.2 Mode curve fitting

After conducting optimization techniques and the optimum solution is found, verification of the coincident between the modal test results with the FE modal analysis results is essential to verify the accuracy of the FE model. Therefore, the following steps are conducted for this purpose:

1. Extracting a modal imaginary response curve for each excitation axis from the previous shaker table modal test results which was in magnitude-frequency to use it to compare with the FE modal curve.
2. Using the optimum solution no-27 for the bushings stiffness from Table 5.1 above to conduct FE modal analysis. This solution gives closer modes of vibration to the test results.
3. Conduct FE modal analysis for each axis and plot the imaginary Transfer Function vs. Frequency.
4. Compare the results for each axis between steps 1 & 2 above to verify the FE model accuracy.

The plots are shown in Figure 5.2

5.3.3 Stress-Strain history

Stress-strain history is always considered as a significant indication of the FE model accuracy. For this reason two strain gages are fixed in the critical location of the bracket to record strain history as mentioned in chapter four, and used to compare with the FEA strain results in the same location as shown in Table 5.2.

5.4 Frequency response and random vibration analysis

From the results below, and after conducting all the above steps, the FE model is considered accurate and observes the real component dynamic behavior. Based on this correlated model, frequency response and random vibration analysis are conducted; the stresses and strains are calculated in the critical locations (Table 5.2).

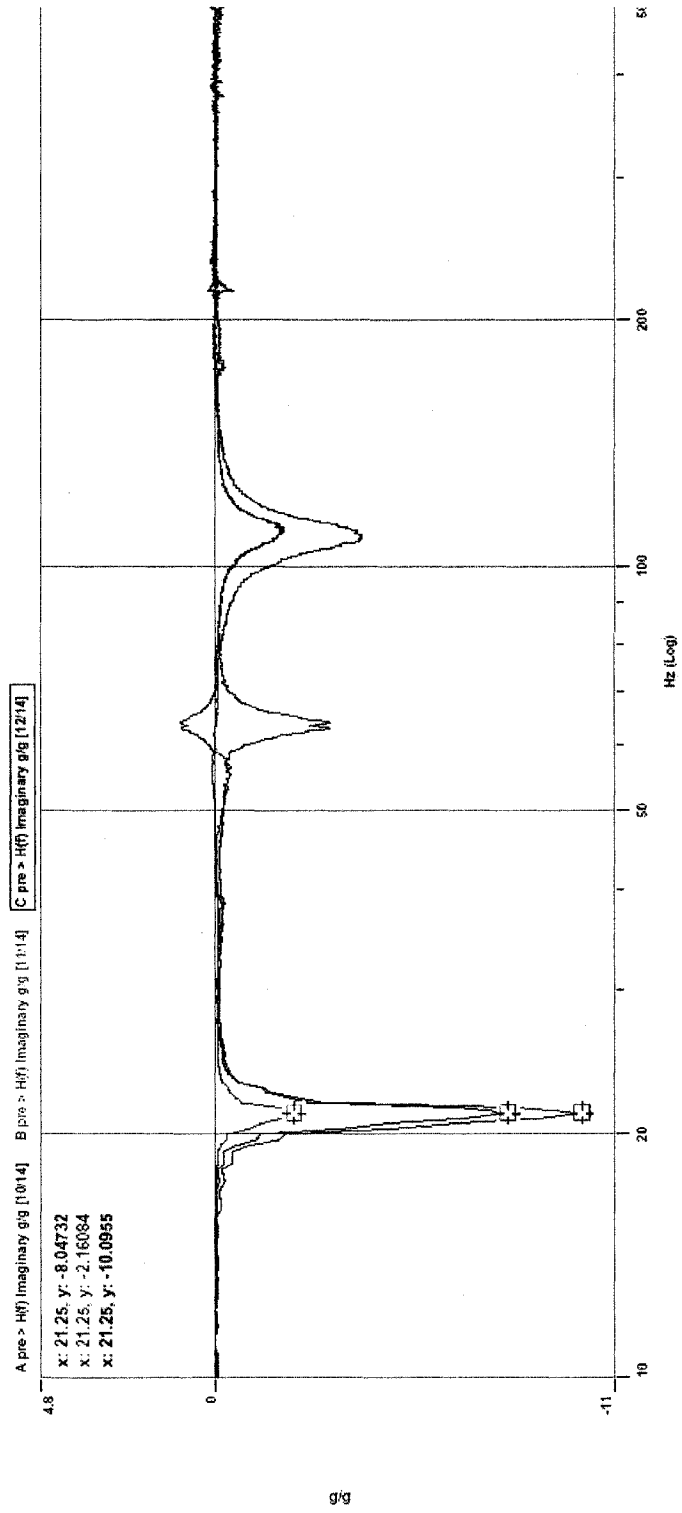

Figure 5.2 (a) Imaginary Transfer Function vs. Frequency plot for modal test in X-direction

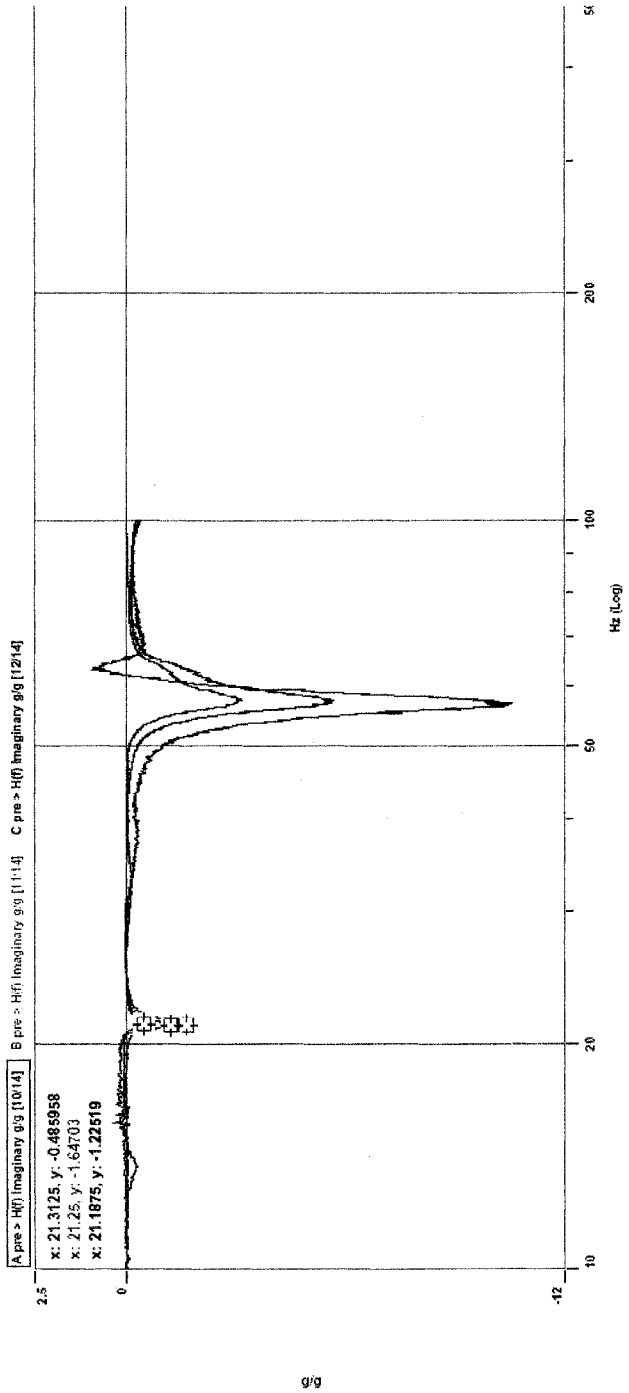

Figure 5.2 (b) Imaginary Transfer Function vs. Frequency plot for modal test in Z-direction

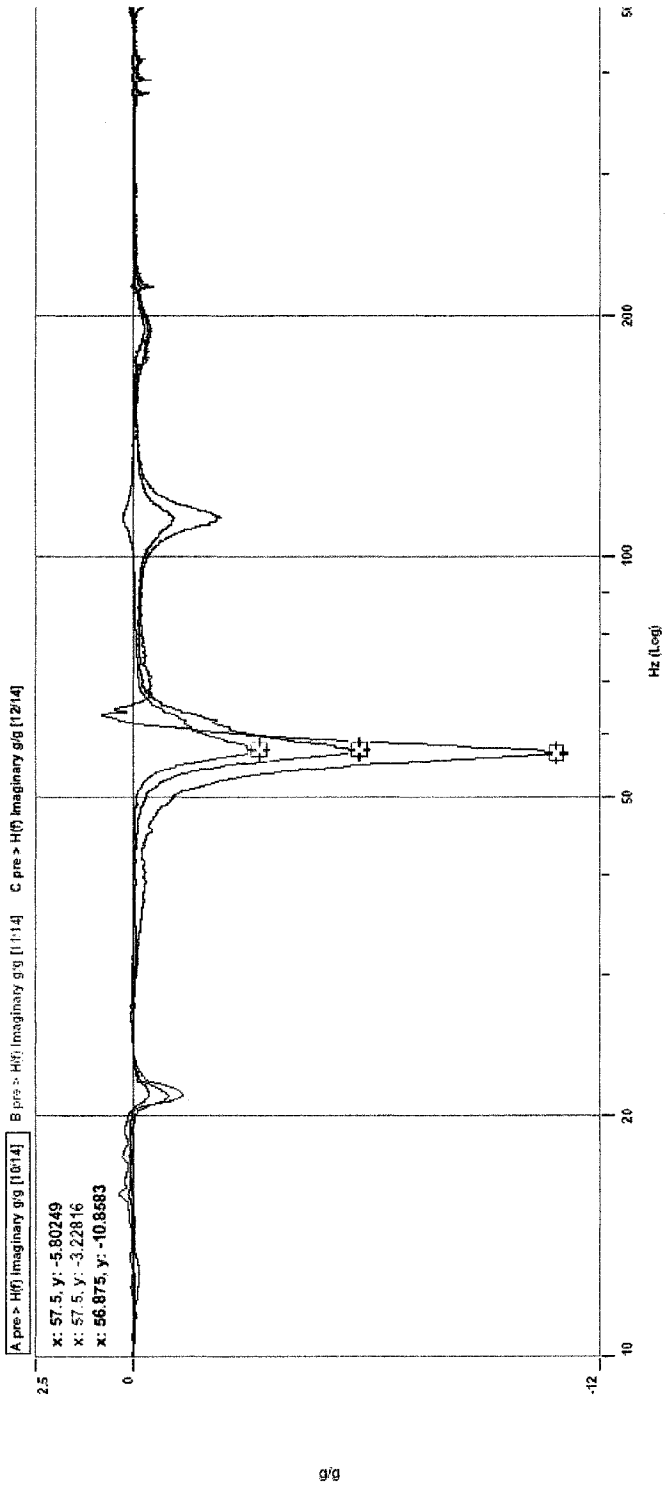

Figure 5.2 (c) Imaginary Transfer Function vs. Frequency plot for modal test in Z-direction

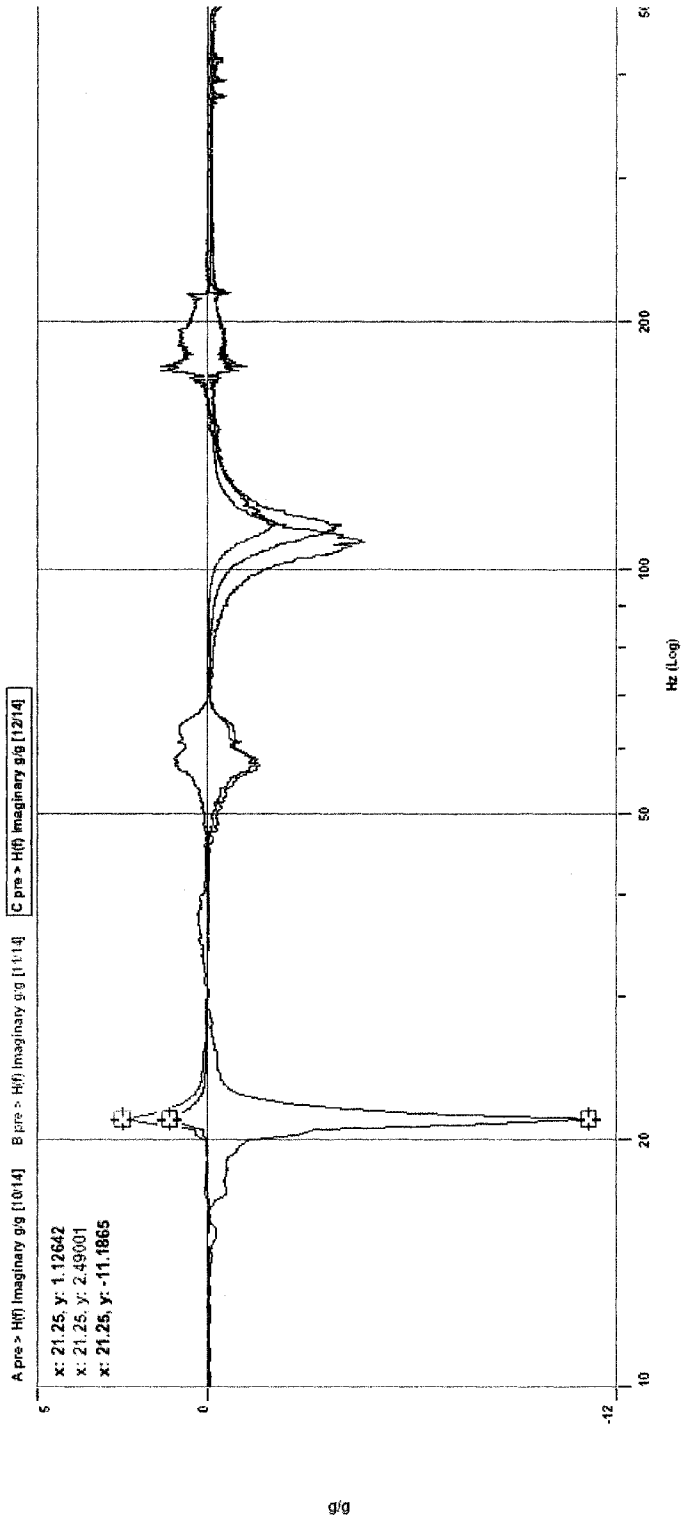

Figure 5.2(d) Imaginary Transfer Function vs. Frequency plot for modal test in Y-direction

Table 5.2 FE results for the stresses and strains and there critical node locations for the X-direction

FINITE LEMENT RESULTS					
NODE NO.	STRAIN	NODE NO.	STRESS IN Z1(MPa)	NODE NO.	STRESS IN Z2(MPa)
Area "A"	5.22E-04	Area"B"	146.678	Area"C"	122.112
Area "A"	5.20E-04	Area"B"	144.293	Area"C"	120.681
Area "A"	5.03E-04	Area"B"	141.431	Area"C"	119.012

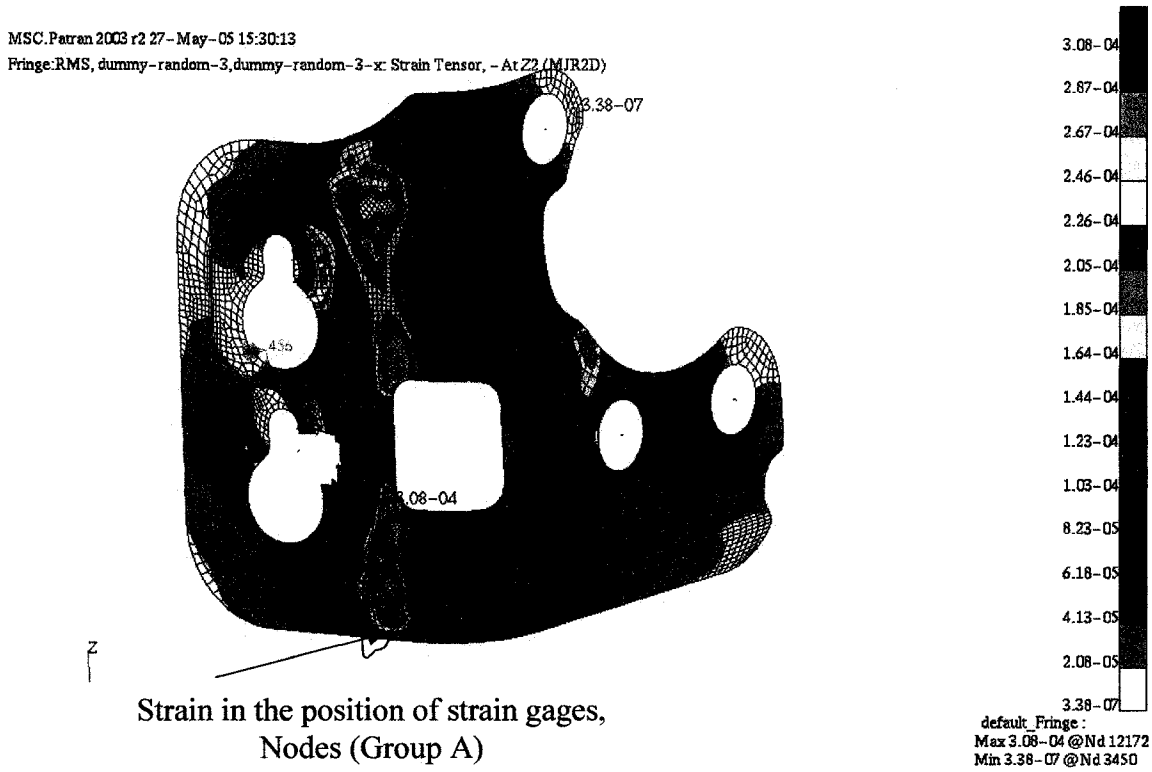

Figure 5.3 FE strain plots in Z2 highlighting the strain in the location of the strain gages

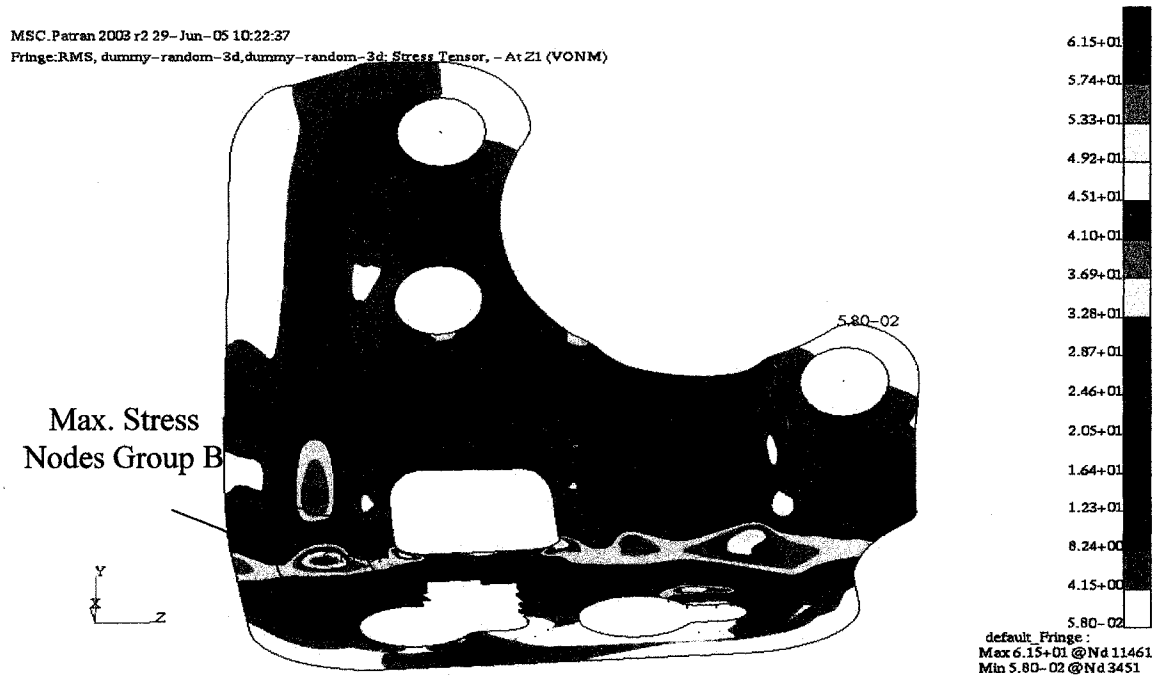

Figure 5.4 Maximum stresses in Z1 using PSD excitation in X-direction

From the strain results shown in table chapter four is which is found is equal to the FEA results shown in Table 5.2. The failure location in the test where the first crack is detected is lies in the region area B where the high stresses is recorded in the finite element model.

5.5 Fatigue assessment

After calculating the stresses, the final step is the fatigue assessment of the component using MSC.Fatigue software and the stresses calculated from the previous random vibration analysis. Two analysis methods, Tunna and Dirlik are available in MSC.Fatigue are used for fatigue assessment. Dirlik method is more accurate when the response of the signal is wide band and it is found far superior in most engineering applications, but it gives conservative results when the signal is narrow band. Tunna method is developed specifically for components made of steel and subjected to random vibration signal. It is found that this method works good when the response of the signal is narrow band (MSC. Fatigue software, 1999). Three types of stamping steel materials are used; each one has a slightly different S-N curve as shown in Figure 5.5(a) and 5.5(b), the fatigue life results are shown in Table 5.3 below for X, Y and Z directions.

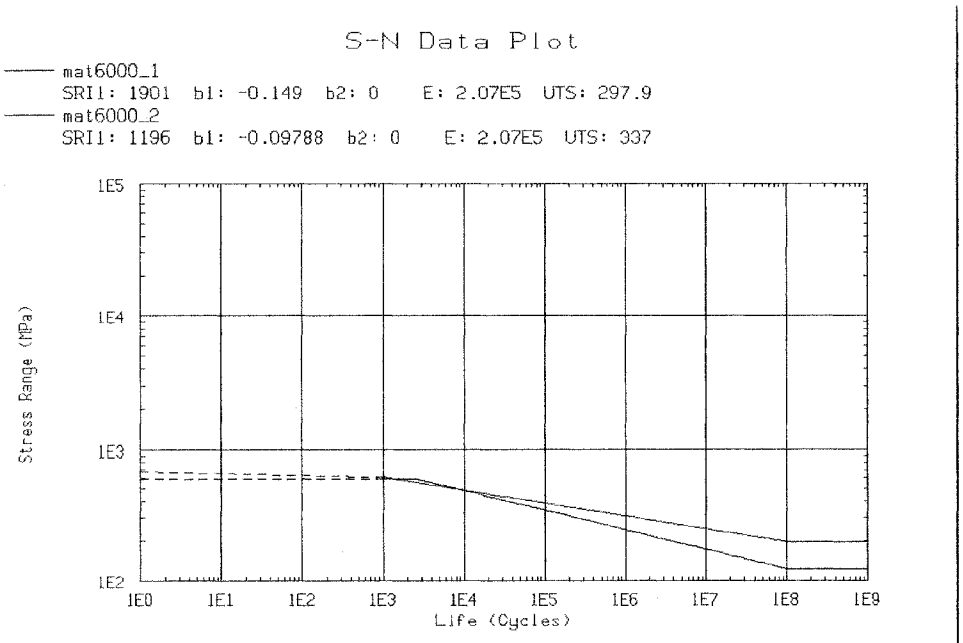

Figure 5.5 (a) S-N curve for MAT-1 and MAT-2 stamped steel

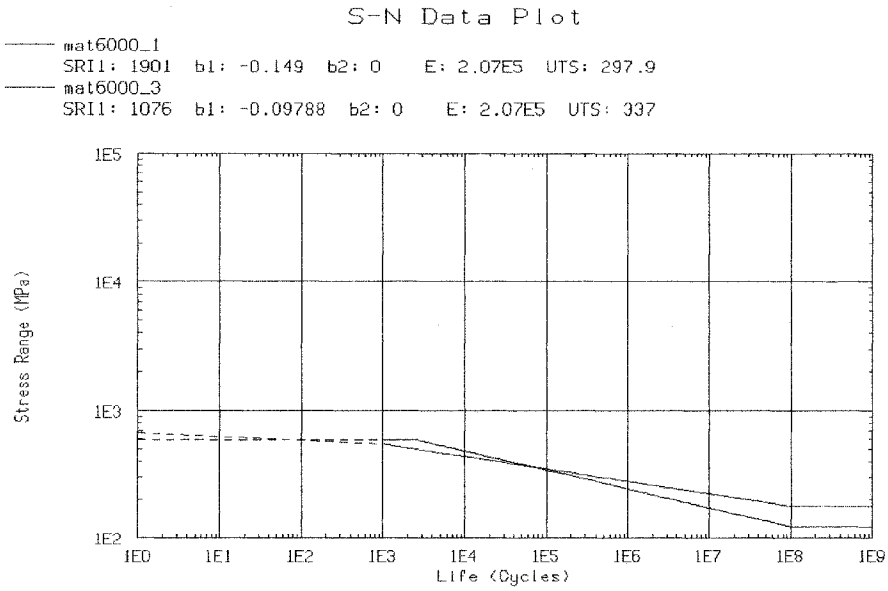

Figure 5.5 (b) S-N curve for MAT-1 and MAT-3 stamped steel

Table 5.3 Fatigue life (seconds) for the most damage nodes in the bracket using Tunna and Dirlik methods for vibration fatigue analysis

DUMMY MASS FATIGUE LIFE X-DIR. (SECONDS)					
NODE	DIRLIK MAT-1	TUNNA MAT-1	IRREGULARITY FACTOR	TUNNA MAT-2	TUNNA MAT-3
11461	11424.15	575731.85	0.4936	5.13E+06	1748147.8
11466	11529.09	578863.35	0.4939	5.15E+06	1762321.8
11462	11576.79	587399.27	0.493	5.29E+06	1804870.2
11467	11674.575	591029.24	0.4932	5.34E+06	1821550.9
DUMMY MASS FATIGUE LIFE Y-DIR. (SECONDS)					
13119	94965.93	4.87E+09	0.137	5.13E+06	1.75E+06
13175	96396.93	4.94E+09	0.1371	5.15E+06	1.76E+06
13120	111119.54	5.72E+09	0.1369	5.29E+06	1.80E+06
13174	111577.46	5.70E+09	0.1371	5.34E+06	1.82E+06
DUMMY MASS FATIGUE LIFE Z-DIR. (SECONDS)					
5196	62642.025	4.29E+05	0.7056	3.89E+06	1.33E+06
13178	63937.08	4.44E+05	0.704	4.10E+06	1.40E+06
13124	65432.475	4.48E+05	0.7054	4.17E+06	1.42E+06
13180	65749.68	4.58E+05	0.7037	4.29E+06	1.46E+06

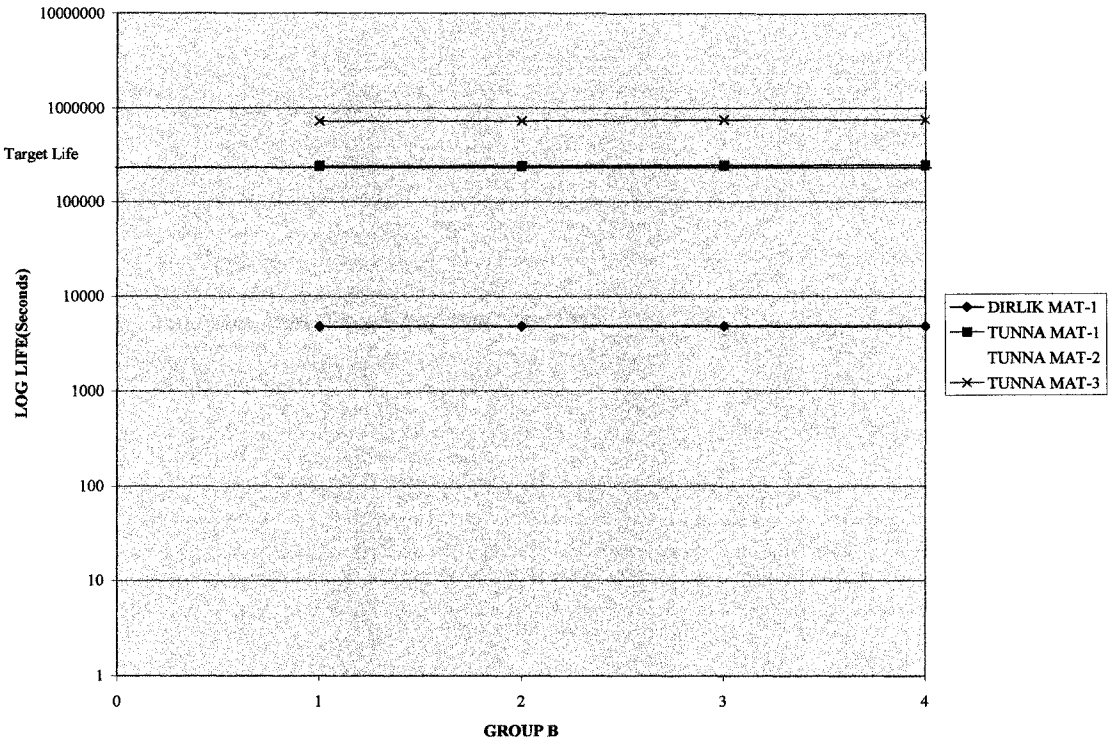

Figure 5.6 Log Life for the bracket supporting the Dummy mass using Dirlik and Tunna methods and three types of steel

From the results in Table 5.3 the fatigue life predicted from the finite element analysis using Dirlik method and MAT-1 is too small compared to the target life while the life predicted using Tunna method and MAT-1 is very close to the target life in the X,Y, and Z directions. The fatigue life predicted using Tunna method and MAT-2 and MAT-3 are higher than the target life.

From the above analysis and results, the best model that fits the modes of vibration, the stress-strain history, and the fatigue life is the model with the following input parameters:

1) ECU bushings stiffness are: 371, 840, 830 N/mm for the translational stiffness and 26630, 32143, 42000 N*mm/rad for the rotational stiffness
2) Base bushings stiffness are: 1404900, 1677900, 1677900 N/mm for the translational stiffness and 23163000, 16380000, 29820000 N*mm/rad for rotational stiffness
3) Viscous damping of 4%
4) Material properties are: MAT-1

5.6 Fatigue assessment of the real component

After correlating the results between the FE model and the test results for the dummy mass, now the FE model is considered accurate and can rely on it to conduct the final step which is the fatigue assessment for the bracket supporting the real ECU which weighted 3.15 kg.

5.6.1 Modal analysis and random vibration analysis

Conducting modal analysis and random vibration analysis, the results are shown in Table 5.4:

Table 5.4: Modes of vibration and critical stresses and their locations for the real ECU

MODES(Hz)	GROUP	CRITICAL STRESS IN X-DIR.(MPa)	GROUP	CRITICAL STRESS IN Y-DIR.(MPa)	GROUP	CRITICAL STRESS IN Z-DIR.(MPa)
37.4	B	102.3	B	93.0	C	100.6
95.8						
122.0						
126.0						
174.0						
321.8						
686.0						
1186.0						
1479.0						

5.6.2 Fatigue assessment

The results from the previous analysis were used to conduct fatigue assessments using two methods for vibration analysis in MSC.Fatigue (Dirlik method and Tunna method). The results are shown in Table 5.5 and Figure 5.7.

Table 5.5: Fatigue assessment for the real ECU using two methods of analysis (Dirlik and Tunna)

ECU MASS FATIGUE LIFE X-DIR. (SECONDS)					
GROUP	DIRLIK MAT-1	TUNNA MAT-1	IRREGULARITY FACTOR	TUNNA MAT-2	TUNNA MAT-3
B	24918	776034	0.528	1.39E+07	4.75E+06
B	25179	7.81E+05	0.528	1.41E+07	4.79E+06
B	25243	7.88E+05	0.528	1.43E+07	4.86E+06
B	25456	7.93E+05	0.528	1.44E+07	4.91E+06
ECU MASS FATIGUE LIFE Y-DIR. (SECONDS)					
B	1.36E+05	2.80E+09	0.1674	1.05E+13	3.59E+12
B	1.39E+05	2.87E+09	0.1673	1.09E+13	3.72E+12
B	1.71E+05	3.43E+09	0.1682	1.43E+13	4.86E+12
B	1.94E+05	3.94E+09	0.1679	1.76E+13	6.02E+12
ECU MASS FATIGUE LIFE Z-DIR. (SECONDS)					
D	46335	1.15E+05	0.8448	8.71E+05	2.97E+05
D	47178	1.17E+05	0.8445	8.99E+05	3.06E+05
D	47864	1.18E+05	0.8448	9.16E+05	3.12E+05
D	49499	1.23E+05	0.8444	9.68E+05	3.30E+05

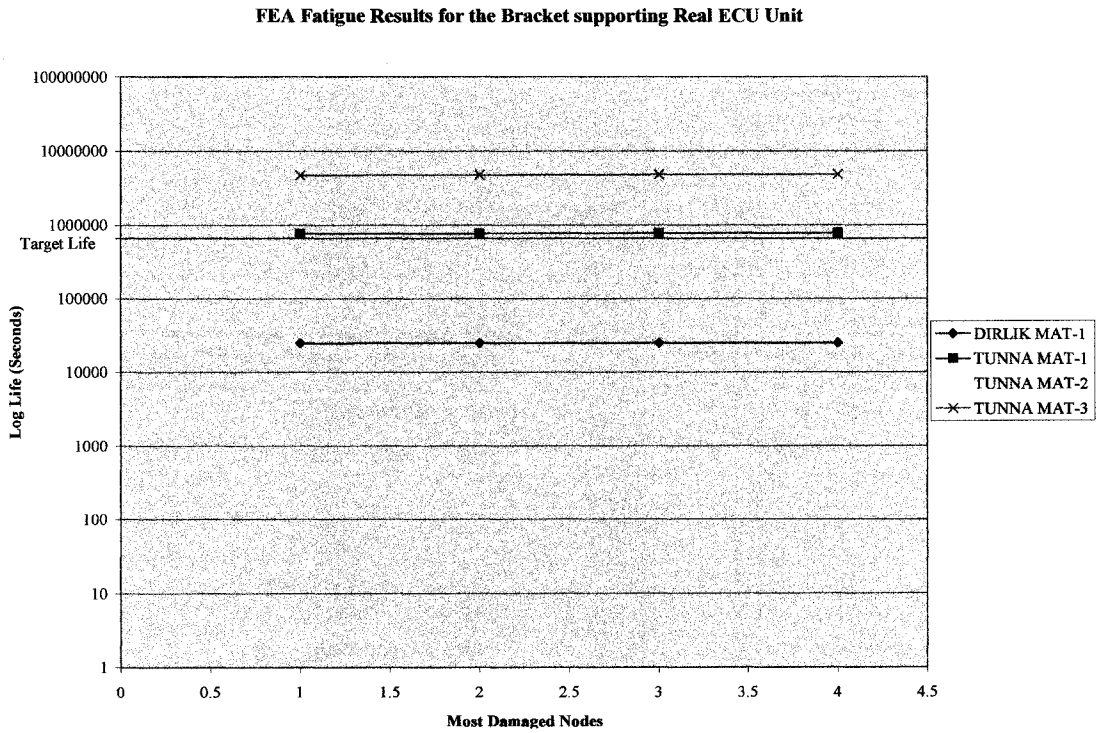

Figure 5.7 Log Life for the bracket supporting the real ECU using Dirlik and Tunna methods and three types of steel

From the results in Table 5.5 we can determine that Dirlik method is still gives life less than target life, while Tunna method and MAT-1, MAT-2 and MAT-3 gives better life assessment and the fatigue life for the real component is higher than target life in the three excitation axes X,Y, and Z.

CHAPTER SIX
CONCLUSION

6.1 Summary

Fatigue assessment is one of the most important phenomenons in today industrial and automotive applications that may cause more than 90% of the failures in structures and components. Studying and modeling fatigue is done in conjunction with finite element which is considered a very useful tool in today engineering applications.

Using finite element analysis in engineering applications saves efforts, time and money, however, physical testing on the other hand are essential in most of the cases to verify the analysis results and validate accuracy and the component behavior. In most of the durability cases finite element analysis cannot be considered as the only analysis method and used to replace or eliminate the physical test, however, it is used to reduce the number of tests or the testing time needed for a specific application. Finite element analysis gives fast and important idea about the dynamic behavior of the structure, the critical location of the stresses and the strains, the fatigue assessment and life in the design stage. In automotive industry, more need to use finite element exist in today applications because it provide a shorter time in the design stage and prototyping than the conventional methods. The competition in today's industry increases the demand to use finite element analysis in the engineering applications in the design stage to save time and to get the product ready in a period between 12-24 months.

Finite element analysis observed some discrepancies from the real test due to approximation, discretization, and other parameters related to the boundary conditions, meshing, material properties, etc..., when modeling a component or structure. This may lead to differences between the results obtained from the finite element analysis and the real component behavior like stresses, strains, accelerations, fatigue life, etc. Therefore, a need to correlate the FE model to observe the real component dynamic behavior is

essential to decrease the error and increase results accuracy for a future FEA based fatigue simulation.

6.2 Conclusions

The following conclusions can be drawn from this project:

- The important parameters affecting the accuracy of the FE model are: meshing quality, boundary conditions, material properties, bushings stiffness, and damping ratio.
- Finite element model is very sensitive to bushing elements; therefore, care should be taken when modeling bushings in FE, especially their properties, stiffness and damping.
- Bushings behavior is nonlinear in nature, and the need to measure the force over the displacement ratio is important in modeling them accurately; this is difficult to measure in reality. However, in the case of the random vibration analysis in frequency domain the relation is linear and this is one of the approximations that may affect the FE model accuracy. The stiffness and damping vs. frequency was constant too, this will cause another effect to the accuracy of the model.
- Fatigue assessment formulas are empirical; therefore, small differences in strains or stresses may cause differences of a few orders of magnitude in fatigue life.
- Vibration fatigue model in MSC.Fatigue is stress based only, strain based approach for random signal may give better results.
- Using a suitable analysis method in fatigue assessment is important and may cause that the results to be far away from reality (more conservative or over estimate the life). Dirlik method is considered a good analysis method in most of the cases especially when the response of a random signal is wide band, but it gives more conservative results when the response of a signal is narrow band.
- Tunna method is more appropriate for steel components and when the response of a random signal is narrow band like in the case of the ABS-bracket which is the subject of this thesis.

- From the above analysis methodology a reasonable accuracy for the FE model is achieved and a good FE simulation and FEA results for the measured strain and life of the component is predicted and correlated with tests results. This correlated results are achieved by using Tunna method for the ABS-bracket in two cases when the bracket is supporting dummy mass and then when supporting actual ECU unit. However, small discrepancy in Z-direction is observed when MAT-1 is used, this is mainly due to the material S-N curve and the endurance limit of the material as shown in Figure 5.5 a and b.

6.3 Recommendations for future researches

- Extracting the S-N curve from a fatigue properties test for the actual ABS-bracket material and use this S-N curve to model the material properties and conduct fatigue assessments to check the differences.
- Conducting vibration fatigue analysis based on strain and find out what are the differences between the two methods.
- Studying the factors that cause the difference in Z-direction if the suggested extracted S-N curve for the actual material doesn't correlate the life in Z-direction.
- Using solid elements instead of shell elements to find out how are the results will be affected.
- Convert the PSD to time and run the analysis and fatigue simulation based on a time history.

REFERENCES

1. Bannentine J. A., Comer J. J., and Handrock J. L., (1990), "Fundamental of Metal Fatigue Analysis", Prentice Hall, Englewood Cliffs, New Jersy 07632.

2. Basquin, O. H., (1910), " The Experimental Law of Endurance Tests", American Society for Testing and Materials", Vol. 10, pp. 625-630.

3. Bishop, N. W. M., and Sherrat, F., (1990), " A Theoretical Solution For the Estimation of Rainflow Ranges from Power Spectral Density Data", Fatigue Fracture Engineering material structures, pp. 311-326.

4. Coffin, L. F., Jr., (1954), "A Study of the Effects of Cyclic Thermal stresses on a Ductile Metal", American society of Mechanical Engineers, Vol. 76, pp. 931-950.

5. Collins, J. A., (1981), "Failure of Materials in Mechanical design", A Wiley-Interscience Publication, John Wiley & Sons.

6. Draper, J., (1999), "Modern Metal Fatigue Analysis", ABAQUS Inc., ABAQUS Series.

7. Dirlik, T. (1985), "Application of Computers in Fatigue Analysis, University of Warwick Thesis, UK.

8. Ewins D. J., (2000), "Modal Testing, Theory, Practice and Application", Research Studies Press Ltd.

9. Hoffmann, M., and Seeger, T., (1985), "A New Approach to the Evaluating of Fatigue Under Multiaxial Loading", Journal of Engineering Materials and Technology, Vol. 103, pp. 118-125.

10. Maia N. M. M., Silva J. M. M., (1997), "Theoretical and Experimental Modal Analysis", Research Studies Press Ltd, John Wiley & Sons Inc.

11. Manson, S. S., (1953), "Behavior of Materials under Conditions of Thermal Stress", Heat Transfer Symposium, University of Michigan Engineering Research Institute, pp. 9-75.

12. Morrow, J., (1965), "Cyclic Plastic Strain energy and Fatigue of Metals", American Society for Testing and Materials, Philadelphia.

13. MSC.Software, 1999, "Patran v.9 volume 1 and 2 User's Guide", The MacNeal-Schwendler Corporation, CA, USA.

14. MSC.Software, 2001, "Nastran User's Guide", The MacNeal-Schwendler Corporation, CA, USA.

15. MSC.Software, 1994, "Nastran v.68 Linear Static Analysis, User's Guide", The MacNeal-Schwendler Corporation, CA, USA.

16. MSC.Software, 1994, "Nastran v.68 Basic Dynamic Analysis, User's Guide", The MacNeal-Schwendler Corporation, CA, USA.

17. MSC.Software, 1994, "Nastran v.68 Design Sensitivity and Optimization, User's Guide", The MacNeal-Schwendler Corporation, CA, USA.

18. MSC.Software, 1999, "Nastran v.2 Random Vibration Analysis, User's Guide", The MacNeal-Schwendler Corporation, CA, USA.

19. MSC.Software, 1999, "Fatigue version 8, volume 1 and 2, User's Guide", The MacNeal-Schwendler Corporation, CA, USA.

20. nCode International, (2001), "FE-Fatigue Theory Manual", Michigan, USA.

21. Neuber, H., (1946), "Theory of Notch Stress: Principle for Exact Stress Calculations", Edwards, Ann Arbor, Michigan.

22. Peterson, R., E., (1974), "Stress Concentration Factors", Wiley Publication, New York.

23. Stephens R. I., Fatemi A., Stephens R. R., Fuchs H. O., (2001),"Metal Fatigue in Engineering", Wiley-Interscience Publication, John Wiley & Sons.

24. Smith, R. N., Watson, P., and Topper, T. H., (1970), " A Stress-Strain Parameter for the Fatigue of Metals", Journal of Materials, Vol.5, No.4, pp. 767-778.

25. Tunna, J. M., BA, (1985), " Random Load Fatigue: Theory and Experiment", Proctor Institutes of Mechanical Engineers, pp. 249-257, UK.

26. Tunna, J. M., (1986), "Fatigue Life Prediction for Gaissian Random Loads at the Design Stage", Fatigue Fracture Engineering for Materials and Structures, pp. 169-184, UK.

VITA AUCTORIS

Ziad Abdul–Hafidh Hanna was born on February 2nd, 1967 in Baghdad, Iraq. He graduated in 1984 from Al-Mansour High School in Baghdad, Iraq. He attended the University of Baghdad , which is located in Baghdad, Iraq, where he earned his Bachelor of science in Civil engineering with Honours in 1988. In 2003, Ziad attended the University of Windsor, located in Windsor, Ontario, Canada to complete his post graduate study. He is currently enrolled as Masters candidate at this institution, and is sceduelled to graduate in October, 2005.